

1 **Effective radiative forcing from emissions of reactive gases and** 2 **aerosols – a multi-model comparison**

3 Gillian D. Thornhill¹, William J. Collins¹, Ryan J. Kramer², Dirk Olivié³, Ragnhild B. Skeie⁴,
4 Fiona O'Connor⁵, Nathan L. Abraham⁶, Ramiro Checa Garcia⁷, Susanne E. Bauer⁸, Makoto
5 Deushi⁹, Louisa K. Emmons¹⁰, Piers M. Forster¹¹, Larry W. Horowitz¹², Ben Johnson⁵, James
6 Keeble⁶, Jean-Francois Lamarque¹⁰, Martine Michou¹³, Michael J. Mills¹⁰, Jane P. Mulcahy⁵,
7 Gunnar Myhre⁴, Pierre Nabat¹³, Vaishali Naik¹², Naga Oshima⁹, Michael Schulz³, Christopher
8 J. Smith¹¹, Toshihiko Takemura¹⁴, Simone Tilmes¹⁰, Tongwen Wu¹⁵, Guang Zeng¹⁶, Jie
9 Zhang¹⁵.

10 ¹Department of Meteorology, University of Reading, Reading, RG6 6BB, UK

11 ²Climate and Radiation Laboratory, NASA Goddard Space Flight Center, Greenbelt, MD 20771, USA, and
12 Universities Space Research Association, 7178 Columbia Gateway Drive, Columbia, MD 21046, USA

13 ³Norwegian Meteorological Institute, Oslo, Norway

14 ⁴CICERO – Centre for International Climate and Environmental Research Oslo, Oslo, Norway

15 ⁵Met Office, Exeter, UK

16 ⁶Department of Chemistry, University of Cambridge, Lensfield Road, Cambridge, CB2 1EW, U.K., National
17 Centre for Atmospheric Science, U.K

18 ⁷IPSL/LSCE CEA-CNRS-UVSQ-UPSaclay UMR Gif sur Yvette, FRANCE

19 ⁸NASA Goddard Institute for Space Studies, USA

20 ⁹Meteorological Research Institute, Tsukuba, Japan

21 ¹⁰National Center for Atmospheric Research, Boulder, CO, USA

22 ¹¹University of Leeds, Leeds, UK and International Institute for Applied Systems Analysis (IIASA), Laxenburg,
23 Austria

24 ¹²NOAA, Geophysical Fluid Dynamics Laboratory (GFDL), Princeton, NJ 08540-6649

25 ¹³Centre National de Recherches Météorologiques, Meteo-France, Toulouse Cedex, France

26 ¹⁴Research Institute for Applied Mechanics, Kyushu University, Japan

27 ¹⁵Climate System Modeling Division, Beijing Climate Center, Beijing, China

28 ¹⁶NIWA, Wellington, New Zealand

29 *Correspondence to:* Gillian D. Thornhill (g.thornhill@reading.ac.uk)

30 **Abstract**

31 This paper quantifies the pre-industrial (1850) to present-day (2014) effective radiative forcing (ERF) of
32 anthropogenic emissions of NO_x, VOCs (including CO), SO₂, NH₃, black carbon, organic carbon, and
33 concentrations of methane, N₂O and ozone-depleting halocarbons, using CMIP6 models. Concentration and
34 emission changes of reactive species can cause multiple changes in the composition of radiatively active species:

35 tropospheric ozone, stratospheric ozone, stratospheric water vapour, secondary inorganic and organic aerosol and
36 methane. Where possible we break down the ERFs from each emitted species into the contributions from the
37 composition changes. The ERFs are calculated for each of the models that participated in the AerChemMIP
38 experiments as part of the CMIP6 project, where the relevant model output was available.

39 The 1850 to 2014 multi-model mean ERFs (\pm standard deviations) are $-1.03 \pm 0.37 \text{ Wm}^{-2}$ for SO_2 emissions, -
40 $0.25 \pm 0.09 \text{ Wm}^{-2}$ for organic carbon (OC), $0.15 \pm 0.17 \text{ Wm}^{-2}$ for black carbon (BC) and for NH_3 it is $-0.07 \pm$
41 0.01 Wm^{-2} . For the combined aerosols (in the piClim-aer experiment) it is $-1.01 \pm 0.25 \text{ Wm}^{-2}$. The multi-model
42 means for the reactive well-mixed greenhouse gases (including any effects on ozone and aerosol chemistry) are
43 $0.67 \pm 0.17 \text{ Wm}^{-2}$ for methane (CH_4), $0.26 \pm 0.07 \text{ Wm}^{-2}$ for nitrous oxide (N_2O) and $0.12 \pm 0.2 \text{ Wm}^{-2}$ for ozone-
44 depleting halocarbons (HC). Emissions of the ozone precursors nitrogen oxides (NO_x), volatile organic
45 compounds (VOC) and both together (O_3) lead to ERFs of $0.14 \pm 0.13 \text{ Wm}^{-2}$, $0.09 \pm 0.14 \text{ Wm}^{-2}$ and 0.20 ± 0.07
46 Wm^{-2} respectively. The differences in ERFs calculated for the different models reflect differences in the
47 complexity of their aerosol and chemistry schemes, especially in the case of methane where tropospheric
48 chemistry captures increased forcing from ozone production.

49

50 **1. Introduction**

51 The characterisation of the responses of the atmosphere, climate, and earth systems to various forcing agents is
52 essential for understanding, and countering, the impacts of climate change. As part of this effort there have been
53 several projects directed at using climate models from different groups around the world to produce a systematic
54 comparison of the simulations from these models, via the Coupled Model Intercomparison Project (CMIP), which
55 is now in its 6th iteration (Eyring et al., 2016). This CMIP work has been subdivided into different areas of interest
56 for addressing specific questions about climate change, such as the impact of aerosols and reactive greenhouse
57 gases, and the AerChemMIP (Collins et al., 2017) project is designed to examine the specific effects of these
58 factors on the climate. The aerosol and aerosol precursor species considered are sulphur dioxide (SO_2), black
59 carbon (BC), organic carbon (OC). The reactive greenhouse gases and ozone precursors are methane (CH_4),
60 nitrogen oxide (NO_x), volatile organic compounds (VOCs – including carbon monoxide), nitrous oxide (N_2O)
61 and ozone-depleting halocarbons (HC).

62 The focus of this work is to characterise the effect of the change from pre-industrial (1850) to present day (2014)
63 in aerosols and their precursors, and chemically-reactive greenhouse gases (including species that affect ozone)
64 on the radiation budget of the planet, referred to as radiative forcing, as an initial step to understanding the response
65 of the atmosphere and earth system to changes in these components. In previous reports of the Intergovernmental
66 Panel on Climate Change (IPCC) the effect of the various forcing agents on the radiation balance has been
67 investigated in terms of the radiative forcing, (RF), which is a measure of how the radiative fluxes at the top of
68 atmosphere (TOA) change in response to changes in, e.g., concentrations or emissions of greenhouse gases and
69 aerosols. There have been several definitions of radiative forcing, (Forster et al., 2016; Sherwood et al., 2015),
70 which generally considered the instantaneous radiative forcing (IRF), or a combination of the IRF including the
71 adjustment of the stratospheric temperature to the driver, generally termed the stratospheric-temperature adjusted
72 radiative forcing. More recently (Boucher, 2013; Chung and Soden, 2015) there has been a move towards using
73 the effective radiative forcing (ERF) as the preferred metric, as this includes the rapid adjustments of the

74 atmosphere to the perturbation, e.g. changes in cloud cover or type, water vapour, tropospheric temperature, which
75 may affect the overall radiative balance of the atmosphere. In this work, ERF is calculated using two atmospheric
76 model simulations both with the same prescribed sea-surface temperatures (SSTs) and sea ice, but one having the
77 perturbation we are interested in investigating, e.g. a change in emissions or concentrations of aerosols or reactive
78 gases. The difference in the net TOA flux between these two simulations is then defined as the ERF for that
79 perturbation.

80 Previous efforts to understand the radiative forcing due to aerosols and reactive gases in CMIP simulations have
81 resulted in a wide spread of values from the different climate models, in part due to a lack of suitable model
82 simulations for extracting the ERF from, e.g., a specific change to an aerosol species. The experiments in the
83 AerChemMIP project have been designed to address this in part, by defining consistent model set-ups to be used
84 to calculate the ERFs, although the individual models will still have their own aerosol and chemistry modules,
85 with varying levels of complexity and different approaches.

86 There are complexities in assessing how a particular forcing agent affects the climate system due to the interactions
87 between some of the reactive gases; for example methane and ozone are linked in complex ways, and this increases
88 the problem of understanding the specific contribution of each to the overall ERF when one of them is perturbed.

89 An attempt to understand some of these interactions is discussed in Section 4.2 below.

90 The experimental set-up and models used are described in Section 2, the methods for calculating the ERFs for the
91 aerosol and chemistry experiments are described in Section 3, and the results are discussed in section 4. Final
92 conclusions are drawn in Section 5.

93 **2. Experimental Setup**

94 **2.1 Models**

95 This analysis is based on models participating in the Coupled Model Intercomparison Project (CMIP6) (Eyring et
96 al., 2016), which oversees climate modelling efforts from a number of centres with a view to facilitating
97 comparisons of the model results in a systematic framework. The overall CMIP6 project has a number of sub-
98 projects, where those with interests in specific aspects of the climate can design and request specific experiments
99 to be undertaken by the modelling groups. To understand the effects of aerosols and reactive gases on the climate,
100 a set of experiments was devised under the auspices of AerChemMIP (Collins et al., 2017), described in Section
101 2.2.

102 The anthropogenic emissions of the aerosols, aerosol precursors and ozone precursors (excluding methane) for
103 use in the models are given by Hoesly et al. (2018) and van Marle et al. (2017). Models use their own natural
104 emissions (Eyring et al., 2016). The well-mixed greenhouse gases (WMGHG), CO₂, CH₄, N₂O and halocarbons
105 are specified as concentrations either at the surface or in the troposphere. Not all of the models include interactive
106 aerosols, tropospheric chemistry and stratospheric chemistry, which is the ideal for the AerChemMIP experiments,
107 but those models which do not include all these processes provide results for a subset of the experiments described
108 in Section 2.2.

109 The models included in this analysis are summarised below, and in Table 1 with an overview of the model set-up,
110 aerosol scheme and type of chemistry models used included. A more detailed description of each model and the
111 aerosol and chemistry schemes used in each is available in the supplementary materials, Table S1.

112 The CNRM-ESM2-1 model (Séférian et al., 2019; Michou et al., 2020) includes an interactive tropospheric aerosol
113 scheme, and an interactive gaseous chemistry scheme only above the level of 560 hPa. The sulfate precursors
114 evolve to SO₄ using a simple dependence on latitude. The cloud droplet number concentration (CDNC) depends
115 on SO₄, organic matter and sea-salt concentrations, so the aerosol cloud-albedo effect is represented, although
116 other aerosol-cloud interactions are not.

117 The UKESM1 model (Sellar et al., 2020) includes an interactive stratosphere-troposphere gas-phase chemistry
118 scheme (Archibald et al., 2020) using the UK Chemistry and Aerosol (UKCA); (Morgenstern et al.,
119 2009; O'Connor et al., 2014) model. The UKCA aerosol scheme, called GLOMAP-mode is two-moment
120 simulation of tropospheric black carbon, organic carbon, SO₄ and sea salt. Dust is modelled independently using
121 the bin scheme of Woodward (2001). A full description and evaluation of the chemistry and aerosol schemes in
122 UKESM1 can be found in Archibald et al. (2020) and Mulcahy et al. (2020) respectively.

123 The MIROC6 model includes the Spectral Radiation-Transport Model for Aerosol Species (SPRINTARS) aerosol
124 model which predicts mass mixing ratios of the main tropospheric aerosols and models aerosol-cloud interactions
125 in which aerosols alter cloud microphysical properties and affect the radiation budget by acting as cloud
126 condensation and ice nuclei (Takemura et al., 2005; Watanabe et al., 2010; Takemura and Suzuki, 2019; Takemura,
127 2018; Tatebe et al., 2019).

128 The MRI-ESM2 model (Yukimoto et al., 2019) has the Model of Aerosol Species in the Global Atmosphere mark-
129 2 revision 4-climate (MASINGAR mk-2r4c) aerosol model, and a chemistry model, MRI-CCM2 (Deushi and
130 Shibata, 2011) which models chemistry processes for ozone and other trace gases from the surface to middle
131 atmosphere. The model includes aerosol-chemistry interactions, and aerosol-cloud interactions (Kawai et al.,
132 2019). The ERFs of anthropogenic gases and aerosols under present-day conditions relative to preindustrial
133 conditions estimated by MRI-ESM2 as part of the Radiative Forcing Model Intercomparison Project (RFMIP)
134 (Pincus et al., 2016) and AerChemMIP are summarized in Oshima et al. (2020).

135 The BCC-ESM1 model (Wu et al., 2019; Wu et al., 2020) models major aerosol species including gas-phase
136 chemical reactions, secondary aerosol formation, and aerosol-cloud interactions including indirect effects are
137 represented. It does not include stratospheric chemistry, so concentrations of ozone, CH₄, and N₂O at the top two
138 model levels are the zonally and monthly values derived from the CMIP6 data package.

139 The NorESM2 model contains interactive aerosols and uses the OsloAero6 aerosol module (Seland et al., 2020),
140 (Olivie et al., in prep.) describes the formation and evolution of BC, OC, SO₄, dust, sea-salt and SOA. There is a
141 limited gas-phase chemistry describing the oxidation of the aerosol precursors DMS, SO₂, isoprene, and
142 monoterpenes and oxidant fields of OH, HO₂, NO₃ and ozone are prescribed climatological fields, and there is no
143 ozone chemistry in the model.

144 The GFDL-ESM4 model consists of the GFDL AM4.1 atmosphere component, (Dunne et al., 2020; Horowitz et
145 al., 2020) which includes an interactive tropospheric and stratospheric gas-phase and aerosol chemistry scheme.
146 Nitrate aerosols are explicitly treated in this model.

147 The CESM2-WACCM model includes interactive chemistry and aerosols for the troposphere, stratosphere and
148 lower thermosphere (Emmons et al., 2010); (Gettelman et al., 2019). The representation of secondary organic
149 aerosols follows the Volatility Basis Set approach (Tilmes et al., 2019).

150 The IPSLCM6A-LR-INCA (referred to subsequently as IPSL-INCA) model used for this analysis has interactive
151 aerosols but a limited gas-phase model. The aerosol scheme is based on a sectional approach with to represent the

152 size distribution of dust, sea- salt (which has an additional super-coarse mode to model largest emission of spray-
 153 salt aerosols), BC, NH₄, NO₃, SO₄, SO₂ and OA with a combination of accumulation and coarse log-normal modes
 154 with both soluble and insoluble treated as independent modes. DMS emissions are prescribed and not interactively
 155 calculated. BC is modelled as internally mixed with sulphate (Wang et al. (2016), where the refractive index is
 156 relies on Garnet-Maxwell method. Its emissions are derived from inventories. A new dust refractive index is
 157 implemented (Di Biagio et al., 2019). Well mixed trace gases concentrations/emissions are forced with
 158 AMIP/CMIP6 datasets (Lurton et al., 2020) ozone using Checa-Garcia et al. (2018) and solar forcing from Matthes
 159 et al. (2017).

160 The GISS-E2-1 model aerosol scheme (One-Moment Aerosol (OMA)) module, which includes sulfate, nitrate,
 161 ammonium, carbonaceous aerosols (BC and OC), is coupled to both the tropospheric and stratospheric chemistry
 162 scheme. For the results reported here, the physics version 3 of this model configuration was used, which includes
 163 the aerosol impacts on clouds. For details of the model, see Bauer et al. (2020).

164

165 **Table 1 Components used in the Earth system models (detailed Table is in Supplementary material, Table S1)**

	Aerosols	Tropospheric chemistry	Stratospheric chemistry
IPSL-CM6A-LR-INCA	Interactive	No	No
NorESM2-LM	Interactive	SOA and sulfate precursor chemistry	No
UKESM1-LL	Interactive Tropospheric. Prescribed stratospheric	Interactive	Interactive
CNRM-ESM2-1	Interactive	Chemical reactions down to 560 hPa	Interactive
MRI-ESM2	Interactive	Interactive	Interactive
MIROC6	Interactive	SOA and sulfate precursor chemistry	No
BCC-ESM1	Interactive	Interactive	No
GFDL-ESM4	Interactive	Interactive	Interactive
CESM2-WACCM	Interactive	Interactive	Interactive
GISS-E2-1	Interactive	Interactive	Interactive

166 **2.2 Experiments**

167 The AerChemMIP timeslice experiments (Table 2) are used to determine the present-day (2014) ERFs for the
 168 changes in emissions or concentrations of reactive gases, and aerosols or their precursors (Collins et al., 2017).

169 The ERFs are calculated by comparing the change in net TOA radiation fluxes between two runs with the same

170 prescribed sea surface temperatures (SSTs) and sea ice, but with near-term climate forcers (NTCFs - also referred
171 to as short-lived climate forcers - SLCFs), reactive gas and aerosol emissions, and well-mixed greenhouse gases
172 (WGMHG - methane, nitrous oxide, halocarbon) concentrations perturbed. It should be noted that in
173 AerChemMIP the NTCF experiment excludes CH₄ the experimental design. The control run uses set 1850 pre-
174 industrial values for the aerosol and aerosol precursors, CH₄ N₂O, ozone precursors and halocarbons, either as
175 emissions or concentrations (Hoesly et al., 2018; van Marle et al., 2017; Meinshausen et al., 2017). Monthly
176 varying prescribed SSTs and sea-ice are taken from the CMIP6 DECK coupled pre-industrial (1850) control
177 simulation. Each experiment then perturbs the pre-industrial value by changing one (or more) of the species
178 (emissions or concentrations) to the 2014 value, while keeping SSTs and sea-ice prescribed as in the pre-industrial
179 control. Note adding individual species to a pre-industrial control will likely give different results to a setup where
180 species were individually subtracted from a present-day control. The NTCFs are perturbed individually or in
181 groups. This provides ERFs for the specific emission or concentration change, but also for all aerosol precursor
182 or NTCFs combined (Collins et al., 2017). For models without interactive tropospheric chemistry “NTCF” and
183 “aer” experiments are the same; in the case of NorESM2 for the NTCF experiments the model attempts to mimic
184 the full chemistry by setting the oxidants and ozone to 2014 values. The WGMHG experiments include the effects
185 on aerosol oxidation, tropospheric and stratospheric ozone, and stratospheric water vapour depending on the
186 model complexity.
187 Thirty years of simulation are required to minimise internal variability (mainly from clouds) (Forster et al, 2016.),
188 and one ensemble member was used for each experiment (almost all models provided only a single ensemble
189 member).

191 **Table 2 List of fixed SST ERF simulations. (NTCF in (Collins et al., 2017) is also referred to as 'SLCF' - short-lived**
192 **climate forcers - in other publications) and for the purposes of this study excludes methane.**

Experiment ID	CH ₄	N ₂ O	Aerosol Precursors	Ozone Precursors	CFC/ HCFC	Number of models
<i>piClim-control</i>	1850	1850	1850	1850	1850	11
<i>piClim-NTCF</i>	1850	1850	2014	2014	1850	8
<i>piClim-aer</i>	1850	1850	2014	1850	1850	9
<i>piClim-BC</i>	1850	1850	1850 (non BC) 2014 (BC)	1850	1850	7
<i>piClim-O3</i>	1850	1850	1850	2014	1850	4
<i>piClim-CH4</i>	2014	1850	1850	1850	1850	8
<i>piClim-N2O</i>	1850	2014	1850	1850	1850	5
<i>piClim-HC</i>	1850	1850	1850	1850	2014	6
<i>piClim-NOX</i>	1850	1850	1850	1850 (non NO _x) 2014 (NO_x)	1850	5
<i>piClim-VOC</i>	1850	1850	1850	1850 (non CO/VOC) 2014 (CO/VOC)	1850	5
<i>piClim-SO2</i>	1850	1850	1850 (non SO ₂) 2014 (SO₂)	1850	1850	6

<i>piClim-OC</i>	1850	1850	1850 (non OC) 2014 (OC)	1850	1850	6
<i>piClim-NH3</i>	1850	1850	1850 (non NH ₃) 2014 (NH₃)	1850	1850	2

193 3. Methods

194 In the following analysis we use several methods to analyse the ERF and the relative contributions from different
195 aerosols, chemistry and processes to the overall ERF for the models and experiments described above, where the
196 appropriate model diagnostics were available.

197 3.1 Calculation of ERF using fixed SSTs

198 The ERF is calculated from the experiments described above, where the sea surface temperatures and sea-ice are
199 fixed to climatological values. Here the ERF is defined as the difference in the net TOA flux between the perturbed
200 experiments and the piClim-control experiment (Sherwood et al., 2015), calculated as the global mean for the 30
201 years of the experimental run (where the models were run longer than 30 years, only the last 30 years was used).
202 This allows us to calculate the ERF for the individual species based on the changes to the emission or
203 concentrations between the control and perturbed runs of the models. The assumption is that there is minimal
204 contribution from the climate feedback when the SSTs are fixed, but the resultant ERF includes rapid adjustments
205 to the forcing agent in the atmosphere (Forster et al., 2016).

206 The ERF calculated using this method includes any contributions to the ERF resulting from changes in the land
207 surface temperature (T_s), which ideally should be removed (Shine et al., 2003; Hansen et al., 2005; Vial et al., 2013)
208 (as the ocean temperature changes are removed by using fixed SSTs). However, there is no simple way to prescribe
209 land surface temperatures in the models considered here analogous to the fixing the SSTs, so we make the land
210 surface temperature correction by calculating the surface temperature adjustment from the radiative kernel (see
211 Section 3.2) and subtracting it from the standard ERF as calculated above (see also Smith et al. (2020a); (Tang et
212 al., 2019)). This is designated the ERF_{ts} to differentiate it from the standard ERF as described above.

214 3.2 Kernel Analysis

215 Where the relevant data are available, we use the radiative kernel method (Smith et al., 2018; Soden et al.,
216 2008; Chung and Soden, 2015) to break down the ERF into the instantaneous radiative forcing (IRF) and individual
217 rapid adjustments (designated by A) which are radiative responses to changes in atmospheric state variables that
218 are not coupled to surface warming. In this approach, ERF is defined as:

$$219 \text{ ERF} = \text{IRF} + A_{t_trop} + A_{t_strat} + A_{ts} + A_q + A_a + A_c + e \quad (1)$$

220 where A_{t_trop} is the troposphere temperature adjustment, A_{t_strat} is the troposphere temperature adjustment, A_{ts} is
221 the surface temperature adjustment, A_q is the water vapour adjustment, A_a is the albedo adjustment, A_c is the cloud
222 adjustment, and e is the radiative kernel error. Individual rapid adjustments (A_x) are computed as:

223

224
$$A_x = \frac{\delta R}{\delta x} dx \tag{2}$$

225 where $\frac{\delta R}{\delta x}$ is the radiative kernel, a diagnostic tool typically computed with an offline version of a GCM radiative
 226 transfer model that is initialized with climatological base state data and dx is the climate response of atmospheric
 227 state variable x , diagnosed directly from each model. Cloud rapid adjustments (A_c) are estimated by diagnosing
 228 cloud radiative forcing from model flux diagnostics and correcting for cloud masking using the kernel-derived
 229 non-cloud adjustments and IRF, following common practice (e.g. (Soden et al., 2008;Smith et al., 2018)),
 230 whereby:

231
$$A_c = (ERF - ERF^{clr}) - (IRF - IRF^{clr}) - \sum_{x=[T,ts,q,a]} (A_x - A_x^{clr}) \tag{3}$$

232 For the calculation of the IRF (for aerosols this is the direct effect) here, the clear-sky IRF (IRF^{clr}) is estimated
 233 as the difference between clear-sky ERF (ERF^{clr}) and the sum of kernel-derived clear-sky rapid adjustments
 234 (A_x^{clr}). Since estimates of A_c are dependent on IRF, the same differencing method cannot be used to estimate IRF
 235 under all-sky conditions without special diagnostics (in particular the International Satellite Cloud Climatology
 236 Project diagnostics (ISCCP) diagnostics) not widely available in the AerChemMIP archive. Instead, for the
 237 calculations presented here all-sky IRF is computed by scaling IRF^{clr} by a species-specific factor to account for
 238 cloud masking (Soden et al. 2008).

239 Kernels are available from several sources, and for this analysis we used kernels from CESM, (Pendergrass et al.,
 240 2018), GFDL (Soden et al., 2008), HadGEM3, (Smith et al., 2020b), and ECHAM6 (Block and Mauritsen, 2013)
 241 and took the mean from the four kernels for each model. Overall the individual kernels produced very similar
 242 results for each model, as reported in Smith et al. (2018).

243 **3.3 Calculation of ERF using aerosol-free radiative fluxes**

244 To understand the contributions of various processes to the overall ERF we can attempt to separate the ERF that
 245 is due to direct radiative forcing from that due to the effects of clouds. Greenhouse gases and aerosols can alter
 246 the thermal structure of the atmosphere and hence cloud thermodynamics (the semi-direct effect, (Ackerman et
 247 al., 2000)), and aerosols can act via microphysical effects (e.g. increasing the number of condensation nuclei and
 248 decreasing the effective radii of cloud droplets, referred to as the aerosol cloud albedo effect and the cloud lifetime
 249 effect (Twomey, 1974;Albrecht, 1989;Pincus and Baker, 1994). Following the method of Ghan (2013) the
 250 contribution of the aerosol-radiation interactions to the ERF can be distinguished from that of the aerosol-cloud
 251 interactions by using a ‘double-call’ method. This means that the model radiative flux diagnostics are calculated
 252 a second time but ignoring the scattering and absorption by the aerosol – referred to in the equations below with
 253 the subscript ‘af’. The other effects of the aerosol on the atmosphere (i.e. cloud changes, stability changes,
 254 dynamics changes) will still be present, however. The IRF_{af} as defined here is the direct radiative forcing from
 255 the aerosol, due to scattering and absorption of radiation. The cloud radiative forcing (ERF_{af}) due to the aerosol-
 256 cloud interactions is then obtained by using the difference between the aerosol-free all-sky fluxes and the aerosol-
 257 free clear-sky fluxes, which isolates the cloud effects (see Eqns. 4-6, where Eqn. (6) is included for completeness).
 258 The ERF_{af} may include non-cloud rapid adjustments in cloudy regions of the atmosphere. The final term is the
 259 ERF as calculated from fluxes with neither clouds nor aerosols (ERF_{cs,af}).

260 The ERFs are calculated in the same way as for the all-sky ERF described in Section 3.1, except that the all-sky
 261 radiative flux diagnostics are replaced by the relevant aerosol-free fluxes for both the clear-sky and all-sky cases.

262

263 $IRF_{ari} = (ERF - ERF_{af})$ (4)

264 $ERF_{afi} = ERF_{af} - ERF_{cs,af}$ (5)

265 $ERF_{cs,af} = ERF_{cs,af}$ (6)

266 Separating the IRF in Eqn. (1) into aerosols and greenhouse gas contributions, $IRF = IRF_{aer} + IRF_{GHG}$, we can re-
 267 write Eqns. 4-6.

268 $IRF_{ari} = IRF_{aer}$ (7)

269 $ERF_{afi} = A_C + \sum_{x=[T,ts,q,a]} (A_x - A_x^{clr}) + (IRF_{GHG} - IRF_{GHG}^{clr})$ (8)

270 $ERF_{cs,af} = \sum_{x=[T,ts,q,a]} A_x^{clr} + IRF_{GHG}^{clr}$ (9)

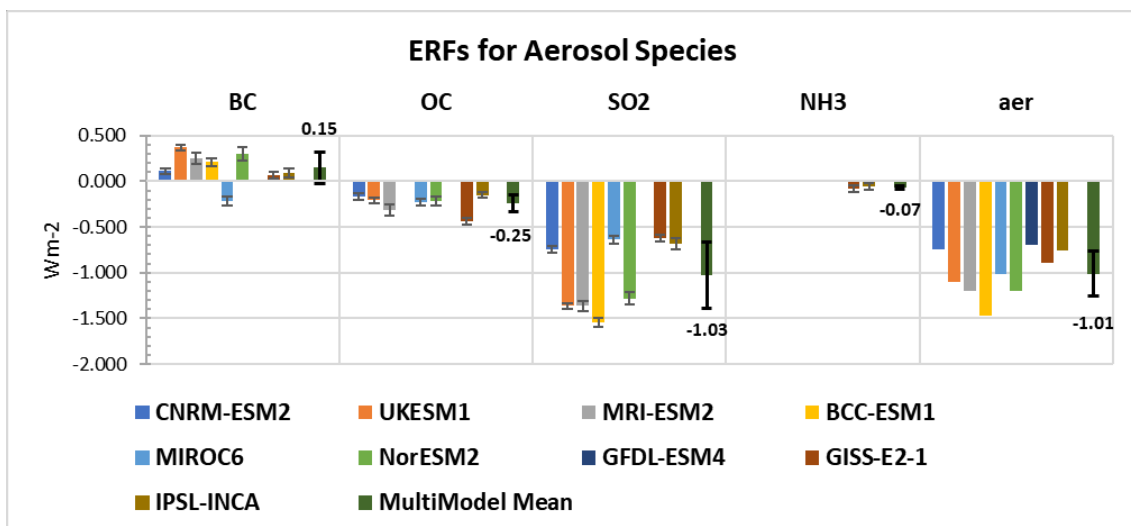
271 So ERF_{afi} is equivalent to A_C in Eqn. (3) with extra terms to account for the all-sky - clear-sky difference in the
 272 non-cloud adjustments and all-sky - clear-sky difference in any greenhouse gas IRF. With no greenhouse gas
 273 changes $ERF_{cs,af}$ is the total clear-sky non-cloud adjustment. Ghan (2013) attributes this mostly to the surface
 274 albedo change A_{α}^{clr} , however the kernel analysis shows other non-cloud adjustments are larger (Table S4). For
 275 greenhouse gases $ERF_{cs,af}$ is the total clear-sky ERF. Assuming the non-cloud adjustments are small apart from
 276 T_{strat} (Table S4), $ERF_{cs,af}$ is approximately $SARF_{GHG}^{clr}$. The $SARF_{GHG}^{clr}$ is expected to be an overestimate of
 277 $SARF_{GHG}$ by 10-40% due to cloud masking (Myhre and Stordal 1997). Thus for greenhouse gases the ERF_{afi} will
 278 be a combination of the cloud adjustment and cloud-masking.

279 **4. Results**

280 **4.1 Aerosols and precursors**

281 **4.1.1 Inter-model Variability**

282 The ERFs are calculated as described in Section 3.1, and the summary chart of the ERFs is shown in Fig. 1 for
 283 those models with available results – it should be noted that not all models ran all the experiments. The multimodel
 284 mean is shown as a separate bar in Fig. 1, with the value given and the standard error indicated with error bars. A
 285 table of the individual values for each model and the multimodel mean are included Table S2 in the supplementary
 286 materials.



287 **Fig. 1 Aerosol ERFs for the models with the available diagnostics for the aerosol species experiments, with interannual**
288 **variability represented by error bars showing the standard error. The piClim-aer experiments include the BC, OC**
289 **SO₂ aerosols, and for GISS-E2-1 and IPSL-INCA NH₃ aerosols are also included. The multimodel mean is shown with**
290 **the mean value and error bars indicating the standard deviation.**

291 For the piClim-BC results, the range of values is from -0.21 Wm^{-2} to 0.37 Wm^{-2} , while the MIROC6 model has a
292 negative ERF for BC, contrasting with the positive values from the other models - see further discussion on this
293 in Section 4.1.2.

294 The experiments for the OC (organic carbon) have a range from -0.44 Wm^{-2} to -0.15 Wm^{-2} , and the variability
295 between the models is much less than for the other experiments. The calculated ERFs for the SO₂ experiment
296 show a variation from -1.54 Wm^{-2} to -0.62 Wm^{-2} , with CNRM-ESM2-1, MIROC6, IPSL-INCA and GISS-E2-1
297 at the lower end of the range. These models show a smaller rapid adjustment to clouds which would account for
298 this (see fig S1); also note that CNRM-ESM2-1 does not include aerosol effects apart from the cloud-albedo
299 effect. The two models with results for the NH₃ (GISS-E2-1 and IPSL-INCA) experiment have ERFs of -0.08 and
300 -0.06 Wm^{-2} respectively.

301 The piClim-aer experiment which uses the 2014 values of aerosol precursors and PI (pre-industrial) values for
302 CH₄, N₂O and ozone precursors shows a range from -1.47 Wm^{-2} to -0.7 Wm^{-2} among the models, making it
303 difficult to narrow the range of uncertainty of aerosols from global models. However, the range in the CMIP6
304 models is consistent with that reported in Bellouin et al. (2019), who suggest a probable range of -1.60 to -0.65
305 Wm^{-2} for the total aerosol ERF, and compares well with the range of -1.37 to -0.63 Wm^{-2} for the set of piClim-
306 aer experiments considered in (Smith et al., 2020a) as part of the RFMIP project. In general, the sum of the ERFs
307 from the individual BC, OC and SO₂ experiments does not equal the piClim-aer experiment, due to non-linearity
308 in the aerosol-cloud interactions, particularly since the aerosol perturbation is added to the relatively pristine pre-
309 industrial atmosphere. In the case of GISS and IPSL-INCA, and GFDL-ESM4 the models also include nitrate
310 aerosols.

311 The issue of the effect of perturbing the pre-industrial atmosphere with the aerosol changes is examined in more
312 detail in the Supplementary material (see section S6) for NorESM2, where a sensitivity analysis was carried out.
313 This analysis does not repeat the AerChemMIP experiments with the perturbation in a present-day atmosphere
314 but examines the effect of adding the SO₂ and combined aerosol perturbation to an already polluted present day
315 atmosphere. In this simplified sensitivity study the differences are 13% for the SO₂ experiment, and 20% for the
316 combined aerosol experiment. However, it should be borne in mind that this is for a specific model, and the
317 perturbed experiment still has the 1850 climate conditions.

318 The ERF_{ts} is a simplified method for corrections of land surface warming in fixed sea surface temperature
319 simulations which in addition to land surface changes leads to changes in land surface albedo changes,
320 tropospheric temperature, water vapor and cloud changes (Smith et al., 2020a; Tang et al., 2019).

321 The ERF_{ts} for the models where the land surface temperature adjustment is removed are also included in
322 Supplemental Tables S2 and S3, for comparison with the standard ERF. In general, the difference between the
323 two values is small, of the order of 5 -10%.

324

325 **4.1.2 Breakdown of the ERF into atmospheric adjustments and IRF**

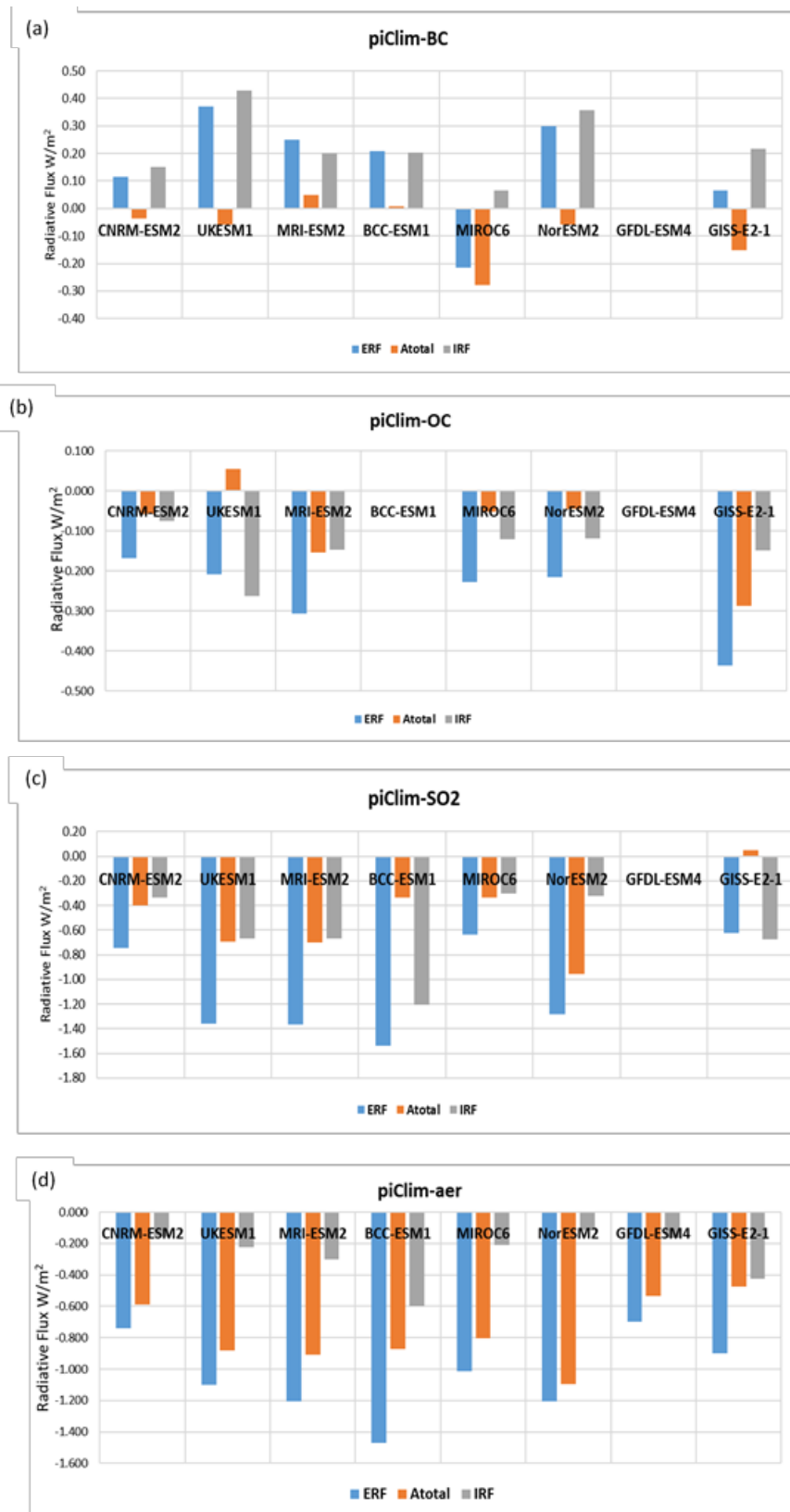


Figure 2 Breakdown of the ERFs into the atmospheric rapid adjustments (Atotal) and IRF (instantaneous radiative forcing) for the aerosols. (a) piClim-BC experiment, (b) piClim-SO2 experiment, (c) piClim-OC experiment, (d) piClim-aer experiment

327 The results in Fig. 2 show the ERF as calculated from the radiative fluxes in the fixed SST experiments (Section
 328 3.1), the total of the atmospheric adjustments, A_{total} , described in Section 3.2 (where $A_{\text{total}} = A_T + A_{\text{ts}} + A_q + A_a +$
 329 A_c c.f. eqn. 1), and the instantaneous radiative forcing (IRF).
 330 The sum of the IRF and the atmospheric adjustments should equal the overall ERF, however as the calculation of
 331 the IRF depends upon an empirical factor for cloud masking to find the all-sky IRF from the clear-sky IRF (see
 332 Section 3.2) the sum of the IRF and the A_{total} will not necessarily equal the ERF as calculated directly from the
 333 model radiative flux diagnostics. However, in general the difference is less than 3%, suggesting that the
 334 approximation used in the calculation of the IRF is reasonable. Using the kernel method described above it is
 335 important to note that the IRF calculated here accounts for the presence of the clouds but does not include cloud
 336 changes such as the cloud albedo effect.
 337 The models show a variability in the IRF for SO_2 , (Fig. 2c) with a range of -0.3 Wm^{-2} to -1.2 Wm^{-2} with the BCC-
 338 ESM1 model being the outlier, having the largest overall ERF. The OC experiments (Fig. 2b) range from -0.08
 339 Wm^{-2} to -0.26 Wm^{-2} , with a range for BC of 0.07 Wm^{-2} to 0.43 Wm^{-2} (Fig. 2a). In MIROC6 the treatment of BC
 340 (Takemura & Suzuki 2019; Suzuki & Takemura 2019) leads to faster wet removal of BC and hence a lower IRF.
 341 For the combined aerosols (Fig 2d) the range is from -0.1 Wm^{-2} to -0.6 Wm^{-2} .
 342 There are significant differences between the models in the A_{total} for SO_2 ; these range from 0.05 Wm^{-2} to -1.0 Wm^{-2}
 343 2 , where the differences are dominated by the cloud adjustments which here include the cloud albedo effect as part
 344 of the adjustment (see Fig S3 for breakdowns of the atmospheric adjustments for all models). The adjustments to
 345 BC are vary in sign and magnitude, with the MRI-ESM2 and BCC-ESM1 models having a slight positive
 346 adjustment. The overall model mean has a weaker negative adjustment to that reported by (Stjern et al.,
 347 2017; Samset et al., 2016; Smith et al., 2018). The MIROC6 model has a large negative adjustment which is large

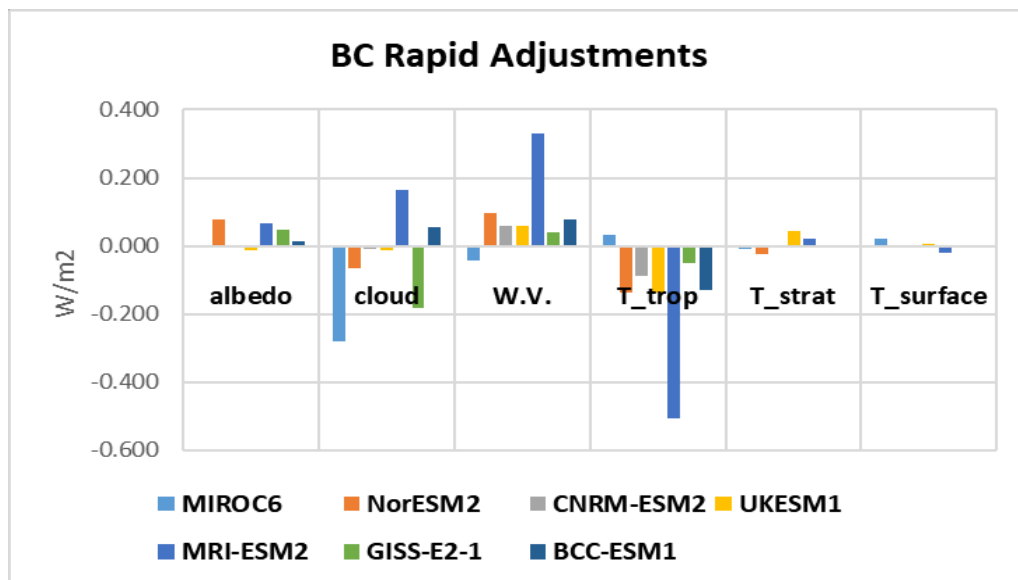


Figure 3 Breakdown of the atmospheric adjustments (albedo, cloud, water vapour, troposphere temperature, stratosphere temperature and surface temperature) for the piClim-BC experiments, showing the variability between models.

348 enough to lead to an overall negative ERF. We explore the contribution of the individual adjustments to BC in
349 more detail in Fig. 3.

350 Examining the breakdown of the rapid adjustments for the piClim-BC experiments (Fig. 3) we see considerable
351 variability in the relative importance of the rapid adjustments; the cloud adjustment dominates in MIROC6,
352 consistent with the increase in low clouds reported for this model, and the treatment of BC as ice nuclei causes
353 the large negative cloud adjustment here (Takemura and Suzuki, 2019; Suzuki and Takemura, 2019). The GISS-
354 E2-1 model also has a strong cloud rapid adjustment, but the larger positive value of the IRF leads to an overall
355 positive ERF for this model. With the exception of MIROC6 the negative tropospheric temperature adjustment is
356 balanced by the water vapour (specific humidity) adjustment, although the magnitude of these adjustments for
357 MRI-ESM2 is at least twice that for the other two models. The interaction of BC with clouds in the MRI-ESM2
358 model is discussed in detail in Oshima et al. (2020), in particular the impact of BC on ice nucleation in high
359 clouds. The larger surface albedo adjustment for both NorESM2 and MRI-ESM2 is most likely due to the
360 representation of deposition of BC on snow and ice in these models (Oshima et al., 2020).

361 The piClim-aer experiments (Fig. 1d) show all models have a negative A_{total} , covering a range from -0.47 to -1.1
362 Wm^{-2} . Overall, the cloud rapid adjustments dominate for the piClim-aer experiments, with a contribution ranging
363 from -0.45 to -1.1 Wm^{-2} (See fig S1). Smith et al. (2020) also recently diagnosed forcing and adjustments in a
364 similar subset of CMIP6 models for the piClim-aer experiment as part of the Radiative Forcing Model
365 Intercomparison Project (RFMIP) efforts. While they also diagnosed IRF as a residual calculation between ERF
366 and the sum of rapid adjustments, they estimated cloud adjustments using a modified version of the APRP method
367 instead of radiative kernels. In their approach, the cloud albedo effect (i.e. Twomey Effect) is considered part of
368 the IRF, whereas in the traditional kernel decomposition, it is considered a cloud adjustment. Table S5 compares
369 the two sets of estimates, highlighting the IRF and total cloud adjustment exhibit a near equal absolute difference
370 between the two studies and the sum of IRF and total cloud adjustment are in close agreement (Mean % difference
371 $\sim 1.0\%$ for this subset of models). This indicates the classification of the first indirect effect is the only noticeable
372 difference between the two approaches.

373 The breakdown of the rapid adjustments for all the models are included in supplementary Figure S1, showing the
374 contributions from each type of rapid adjustment for all the experiments for which we have the relevant
375 diagnostics.

376

377 **4.1.3 Radiation and Cloud interactions**

378 The second method of breaking down the ERF to constituents is described in Section 3.3, (the Ghan method), the
379 results from which are shown in Table 3. The detailed ERF results for MRI-ESM2 are summarized in Oshima et
380 al. (2020), and for UKESM1 in O'Connor et al. (2020a). Only four of the models under consideration have so far
381 produced the necessary diagnostics for this calculation, and the results are presented in Table 3. For the
382 experiments on aerosols (aer, BC, SO_2 , OC) the $\text{ERF}_{\text{cs,af}}$ (non-cloud adjustments) contribution is small, and the
383 ERF is largely a combination of the direct radiative effect IRF_{ari} , and the cloud radiative effect, ERF_{aci} . The
384 IRF_{ari} is the direct effect of the aerosol due to scattering and absorption, while the ERF_{aci} is the contribution
385 from the aerosol-cloud interactions and is approximately equal to the rapid adjustments due to clouds (A_c see
386 Section 3.2).

387
388
389
390

Table 3 Results for IRFari, ERFaci and ERFcs,af for aerosol experiments from several models

	UKESM1			CNRM-ESM2			NorESM2			MRI-ESM2		
	IRFari	ERFcs,af	ERFaci	IRFari	ERFcs,af	ERFaci	IRFari	ERFcs,af	ERFaci	IRFari	ERFcs,af	ERFaci
aer	-0.15	0.05	-1.00	-0.21	0.08	-0.61	0.03	-0.03	-1.21	-0.32	0.09	-0.98
BC	0.37	0.001	-0.005	0.13	0.01	-0.03	0.35	0.07	-0.12	0.26	0.08	-0.09
OC	-0.15	-0.01	-0.07	-0.07	0.04	-0.14	-0.07	0.02	-0.16	-0.07	-0.05	-0.21
SO2	-0.49	0.03	-0.91	-0.29	0.08	-0.53	-0.19	-0.09	-1.01	-0.48	0.05	-0.93

391
392
393
394
395
396
397
398
399
400
401
402

For the BC experiment the contribution of the aerosol-cloud interaction has a strong contribution to the overall ERF, except in the case of UKESM1 where it is much weaker; this may be due to the strong SW and LW cloud adjustments in this model cancelling out (O'Connor et al., 2020; Johnson et al., 2019). The SO₂ experiment shows a large cloud radiative effect, in fact the ERFaci is mostly double the IRFari in all the models, due to the large effect on clouds of SO₂ and sulfates through the indirect effects. For the OC experiments the ERFaci to IRFari comparison is mixed, with the ERFaci general half or less the IRFari, except in the case of UKESM1, where this ratio is reversed.

The IRFari are compared with the IRF calculated via the kernel analysis (Section 3.2) where the relevant model results are available. These are shown in fig S2(a), the agreement is generally good giving confidence in the kernel analysis. Similarly ERFaci compares well with the cloud adjustment Ac (fig S2(b)).

4.1.4 AOD Forcing Efficiencies

In order to break down the contributions of the constituent aerosol species to the overall aerosol ERF, we use the AOD (aerosol optical depth) as a forcing efficiency metric for each of the species, and use this to assess their contributions to the overall ERF. Not all models had diagnostics available for the AOD for the individual species, so the analysis uses a subset of the models.

By looking at the single species piClim-BC, piClim-OC and piClim-SO₂ experiments we can find the change in the AOD for the individual species (e.g. ΔAOD for BC for the piClim-BC experiment), and use this to scale the piClim-BC ERF by the AOD change. This assumes that the ERF in the single-species experiment is wholly due to the change in that species as indicated by the AOD, an assumption which is explored in the Supplementary material in Section S4. Table 5 shows the AOD forcing efficiency for the piClim-BC, piClim-SO₂ and piClim-OC experiments for each of the five models which had the relevant optical depth diagnostics available.

414

415 **Table 4 Values of ERF, Δ AOD and ERF/AOD for aerosol experiments for CNRM-ESM2-, MIROC6, Nor-ESM2, GISS-**
 416 **E2-1 and MRI-ESM2 models.**

BC Exp	BC ERF	Change in BC AOD	ERF/AOD
CNRM-ESM2	0.114	0.0015	77.64
MIROC6	-0.214	0.0006	-339.38
NorESM2	0.300	0.0019	159.75
GISS-E2-1	0.065	0.002	31.65
MRI-ESM2	0.251	0.0073	34.22
OC Exp	OC ERF	Change in OA AOD	ERF/AOD
CNRM-ESM2	-0.169	0.0030	-57.20
MIROC6	-0.227	0.0065	-35.05
NorESM2	-0.215	0.0053	-40.57
GISS-E2-1	-0.438	0.0041	-107.16
MRI-ESM2	-0.317	0.0034	-94.39
SO2 Exp	SO2 ERF	Change in SO4 AOD	ERF/AOD
CNRM-ESM2	-0.746	0.0118	-63.22
MIROC6	-0.637	0.0152	-41.91
NorESM2	-1.281	0.0099	-129.24
GISS-E2-1	-0.622	0.0308	-20.22
MRI-ESM2	-1.365	0.0279	-49.08

417 The MIROC6 model results in a negative scaling for BC due to the negative ERF for this experiment for this
 418 model (Takemura & Suzuki 2019; Suzuki & Takemura 2019) (see Section 4.1.1). The change in the BC AOD is
 419 similar for CNRM-ESM2-1 and Nor-ESM2, and the scale factors reflect the differences in the ERF. The scaling
 420 for the SO4 in the NorESM2 experiment is twice that of the other models, suggesting a larger impact of the SO4
 421 AOD on the ERF in this model. These values differ somewhat from those found in Myhre et al. (2013b) where
 422 they examined the radiative forcing normalised to the AOD using models in the AeroCom Phase II experiments.
 423 They found values for sulfate ranging from -8 Wm^{-2} to -21 Wm^{-2} per unit AOD, much weaker than those in our
 424 results. However, it is important to note that in the AeroCom Phase II experiments the cloud and cloud optical
 425 properties are identical between their control and perturbed runs, so no aerosol indirect effects are included, nor

426 is any rapid adjustments (IRFari in Eqn. 4). For the BC experiment their values range from 84 Wm^{-2} to 216 Wm^{-2}
 427 2 per unit AOD, broadly similar to the results presented here (with the exception of the negative MIROC6 result).
 428 Their results for OA (organic aerosols) which include fossil fuel and biofuel emissions have values ranging from
 429 -10 Wm^{-2} to -26 Wm^{-2} per unit AOD, weaker than our values for the piClim-OC experiments which range from -
 430 35 Wm^{-2} to -107 Wm^{-2} per unit AOD but include the cloud indirect effects here.

431 The sum of the individual AODs from BC, SO_4 , OA, dust and sea salt gives the total aerosol AOD in the piClim-
 432 aer experiment, where the various aerosols were combined. We can then use the AOD for each aerosol in the
 433 piClim-aer experiment and the forcing efficiency above to find the contribution of the individual aerosol to the
 434 overall change in ERF, providing an approximate estimate of the relative contribution of each aerosol to the overall
 435 ERF. In Fig. 4 the relative contributions to the ERF from black carbon (BC), organic aerosols (OA) and sulfate
 436 (SO_4) are shown for three of the models. The sum of the ERFs from the individual species is also compared to the
 437 ERF calculated from the piClim-aer experiment (NB the sea salt and dust contributions to the ERF are less than

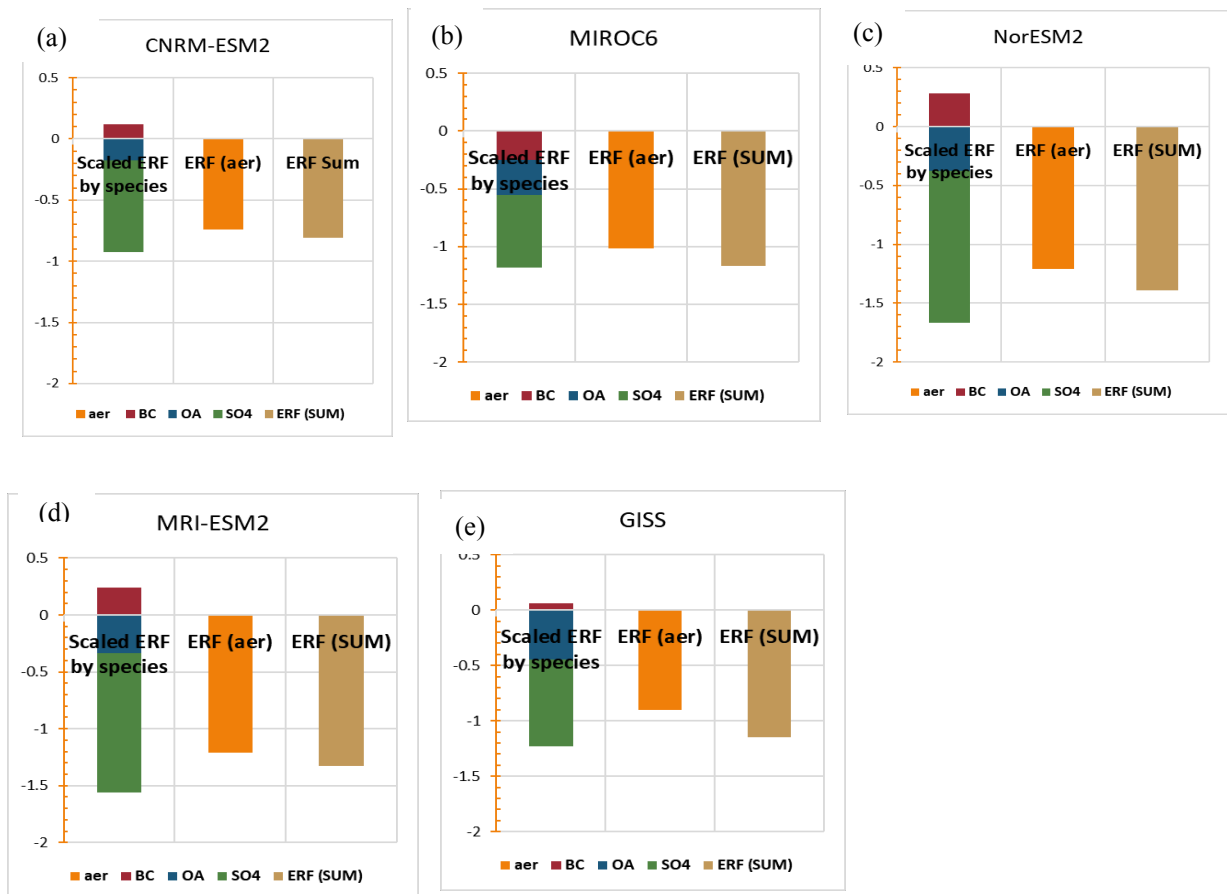


Fig. 4 The contributions to the ERF for piClim-aer from the individual species, the sum of the scaled ERFs and the ERF calculated directly from the piClim-aer experiment for five of the models.

438 1%, and not shown in this figure for clarity - the ERF/AOD forcing efficiency for these is presented in (Thornhill
 439 et al., 2020). There is considerable variation in the ERF for the piClim-aer experiments between models (see
 440 Section 4.1), but from this analysis the SO_4 is the largest contributor in all cases, although in the case of the
 441 MIROC6 model its relative importance is reduced. The positive ERF contribution from the BC tends to partly

442 offset the negative ERF from the OA and SO₄, except in the MIROC6 model, where the BC has a negative
443 contribution to the ERF.

444 The difference between the calculated ERF from the sum of the scaled ERFs is a result of the non-linearity of the
445 aerosol-cloud interactions, a factor which is increased because the aerosols are added to the pre-industrial
446 atmosphere. However, using the IRFari instead of the total ERF to calculate the forcing efficiency and using the
447 same method also results in a difference between the total IRFari derived from the scaled individual experiments
448 and the IRFari for the combined aerosol experiment, suggesting that the difference is not simply a result of the
449 aerosol-cloud interactions.

450 Using the burden as a scaling factor following the same analysis as described for the AOD results in a largely
451 similar result for the scaling factor, although interestingly the burden scaling for SO₂ in the Nor-ESM2 model is
452 similar to the other models (see Table S6 for the burden forcing efficiency).

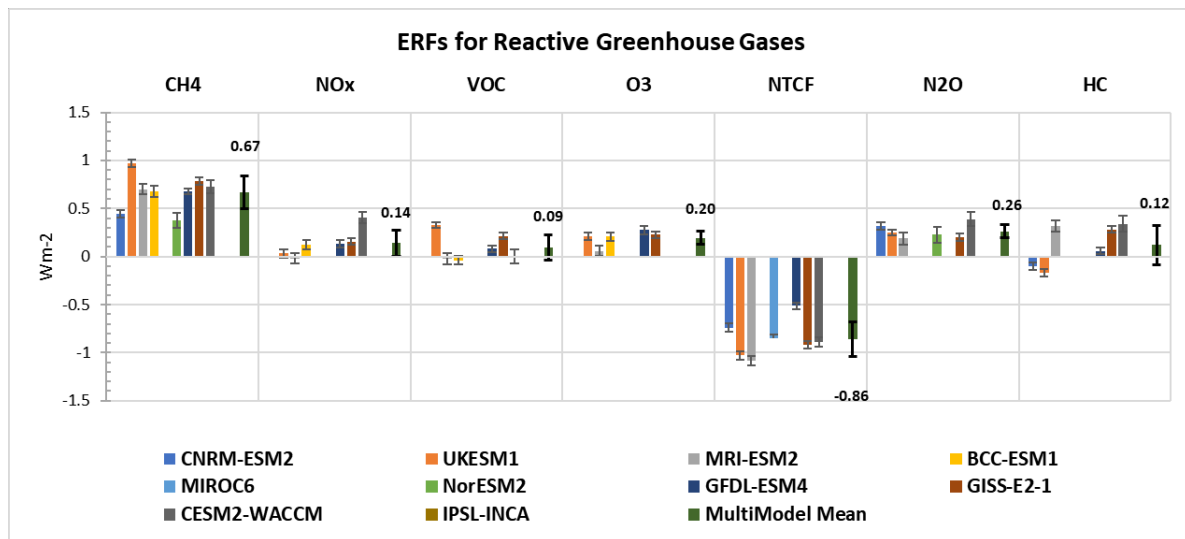
453

454 **4.2 Reactive greenhouse gases**

455 The different Earth system models include different degrees of complexity in their chemistry, so their responses
456 to changes in reactive gas concentrations or emissions differ. NorESM2 has no atmospheric chemistry, so there is
457 no change to ozone (tropospheric or stratosphere) or to aerosol oxidation following changes in methane or N₂O
458 concentrations. CNRM-ESM2-1 includes stratospheric ozone chemistry, but no non-methane hydrocarbon
459 chemistry and so ozone is prescribed below 560 hPa. There are no effects of chemistry on aerosol oxidation. BCC-
460 ESM1 includes tropospheric chemistry, but not stratospheric chemistry. Stratospheric concentrations are relaxed
461 towards climatological values. UKESM1, GFDL-ESM4, CESM2-WACCM, GISS-E2 and MRI-ESM2 all include
462 tropospheric and stratospheric ozone chemistry as well as changes to aerosol oxidation rates. The ERFs calculated
463 for the reactive gases for several models are shown in Fig. 5, with the multi-model means given in Supplementary
464 Table S3.

465 The contributions from gas-phase and aerosol changes to the ERF can be pulled apart to some extent by using the
466 clear-sky and aerosol-free radiation diagnostics (Table 5). The direct aerosol forcing (IRFari) is diagnosed as for
467 the aerosol experiments (section 3.3). The diagnosed changes in aerosol mass are shown in Table S8. GFDL-
468 ESM4 and GISS-ES-1 include nitrate aerosol and show expected responses from NO_x emissions (including O₃
469 experiment). CESM2-WACCM shows an increase in secondary organic aerosol from VOC emissions. Sulphate
470 responses are generally inconsistent across the models. There seems little correlation between aerosol mass
471 changes and diagnosed IRFari.

472 For gas-phase experiments the diagnosed cloud interactions (ERFaf-ERFcs,af) comprise the ERFaci from effects
473 on aerosol chemistry (as in section 3.3) but also any cloud adjustments and effects of cloud masking on the gas-
474 phase forcing (Eqn. 8). The clear-sky aerosol-free diagnostic (ERFcs,af) is an indication of the greenhouse gas
475 forcing however this will be an over-estimate as it neglects cloud masking effects (section 3.3).



477 **Fig. 5** Reactive gas ERFs for the models with the available diagnostics for the reactive gas experiments with interannual
 478 variability represented by error bars showing the standard error. The multimodel mean is shown with the mean value
 479 and error bars indicating the standard deviation.

480 4.2.1 ERF vs SARF

481 For the reactive greenhouse gases the kernel analysis is used to break down the ERF into the stratospherically
 482 adjusted radiative forcing (SARF), which is calculated using the IRF from the kernel analysis (Section 3.2) and
 483 the stratospheric temperature adjustment (A_{t_strat}) ($SARF = IRF + A_{t_strat}$), and the tropospheric adjustments, A_{t_trop} ,
 484 which is the sum of the tropospheric atmospheric adjustments. These quantities are plotted in Fig. 6.

485 For methane the ERFs are largest for those models that include tropospheric ozone chemistry reflecting the
 486 increased forcing from ozone production, see section 4.2.2. The analytic calculation for CH_4 -only based on
 487 Etminan et al. (2016) gives a SARF of 0.56 Wm^{-2} . The tropospheric adjustments are negative for all models except
 488 UKESM1 (Fig 6). The negative cloud adjustment comes from an increase in the LW emissions, possibly due to
 489 less high cloud. In UKESM1 (O'Connor et al., 2020b) show that methane decreases sulfate new particle
 490 formation, thus reducing cloud albedo and hence a positive cloud adjustment in that model.

491 For N_2O results are available for models CNRM-ESM2, NorESM2, MRI-ESM2, and GISS-E2 (the analytic N_2O -
 492 only calculation gives a SARF of 0.17 Wm^{-2}). There appears little net rapid adjustment to N_2O apart from CESM2-
 493 WACCM. Note that due to the method of calculating the all-sky IRF (section 3.2), the IRF and the adjustment
 494 terms do not sum to give the ERF.

495 The models respond very differently to changes in halocarbons. The expected halocarbon-only SARF is $+0.30$
 496 Wm^{-2} depending on exact speciation used in the model (WMO 2018). For CNRM-ESM2, UKESM1 and GFDL-
 497 ESM4 the ERFs are negative or only slightly positive (see also Morgenstern et al. (2020)), whereas for GISS-E2-1
 498 and MRI-ESM2 the ERFs and SARF are both strongly positive. The differences in stratospheric ozone destruction
 499 in these models can partially explain the inter-model differences (section 4.2.2).

500

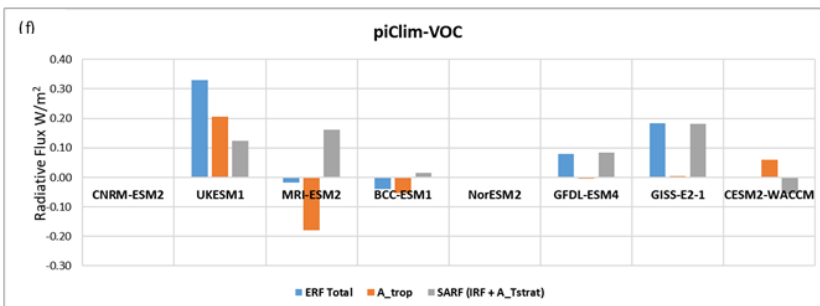
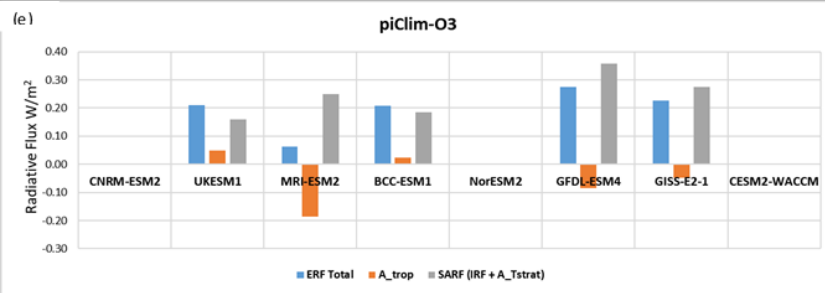
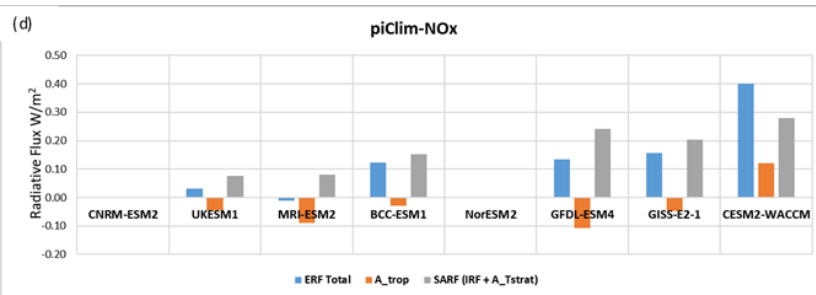
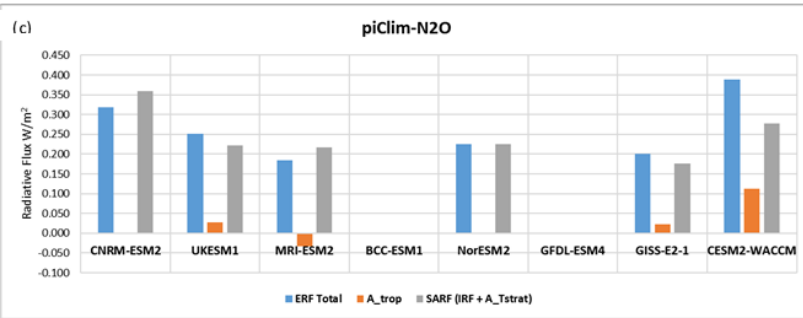
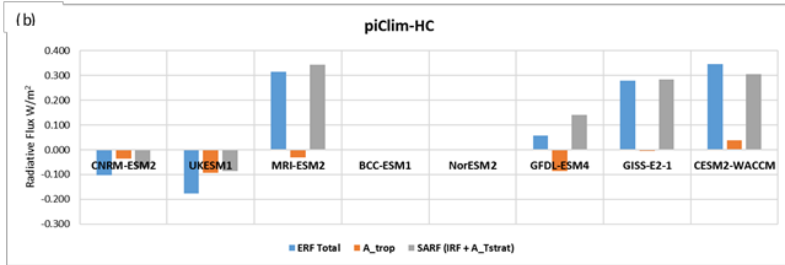
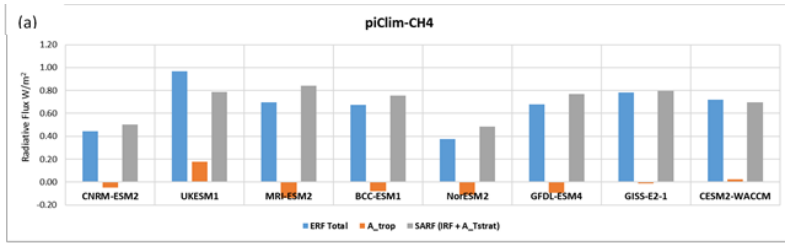


Figure 6 Breakdown of the ERF into SARF ($IRF + A_{t, strat}$) and tropospheric rapid adjustments (A_{trop}) for the chemically reactive species (a) for piClim-CH₄ experiments, (b) for piClim-HC experiments, (c) for piClim-N₂O experiments, (d) for piClim-NO_x experiments, (e) for piClim-O₃ experiments, and (f) for piClim-VOC experiments

502

503

504 **Table 5 Calculations of IRFari, ERFaci (cloud) and ERFcs,af for the chemically reactive species**

	UKESM			GFDL-ESM4			CNRM-ESM2			NorESM2			MRI-ESM2		
	IRFari	ERFcs,af	cloud	IRFari	ERFcs,af	cloud	IRFari	ERFcs,af	cloud	IRFari	ERFcs,af	cloud	IRFari	ERFcs,af	cloud
CH ₄	-0.01	0.86	0.12	-0.01	0.91	-0.22	0.00	0.56	-0.12	-0.01	0.48	-0.10	0.00	0.91	-0.21
HC	-0.02	0.02	-0.18	-0.02	0.22	-0.14	-0.01	-0.02	-0.08				-0.02	0.50	-0.17
N ₂ O	-0.01	0.26	0.01				0.00	0.41	-0.09	-0.01	0.24	-0.00	-0.00	0.23	-0.03
O ₃	-0.02	0.16	0.07	-0.04	0.49	-0.18							-0.00	0.24	-0.18
NO _x	-0.03	0.10	-0.05	-0.02	0.25	-0.09							-0.01	0.03	-0.04
VOC	0.00	0.13	0.20	-0.02	0.18	-0.08							0.004	0.17	-0.2

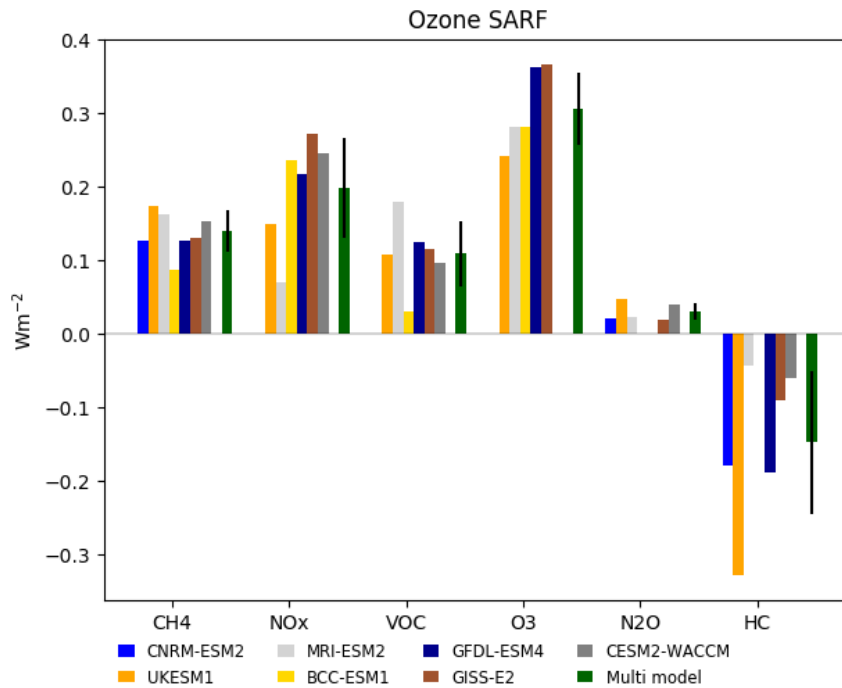
505

506 **4.2.2 Ozone changes**

507 The ozone radiative forcing is diagnosed using a kernel to scale the 3D ozone changes based on Skeie et al. (2020).
508 This kernel includes stratospheric temperature adjustment, but not tropospheric adjustments so gives a SARF.
509 These are shown in Fig. 7. Corresponding changes in the tropospheric and stratospheric ozone columns are shown
510 in figure S5, Increased CH₄ concentrations give a SARF for ozone produced by methane of $0.14 \pm 0.03 \text{ W m}^{-2}$,
511 anthropogenic NO_x emissions and VOC (including CO) emissions give SARFs of 0.20 ± 0.07 and $0.11 \pm 0.04 \text{ W m}^{-2}$
512 respectively. The O₃ experiment comprised both NO_x and VOC emission changes. The SARF in this experiment
513 ($0.31 \pm 0.05 \text{ W m}^{-2}$) is close to the sum of the NO_x and VOC experiments ($0.30 \pm 0.05 \text{ W m}^{-2}$ for the same set of
514 models) showing little non-linearity in the chemistry (Stevenson et al., 2013).

515 There is a larger variation across models in the stratospheric ozone depletion from halocarbons ($-0.15 \pm 0.10 \text{ W m}^{-2}$)
516 with UKESM1 having noticeably larger depletion as seen in Keeble et al. (2020) giving a SARF of -0.33 W m^{-2} .
517 N₂O causes some stratospheric ozone depletion in these models, mainly in the tropical upper stratosphere where
518 depletion causes a positive forcing (Skeie et al., 2020), and increases tropospheric ozone (Fig. S6) giving a small
519 net positive SARF ($0.03 \pm 0.01 \text{ W m}^{-2}$).

520



521

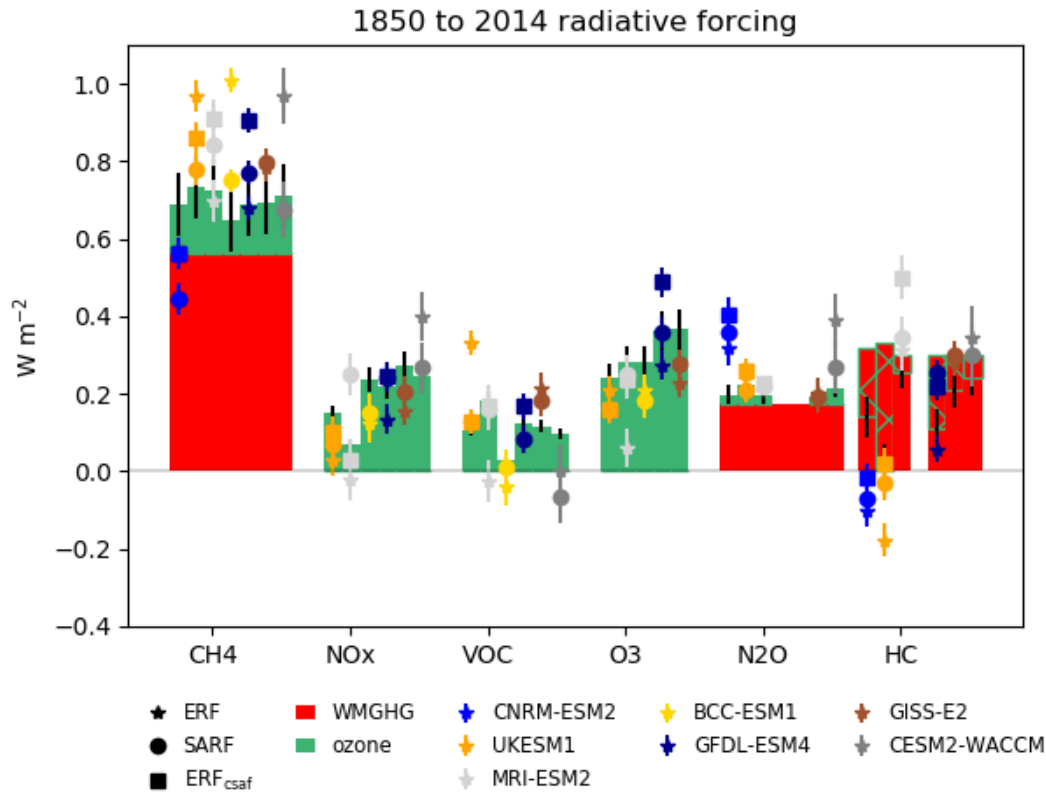
522 **Fig. 7 Changes in ozone stratospheric-temperature adjusted radiative forcing (SARF) for each experiment, diagnosed**
 523 **using kernels (see text). . Uncertainties for the multi model means are standard deviations across models.**

524 **Methane oxidation also leads to water vapour production. Figure S6 shows increases in the stratosphere for the piClim-**
 525 **CH₄ of up to 20% . The kernel analysis however finds very low radiative forcing associated with this increase**
 526 **(-0.002±0.003 Wm⁻²).**

527 4.2.3 Comparison with greenhouse gas forcings

528 The ERFs, ERFcs,af and SARFs diagnosed for the greenhouse gas changes (Fig. 6, Table 5) are compared with
 529 the expected greenhouse gas SARFs in Fig. 8. The expected SARFs from the well-mixed gases are given by
 530 Etminan et al. (2016) for CH₄ and N₂O, and by WMO (2018) for the halocarbons (the halocarbon changes are
 531 slightly different in each model). The expected SARFs from ozone changes are from Fig. 7.

532 For methane the ERFs are typically higher than the expected GHG SARF (except for CNRM-ESM2).The
 533 diagnosed ERFcs,af and SARF agree better with the expected SARF in UKESM1, BCC-ESM1 and CESM2-
 534 WACCM, but not in other models. For N₂O the modelled ERF is larger than the expected SARF for CNRM-
 535 ESM2-1 and CESM2-WACCM, this is explained by the rapid adjustments for CESM2-WACCM, but not for
 536 CNRM-ESM2. For halocarbons the stratospheric ozone depletion offsets the direct SARF and accounts for much
 537 of the spread in the model SARF, although the CNRM-ESM2-1 ERF and SARF is lower than expected. The
 538 modelled HC ERF for UKESM1 is strongly negative due to increased aerosol cloud interactions, (O'Connor et
 539 al., 2020a;Morgenstern et al., 2020) but removing cloud effects using the SARF or ERFcs,af agrees better with
 540 the expected value. The estimated ozone SARF from the NO_x, VOC and O₃ experiments generally agrees with
 541 the model SARF and ERFcs,af. For CESM2-WACCM the ERF from the VOC experiment is zero, and the SARF
 542 negative even though the diagnosed ozone SARF is positive. For all experiments and models ERFcs,af is generally
 543 higher than the expected or diagnosed SARF (see section 3.3).



544

545 **Fig. 8** Estimated SARF from the greenhouse gas changes (WMGHGs and ozone), using radiative efficiencies for the
 546 WMGHGs and kernel calculations for ozone (see text). Hatched bars show decreases in ozone SARF. Symbols show
 547 the modelled ERF, SARF and ERF_{csaf} (estimate of greenhouse gas clear-sky ERF). Uncertainties on the bars are due
 548 to uncertainties in radiative efficiencies. Uncertainties on the symbols are errors in the mean due to interannual
 549 variability in the model diagnostic.

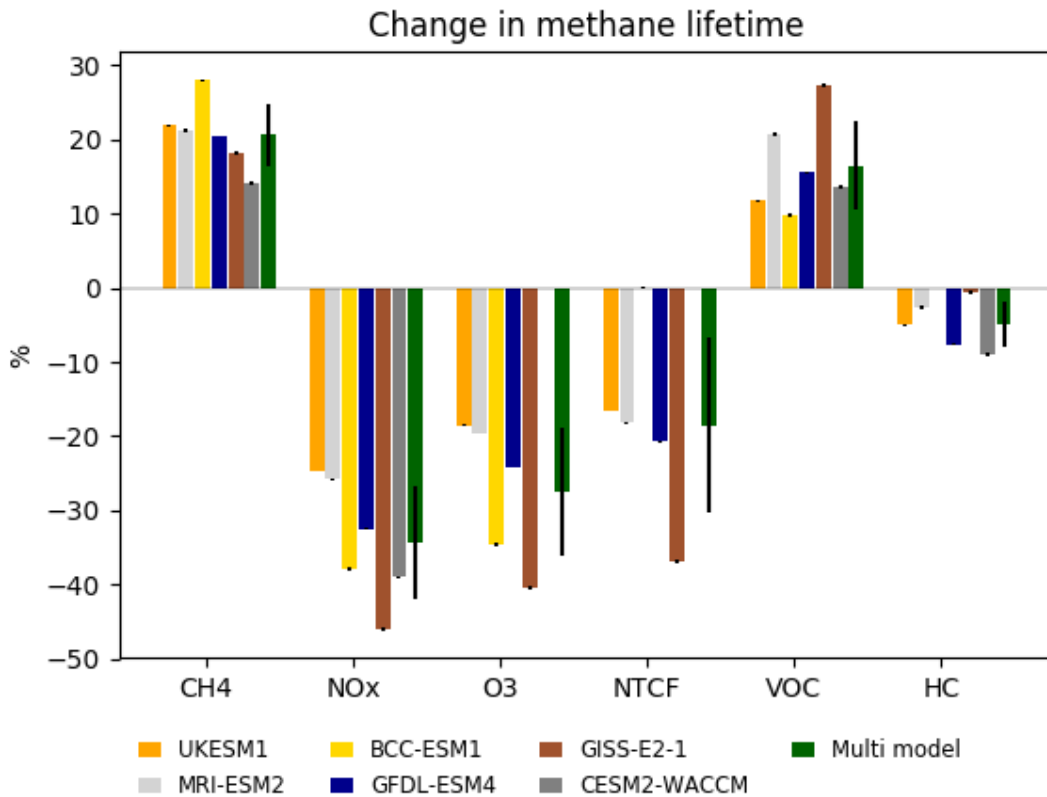
550 4.2.4 Methane Lifetime

551 In the CMIP6 setup the modelled methane concentrations do not respond to changes in oxidation rates. The
 552 methane lifetime is diagnosed (which includes stratospheric loss to OH as parameterised within each model) and
 553 assuming losses to chlorine oxidation and soil uptake of 11 and 30 Tg yr⁻¹ ((Saunois et al., 2020; Myhre et al.,
 554 2013b) and this can be used to infer the methane changes that would be expected if methane were allowed to vary.
 555 Fig. 9 shows the methane lifetime response is large and negative for NO_x emissions, with a smaller positive change
 556 for VOC emissions. Halocarbon concentration increases decrease the methane lifetime, as ozone depletions leads
 557 to increased UV in the troposphere and increased methane loss to chlorine in the stratosphere (Stevenson et al.,
 558 2020). N₂O also decreases the methane lifetime by depleting ozone in the tropics although the effect is less than
 559 for halocarbons. The O₃ experiment has a significantly more negative effect (-27±9 %) than the sum of NO_x and
 560 VOC (-16±8 %) (uncertainties are multi-model standard deviation). This suggests significant non-additivity. Note
 561 that a combined CH₄+NO_x+VOC experiment is not available to test the additivity further.

562 The lifetime response to changing methane concentrations can be used to diagnose the methane lifetime feedback
 563 factor *f* ((Fiore et al., 2009). The results here give *f*=1.32, 1.31, 1.43, 1.30, 1.26, 1.19 (mean 1.30±0.07) for
 564 UKESM1, MRI-ESM2, BCC-ESM1, GFDL-ESM4, GISS-E2-1 and CESM-WACCM. This is in very good
 565 agreement with AR5, although their values are starting from a year 2000 baseline rather than pre-industrial.

566

567



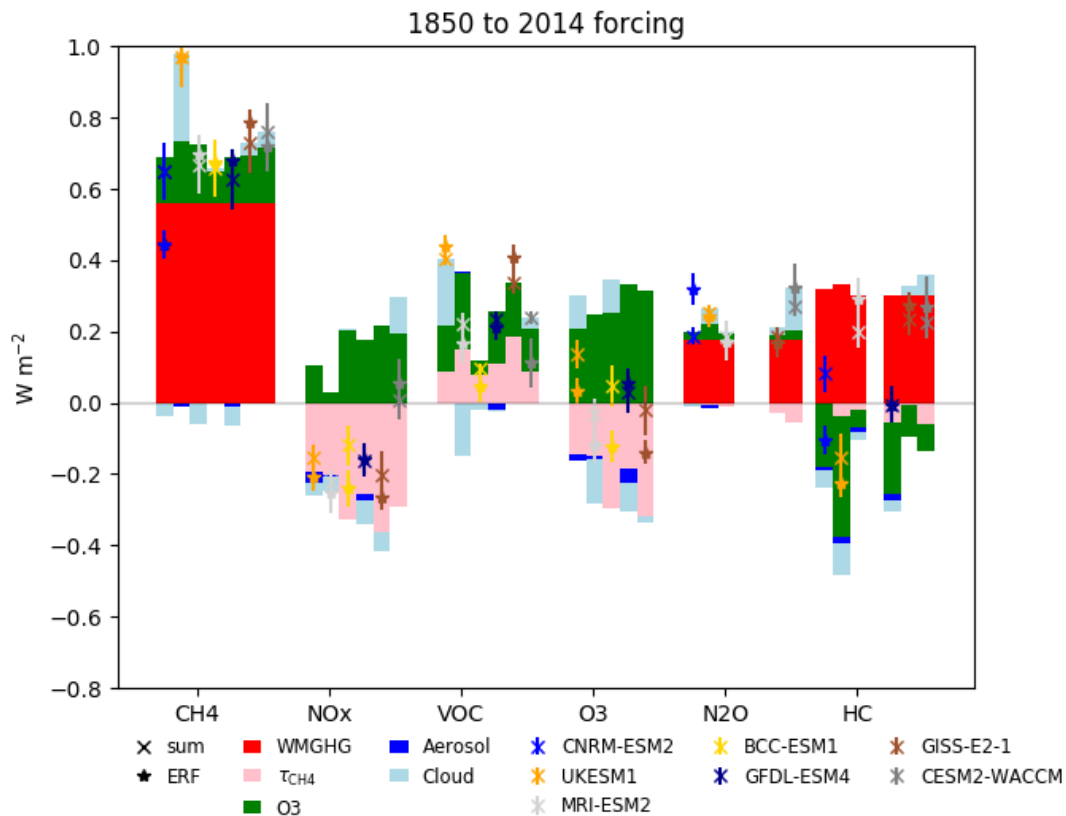
568

569 **Fig. 9** Changes in methane lifetime (%), for each experiment. Uncertainties for individual models are errors on the mean from interannual variability. Uncertainties for the multi model mean are standard deviations across models.
570

571 4.2.5 Total ERFs

572 The methane lifetime changes can be converted to expected changes in concentration if methane were allowed to
573 freely evolve following Fiore et al. (2009), using the f -factors appropriate to each model (section 3.3.4). The
574 inferred radiative forcing is based on radiative efficiency of methane (Etminan et al., 2016). The methane changes
575 also have implications for ozone production, so we assume an ozone SARF per ppb of CH₄ diagnosed for each
576 model from section 4.2.

577 The breakdown of the information from the analyses above is shown in Fig. 10, using the SARF calculated for
578 the gases (WMGHGs and ozone) and kernel-diagnosed cloud adjustments (which include aerosol cloud
579 interactions). Direct contributions from the aerosols IRF_{ari} are shown for models where this is available. The
580 contributions from methane lifetime changes have also been added to the diagnosed ERF as these aren't accounted
581 for in the models. Differences between the diagnosed ERF (stars) and the sum of the components (crosses) then
582 shows to what extent this decomposition into components can account for the modelled ERF. For many of the
583 species, this breakdown is reasonable, and illustrates that cloud radiative effects can make significant contributions
584 to the total radiative impacts of WMGHGs and ozone precursors. This analysis cannot distinguish between cloud
585 effects due to changes in atmospheric temperature profiles or those due to increased cloud nucleation from
586 aerosols.



587

588 **Fig. 10 SARF for WMGHGs, ozone and diagnosed changes in methane. Model diagnosed direct aerosol RF and cloud**
 589 **radiative effect. Crosses mark the sum of the five terms for each model. Stars mark the diagnosed ERF with the effect**
 590 **of methane lifetime (on methane and ozone) added. Differences between stars and crosses shows undiagnosed**
 591 **contributions. Uncertainties on the sum are mainly due to the uncertainties in the radiative efficiencies. Uncertainties**
 592 **in the ERF are errors on the mean due to interannual variability. Note for CESM2-WACCM, BCC-ESM1, GISS-E2-1**
 593 **the direct aerosol effect is unavailable.**

594 5. Discussion

595 For all of the species shown we see considerable variation in the calculated ERFs across the models, which is due
 596 in part to differences in the model aerosol and chemistry schemes; not all models have interactive schemes for all
 597 of the species, and whether or not chemistry is considered will impact the evolution of some of the aerosol species.
 598 We can use the differences in model complexity from the multi-model approach together with the separation of
 599 the effects of the various species in the individual AerChemMIP experiments to understand how the various
 600 components contribute to the overall ERFs we have calculated.

601

602 5.1 Aerosols

603 The 1850-2014 multi-model mean and standard deviation of the ERFs for SO₂, OC and BC are: -1.03 +/- 0.37
 604 Wm⁻² for SO₂, -0.25 +/- 0.09 Wm⁻² for OC, and 0.15 +/- 0.17 Wm⁻² for BC. The total ERF for the aerosols is -
 605 1.01 +/- 0.25 Wm⁻², within the range of -1.65 to -0.6 Wm⁻² reported by (Bellouin et al., 2019).

606 The radiative kernels and double-call diagnostics are used to separate the direct and cloud effects of aerosols for
 607 those models where all the relevant diagnostics are available. These two methods broadly agree on the cloud

608 contribution for the BC, SO₂ and OC experiments. We generally find a weaker total adjustment to black carbon
609 compared to other studies (Samset and Myhre, 2015;Stjern et al., 2017;Smith et al., 2018). The exceptions are
610 MIROC6 and GISS-E2-1. These previous studies used much larger changes in black carbon (up to 10 times)
611 which may cause non-linear effects such as self-lofting.

612 As the ISCCP cloud diagnostics become available for more of the CMIP6 models, it will be possible to do a direct
613 calculation of the cloud rapid adjustments using the kernels from (Zelinka et al., 2014) and compare those with
614 the adjustments calculated using the kernel difference method described in (Smith et al., 2018) and used here
615 (Section 3.2; see also figure 4 and figure S2 from Smith et al. (2020a)).

616 The radiative efficiencies per AOD calculated here are generally larger than those from the AeroCom Phase II
617 experiments (Myhre et al., 2013b), with the caveat that the models included here did not have fixed clouds, so
618 that indirect effects would be included.

619 The values diagnosed for the IRFari (for the models we have available diagnostics for) in CMIP6 are similar to
620 those from CMIP5 (Myhre et al., 2013a) where they reported values for sulfate of -0.4 (-0.6 to -0.2) Wm⁻²
621 compared to our -0.36 (-0.19 to -0.49) Wm⁻² for the SO₂ experiment, for OC they found -0.09 (-0.16 to -0.03)
622 Wm⁻² compared to our value of -0.09 (-0.07 to -0.15) Wm⁻² and for BC they had +0.4 (+0.05 to +0.80) compared
623 to our value of 0.28 (0.13- 0.37) Wm⁻², so broadly the IRFari for the individual species agree with those found in
624 the previous set of models used in CMIP5.

625 The overall aerosol ERF from AR5 is reported as in the range -1.5 to 0.4 Wm⁻², compared to ERF values reported
626 here for the piClim-aer experiment in the range -0.7 to -1.47 Wm⁻².

627

628 **5.2 Reactive greenhouse gases**

629 The diagnosed ERFs from methane, N₂O, halocarbons and ozone precursors are: 0.75±0.10, 0.26±0.07, 0.12±0.21
630 and 0.20±0.07 W m⁻² (excluding CNRM-ESM2-1 for methane as it cannot represent the lower tropospheric ozone
631 changes, and excluding NorESM2 for all as it has no ozone chemistry). These compare with 0.79±0.13, 0.17±0.03,
632 0.18±0.15 and 0.22±0.14 W m⁻² for 1750-2011 from AR5 (Myhre et al., 2013a) - where the effects on methane
633 lifetime and CO₂ have been removed from the AR5 calculations, and the halocarbons are for CFCs and HCFCs
634 only. Section 4.2.5 shows that cloud effects can make a significant contribution to the overall ERF even for
635 WMGHGs. However, clouds cannot explain all the differences. The ERF for N₂O is larger than estimated in AR5.
636 The ozone contribution here is estimated as 0.03±0.01 Wm⁻² whereas it was zero in AR5, but that does not explain
637 all the difference. The multi-model ERF for halocarbons is smaller than AR5, due to larger ozone depletion
638 although the models have a wide spread with some showing significantly lower ERFs and some significantly
639 higher due to varying strengths of ozone depletion in these models.

640 The estimated ozone SARFs from the changes in levels of methane, NO_x and VOC from 1850 to 2014 are
641 0.14±0.03, 0.20±0.07, and 0.11±0.04 W m⁻² compared to 0.24±0.13, 0.14±0.09, and 0.11±0.05 W m⁻² in CMIP5
642 (Myhre et al., 2013a). The ozone from methane contribution is smaller, here only 25% of the direct Etminan et al.
643 (2016) methane SARF compared to 50% in AR5 (or 39% using the Etminan et al. (2016) formula). The NO_x
644 contribution is larger in this study. The CMIP5 results were based on (Stevenson et al., 2013) in which species
645 were reduced from present day levels rather than being increased from pre-industrial levels. The NO_x emission

646 changes are also larger for CMIP6 compared to CMIP5 (Hoesly et al. 2018). The sum of the ozone terms
647 ($\text{CH}_4+\text{N}_2\text{O}+\text{HC}+\text{O}_3$) is $0.33\pm 0.11 \text{ Wm}^{-2}$, agreeing well with the total 1850-2014 ozone SARF of $0.35 \pm 0.16 \text{ Wm}^{-2}$
648 (1.s.d) from Skeie et al. (2020) which included a few additional models.

649

650 The overall effect of NTCF emissions (excluding methane and other WMGHGs) on the 1850-2014 ERF
651 experienced by models that include tropospheric chemistry is strongly negative ($-0.89\pm 0.20 \text{ W m}^{-2}$) due to the
652 dominance of the aerosol forcing over that from ozone. There is a large spread in the NTCF forcing due to the
653 different treatment of atmospheric chemistry within these models. Models without tropospheric and/or
654 stratospheric chemistry prescribe varying ozone levels which are not included in the NTCF experiment. Hence
655 the overall forcing experienced by these models due to ozone and aerosols will be different from that diagnosed
656 here.

657 **6. Conclusion**

658 The experimental setup and diagnostics in CMIP6 have allowed us for the first time to calculate the effective
659 radiative forcing (ERF) for present day reactive gas and aerosol concentrations and emissions in a range of Earth
660 system models. Quantifying the forcing in these models is an essential step to understanding their climate
661 responses.

662 This analysis also allows us to quantify the radiative responses to perturbations in individual species or groups of
663 species. These responses include physical adjustments to the imposed forcing as well as chemical adjustments and
664 adjustments related to the emissions of natural aerosols. The total adjustment is therefore a complex combination
665 of individual process, but the diagnosed ERF implicitly includes these and represents the overall forcing
666 experienced by the models.

667 We find that the ERF from well-mixed greenhouse gases (methane, nitrous oxide and halocarbons) has significant
668 contributions through their effects on ozone, aerosols and clouds, that vary strongly across Earth system models.
669 This indicates that Earth system processes need to be taken into account when understanding the contribution
670 WMGHGs have made to present climate and when projecting the climate effects of different WMGHG scenarios.

671 **7. Acknowledgements**

672 GT, WC, MM, FO'C, DO, MS, acknowledge funding received from the European Union's Horizon 2020 research
673 and innovation programme under grant agreement No 641816 (CRESCENDO).

674 FMO'C, JPM were funded by the Met Office Hadley Centre Climate Programme funded by BEIS and Defra
675 (GA01101). CS was supported by a NERC-IIASA Collaborative Research Fellowship (no. NE/T009381/1). GZ
676 was supported by the NZ government's Strategic Science Investment Fund (SSIF) through the NIWA
677 programme CACV. MD and NO were supported by the Japan Society for the Promotion of Science (grant
678 numbers: JP18H03363, JP18H05292, and JP20K04070), the Environment Research and Technology
679 Development Fund (JPMEERF20172003, JPMEERF20202003, and JPMEERF20205001) of the Environmental
680 Restoration and Conservation Agency of Japan, the Arctic Challenge for Sustainability II (ArCS II), Program
681 Grant Number JPMXD1420318865, and a grant for the Global Environmental Research Coordination System

682 from the Ministry of the Environment, Japan. T. T. was supported by the supercomputer system of the National
683 Institute for Environmental Studies, Japan, and JSPS KAKENHI Grant Number JP19H05669.

684 R.B.S. and G.M. were funded through the Norwegian Research Council project KEYCLIM (grant number
685 295046) and the European Union's Horizon 2020 Research and Innovation Programme under Grant Agreement
686 820829 (CONSTRAIN).

687 The CESM project is supported primarily by the National Science Foundation. This material is based upon work
688 supported by the National Center for Atmospheric Research, which is a major facility sponsored by the NSF
689 under Cooperative Agreement No. 1852977. Computing and data storage resources, including the Cheyenne
690 supercomputer (doi:10.5065/D6RX99HX), were provided by the Computational and Information Systems
691 Laboratory (CISL) at NCAR.

692 We acknowledge the World Climate Research Programme, which, through its Working Group on Coupled
693 Modelling, coordinated and promoted CMIP6. We thank the climate modeling groups for producing and making
694 available their model output, the Earth System Grid Federation (ESGF) for archiving the data and providing
695 access, and the multiple funding agencies who support CMIP6 and ESGF.

696

697 **8. Author Contributions**

698 Manuscript preparation was done by GDT, WJC, RJK, DO and additional contributions from all co-authors.
699 Model simulations were set up, reviewed and/or ran by DO, FMO'C, NLA, MD, LE, LH, J-FL, MMichou,
700 MMills, JM, PN, VN, NO, MS, TT, ST, TW, GZ, JZ. Analysis was carried out by GT, WC, RK, DO, RS.

701

702 **9. Competing Interests**

703 The authors declare that they have no conflict of interest.

704 **10. Data Availability**

705 All data from the various earth system models used in this paper are available on the Earth System Grid Federation
706 Website, and can be downloaded from there. <https://esgf-index1.ceda.ac.uk/search/cmip6-ceda/>

707 **11. References**

708 Ackerman, A. S., Toon, O. B., Taylor, J. P., Johnson, D. W., Hobbs, P. V., and Ferek, R. J.: Effects of
709 Aerosols on Cloud Albedo: Evaluation of Twomey's Parameterization of Cloud Susceptibility Using
710 Measurements of Ship Tracks, *Journal of the Atmospheric Sciences*, 57, 2684-2695, 10.1175/1520-
711 0469(2000)057<2684:eoaoa>2.0.co;2, 2000.

712 Albrecht, B. A.: Aerosols, cloud microphysics, and fractional cloudiness, *Science*, 245, 1227-1230,
713 1989.

714 Archibald, A. T., O'Connor, F. M., Abraham, N. L., Archer-Nicholls, S., Chipperfield, M. P., Dalvi,
715 M., Folberth, G. A., Dennison, F., Dhomse, S. S., Griffiths, P. T., Hardacre, C., Hewitt, A. J., Hill, R.,
716 Johnson, C. E., Keeble, J., Köhler, M. O., Morgenstern, O., Mulchay, J. P., Ordóñez, C., Pope, R. J.,

717 Rumbold, S., Russo, M. R., Savage, N., Sellar, A., Stringer, M., Turnock, S., Wild, O., and Zeng, G.:
718 Description and evaluation of the UKCA stratosphere-troposphere chemistry scheme (StratTrop vn 1.0)
719 implemented in UKESM1, *Geosci. Model Dev. Discuss.*, 2019, 1-82, 10.5194/gmd-2019-246, 2020.

720 Bauer, S. E., Tsigaridis, K., Faluvegi, G., Kelley, M., Lo, K. K., Miller, R. L., Nazarenko, L., Schmidt,
721 G. A., and Wu, J.: Historical (1850–2014) Aerosol Evolution and Role on Climate Forcing Using the
722 GISS ModelE2.1 Contribution to CMIP6, *Journal of Advances in Modeling Earth Systems*, 12,
723 e2019MS001978, 10.1029/2019ms001978, 2020.

724 Bellouin, N., Quaas, J., Gryspeerdt, E., Kinne, S., Stier, P., Watson-Parris, D., Boucher, O., Carslaw,
725 K. S., Christensen, M., Daniau, A.-L., Dufresne, J.-L., Feingold, G., Fiedler, S., Forster, P., Gettelman,
726 A., Haywood, J. M., Lohmann, U., Malavelle, F., Mauritsen, T., McCoy, D. T., Myhre, G.,
727 Mülmenstädt, J., Neubauer, D., Possner, A., Rugenstein, M., Sato, Y., Schulz, M., Schwartz, S. E.,
728 Sourdeval, O., Storelvmo, T., Toll, V., Winker, D., and Stevens, B.: Bounding global aerosol radiative
729 forcing of climate change, *Reviews of Geophysics*, n/a, 10.1029/2019rg000660, 2019.

730 Block, K., and Mauritsen, T.: Forcing and feedback in the MPI-ESM-LR coupled model under abruptly
731 quadrupled CO₂, *Journal of Advances in Modeling Earth Systems*, 5, 676-691, 10.1002/jame.20041,
732 2013.

733 Boucher, O. e. a.: Clouds and Aerosols, In: *Climate Change 2013: The Physical Science Basis.*
734 *Contribution of Working Group I to the Fifth Assessment Report of the Intergovernmental Panel on*
735 *Climate Change*, in, Cambridge University Press, Cambridge, United Kingdom and New York, NY,
736 USA., 2013.

737 Checa-Garcia, R., Hegglin, M. I., Kinnison, D., Plummer, D. A., and Shine, K. P.: Historical
738 Tropospheric and Stratospheric Ozone Radiative Forcing Using the CMIP6 Database, *Geophysical*
739 *Research Letters*, 45, 3264-3273, 10.1002/2017gl076770, 2018.

740 Chung, E.-S., and Soden, B. J.: An Assessment of Direct Radiative Forcing, Radiative Adjustments,
741 and Radiative Feedbacks in Coupled Ocean–Atmosphere Models, *Journal of Climate*, 28, 4152-4170,
742 10.1175/jcli-d-14-00436.1, 2015.

743 Collins, W. J., Lamarque, J. F., Schulz, M., Boucher, O., Eyring, V., Hegglin, M. I., Maycock, A.,
744 Myhre, G., Prather, M., Shindell, D., and Smith, S. J.: AerChemMIP: quantifying the effects of
745 chemistry and aerosols in CMIP6, *Geosci. Model Dev.*, 10, 585-607, 10.5194/gmd-10-585-2017, 2017.

746 Deushi, M., and Shibata, K.: Development of a Meteorological Research Institute Chemistry-Climate
747 Model version 2 for the Study of Tropospheric and Stratospheric Chemistry, *Papers in Meteorology*
748 *and Geophysics*, 62, 1-46, 10.2467/mripapers.62.1, 2011.

749 Di Biagio, C., Formenti, P., Balkanski, Y., Caponi, L., Cazaunau, M., Pangui, E., Journet, E., Nowak,
750 S., Andreae, M., Kandler, K., Saeed, T., Piketh, S., Seibert, D., Williams, E., and Doussin, J.-F.:
751 Complex refractive indices and single scattering albedo of global dust aerosols in the shortwave
752 spectrum and relationship to iron content and size, *Atmospheric Chemistry and Physics Discussions*, 1-
753 42, 10.5194/acp-2019-145, 2019.

754 Dunne, J. P., Horowitz, L. W., Adcroft, A. J., Ginoux, P., Held, I. M., John, J. G., Krasting, J. P.,
755 Malyshev, S., Naik, V., Paulot, F., Shevliakova, E., Stock, C. A., Zadeh, N., Balaji, V., Blanton, C.,
756 Dunne, K. A., Dupuis, C., Durachta, J., Dussin, R., Gauthier, P. P. G., Griffies, S. M., Guo, H., Hallberg,
757 R. W., Harrison, M., He, J., Hurlin, W., McHugh, C., Menzel, R., Milly, P. C. D., Nikonov, S., Paynter,
758 D. J., Ploshay, J., Radhakrishnan, A., Rand, K., Reichl, B. G., Robinson, T., Schwarzkopf, D. M.,
759 Sentman, L. T., Underwood, S., Vahlenkamp, H., Winton, M., Wittenberg, A. T., Wyman, B., Zeng,
760 Y., and Zhao, M.: The GFDL Earth System Model version 4.1 (GFDL-ESM 4.1): Overall coupled

761 model description and simulation characteristics, *Journal of Advances in Modeling Earth Systems*, n/a,
762 e2019MS002015, 10.1029/2019ms002015, 2020.

763 Emmons, L. K., Walters, S., Hess, P. G., Lamarque, J. F., Pfister, G. G., Fillmore, D., Granier, C.,
764 Guenther, A., Kinnison, D., Laepple, T., Orlando, J., Tie, X., Tyndall, G., Wiedinmyer, C., Baughcum,
765 S. L., and Kloster, S.: Description and evaluation of the Model for Ozone and Related chemical Tracers,
766 version 4 (MOZART-4), *Geosci. Model Dev.*, 3, 43-67, 10.5194/gmd-3-43-2010, 2010.

767 Etminan, M., Myhre, G., Highwood, E. J., and Shine, K. P.: Radiative forcing of carbon dioxide,
768 methane, and nitrous oxide: A significant revision of the methane radiative forcing, *Geophysical*
769 *Research Letters*, 43, 12,614-612,623, 10.1002/2016gl071930, 2016.

770 Eyring, V., Bony, S., Meehl, G. A., Senior, C. A., Stevens, B., Stouffer, R. J., and Taylor, K. E.:
771 Overview of the Coupled Model Intercomparison Project Phase 6 (CMIP6) experimental design and
772 organization, *Geosci. Model Dev.*, 9, 1937-1958, 10.5194/gmd-9-1937-2016, 2016.

773 Fiore, A. M., Dentener, F. J., Wild, O., Cuvelier, C., Schultz, M. G., Hess, P., Textor, C., Schulz, M.,
774 Doherty, R. M., Horowitz, L. W., MacKenzie, I. A., Sanderson, M. G., Shindell, D. T., Stevenson, D.
775 S., Szopa, S., Van Dingenen, R., Zeng, G., Atherton, C., Bergmann, D., Bey, I., Carmichael, G., Collins,
776 W. J., Duncan, B. N., Faluvegi, G., Folberth, G., Gauss, M., Gong, S., Hauglustaine, D., Holloway, T.,
777 Isaksen, I. S. A., Jacob, D. J., Jonson, J. E., Kaminski, J. W., Keating, T. J., Lupu, A., Marmer, E.,
778 Montanaro, V., Park, R. J., Pitari, G., Pringle, K. J., Pyle, J. A., Schroeder, S., Vivanco, M. G., Wind,
779 P., Wojcik, G., Wu, S., and Zuber, A.: Multimodel estimates of intercontinental source-receptor
780 relationships for ozone pollution, *Journal of Geophysical Research: Atmospheres*, 114,
781 10.1029/2008jd010816, 2009.

782 Forster, P. M., Richardson, T., Maycock, A. C., Smith, C. J., Samset, B. H., Myhre, G., Andrews, T.,
783 Pincus, R., and Schulz, M.: Recommendations for diagnosing effective radiative forcing from climate
784 models for CMIP6, *Journal of Geophysical Research: Atmospheres*, 121, 12,460-412,475,
785 doi:10.1002/2016JD025320, 2016.

786 Gettelman, A., Mills, M. J., Kinnison, D. E., Garcia, R. R., Smith, A. K., Marsh, D. R., Tilmes, S., Vitt,
787 F., Bardeen, C. G., McNerny, J., Liu, H. L., Solomon, S. C., Polvani, L. M., Emmons, L. K., Lamarque,
788 J. F., Richter, J. H., Glanville, A. S., Bacmeister, J. T., Phillips, A. S., Neale, R. B., Simpson, I. R.,
789 DuVivier, A. K., Hodzic, A., and Randel, W. J.: The Whole Atmosphere Community Climate Model
790 Version 6 (WACCM6), *Journal of Geophysical Research: Atmospheres*, n/a, 10.1029/2019JD030943,
791 2019.

792 Ghan, S. J.: Technical Note: Estimating aerosol effects on cloud radiative forcing, *Atmos. Chem. Phys.*,
793 13, 9971-9974, 10.5194/acp-13-9971-2013, 2013.

794 Hansen, J., Sato, M., Ruedy, R., Nazarenko, L., Lacis, A., Schmidt, G. A., Russell, G., Aleinov, I.,
795 Bauer, M., Bauer, S., Bell, N., Cairns, B., Canuto, V., Chandler, M., Cheng, Y., Del Genio, A., Faluvegi,
796 G., Fleming, E., Friend, A., Hall, T., Jackman, C., Kelley, M., Kiang, N., Koch, D., Lean, J., Lerner, J.,
797 Lo, K., Menon, S., Miller, R., Minnis, P., Novakov, T., Oinas, V., Perlwitz, J., Perlwitz, J., Rind, D.,
798 Romanou, A., Shindell, D., Stone, P., Sun, S., Tausnev, N., Thresher, D., Wielicki, B., Wong, T., Yao,
799 M., and Zhang, S.: Efficacy of climate forcings, *Journal of Geophysical Research: Atmospheres*, 110,
800 10.1029/2005jd005776, 2005.

801 Hoesly, R. M., Smith, S. J., Feng, L., Klimont, Z., Janssens-Maenhout, G., Pitkanen, T., Seibert, J. J.,
802 Vu, L., Andres, R. J., Bolt, R. M., Bond, T. C., Dawidowski, L., Kholod, N., Kurokawa, J.-i., Li, M.,
803 Liu, L., Lu, Z., Moura, M. C. P., O'Rourke, P. R., and Zhang, Q.: Historical (1750–2014) anthropogenic
804 emissions of reactive gases and aerosols from the Community Emissions Data System (CEDS),
805 *Geoscientific Model Development (Online)*, Medium: ED; Size: p. 369-408, 2018.

806 Horowitz, L. W., Naik, V., Paulot, F., Ginoux, P. A., Dunne, J. P., Mao, J., Schnell, J., Chen, X., He,
807 J., John, J. G., Lin, M., Lin, P., Malyshev, S., Paynter, D., Shevliakova, E., and Zhao, M.: The GFDL
808 Global Atmospheric Chemistry-Climate Model AM4.1: Model Description and Simulation
809 Characteristics, *Journal of Advances in Modeling Earth Systems*, n/a, e2019MS002032,
810 10.1029/2019ms002032, 2020.

811 Johnson, B. T., Haywood, J. M., and Hawcroft, M. K.: Are Changes in Atmospheric Circulation
812 Important for Black Carbon Aerosol Impacts on Clouds, Precipitation, and Radiation?, *Journal of*
813 *Geophysical Research: Atmospheres*, 124, 7930-7950, 10.1029/2019jd030568, 2019.

814 Kawai, H., Yukimoto, S., Koshiro, T., Oshima, N., Tanaka, T., Yoshimura, H., and Nagasawa, R.:
815 Significant improvement of cloud representation in the global climate model MRI-ESM2, *Geosci.*
816 *Model Dev.*, 12, 2875-2897, 10.5194/gmd-12-2875-2019, 2019.

817 Keeble, J., Hassler, B., Banerjee, A., Checa-Garcia, R., Chiodo, G., Davis, S., Eyring, V., Griffiths, P.
818 T., Morgenstern, O., Nowack, P., Zeng, G., Zhang, J., Bodeker, G., Cugnet, D., Danabasoglu, G.,
819 Deushi, M., Horowitz, L. W., Li, L., Michou, M., Mills, M. J., Nabat, P., Park, S., and Wu, T.:
820 Evaluating stratospheric ozone and water vapor changes in CMIP6 models from 1850-2100, *Atmos.*
821 *Chem. Phys. Discuss.*, 2020, 1-68, 10.5194/acp-2019-1202, 2020.

822 Lurton, T., Balkanski, Y., Bastrikov, V., Bekki, S., Bopp, L., Braconnot, P., Brockmann, P., Cadule, P.,
823 Contoux, C., Cozic, A., Cugnet, D., Dufresne, J.-L., Éthé, C., Foujols, M.-A., Ghattas, J., Hauglustaine,
824 D., Hu, R.-M., Kageyama, M., Khodri, M., Lebas, N., Levvasseur, G., Marchand, M., Ottlé, C., Peylin,
825 P., Sima, A., Szopa, S., Thiéblemont, R., Vuichard, N., and Boucher, O.: Implementation of the CMIP6
826 Forcing Data in the IPSL-CM6A-LR Model, *Journal of Advances in Modeling Earth Systems*, 12,
827 e2019MS001940, 10.1029/2019ms001940, 2020.

828 Matthes, K., Funke, B., Andersson, M. E., Barnard, L., Beer, J., Charbonneau, P., Clilverd, M. A.,
829 Dudok de Wit, T., Haberreiter, M., Hendry, A., Jackman, C. H., Kretzschmar, M., Kruschke, T., Kunze,
830 M., Langematz, U., Marsh, D. R., Maycock, A. C., Misios, S., Rodger, C. J., Scaife, A. A., Seppälä, A.,
831 Shangguan, M., Sinnhuber, M., Tourpali, K., Usoskin, I., van de Kamp, M., Verronen, P. T., and
832 Versick, S.: Solar forcing for CMIP6 (v3.2), *Geosci. Model Dev.*, 10, 2247-2302, 10.5194/gmd-10-
833 2247-2017, 2017.

834 Meinshausen, M., Vogel, E., Nauels, A., Lorbacher, K., Meinshausen, N., Etheridge, D. M., Fraser, P.
835 J., Montzka, S. A., Rayner, P. J., Trudinger, C. M., Krummel, P. B., Beyerle, U., Canadell, J. G., Daniel,
836 J. S., Enting, I. G., Law, R. M., Lunder, C. R., O'Doherty, S., Prinn, R. G., Reimann, S., Rubino, M.,
837 Velders, G. J. M., Vollmer, M. K., Wang, R. H. J., and Weiss, R.: Historical greenhouse gas
838 concentrations for climate modelling (CMIP6), *Geosci. Model Dev.*, 10, 2057-2116, 10.5194/gmd-10-
839 2057-2017, 2017.

840 Michou, M., Nabat, P., Saint-Martin, D., Bock, J., Decharme, B., Mallet, M., Roehrig, R., Séférian, R.,
841 Sénési, S., and Voldoire, A.: Present-Day and Historical Aerosol and Ozone Characteristics in CNRM
842 CMIP6 Simulations, *Journal of Advances in Modeling Earth Systems*, 12, e2019MS001816,
843 10.1029/2019ms001816, 2020.

844 Morgenstern, O., Braesicke, P., O'Connor, F. M., Bushell, A. C., Johnson, C. E., Osprey, S. M., and
845 Pyle, J. A.: Evaluation of the new UKCA climate-composition model – Part 1: The stratosphere, *Geosci.*
846 *Model Dev.*, 2, 43-57, 10.5194/gmd-2-43-2009, 2009.

847 Morgenstern, O., O'Connor, F. M., Johnson, B. T., Zeng, G., Mulcahy, J. P., Williams, J., Teixeira, J.,
848 Michou, M., Nabat, P., Horowitz, L. W., Naik, V., Sentman, L. T., Deushi, M., Bauer, S. E., Tsigaridis,
849 K., Shindell, D. T., and Kinnison, D. E.: Reappraisal of the climate impacts of ozone-depleting
850 substances., *Gophys. Res. Lett.*, 2020.

851 Mulcahy, J. P., Johnson, C., Jones, C. G., Povey, A. C., Scott, C. E., Sellar, A., Turnock, S. T.,
852 Woodhouse, M. T., Abraham, N. L., Andrews, M. B., Bellouin, N., Browse, J., Carslaw, K. S., Dalvi,
853 M., Folberth, G. A., Glover, M., Grosvenor, D., Hardacre, C., Hill, R., Johnson, B., Jones, A., Kipling,
854 Z., Mann, G., Mollard, J., O'Connor, F. M., Palmieri, J., Reddington, C., Rumbold, S. T., Richardson,
855 M., Schutgens, N. A. J., Stier, P., Stringer, M., Tang, Y., Walton, J., Woodward, S., and Yool, A.:
856 Description and evaluation of aerosol in UKESM1 and HadGEM3-GC3.1 CMIP6 historical
857 simulations, *Geosci. Model Dev. Discuss.*, 2020, 1-59, 10.5194/gmd-2019-357, 2020.

858 Myhre, G., D. Shindell, F.-M. Bréon, W. Collins, J. Fuglestedt, J. Huang, D. Koch, J.-F. Lamarque,
859 D. Lee, B. Mendoza, T. Nakajima, A. Robock, G. Stephens, Takemura, T., and Zhang, H.:
860 Anthropogenic and Natural Radiative Forcing. In: *Climate Change 2013: The Physical Science Basis.*
861 Contribution of Working Group I to the Fifth Assessment Report of the Intergovernmental Panel on
862 Climate Change, 2013a.

863 Myhre, G., Samset, B. H., Schulz, M., Balkanski, Y., Bauer, S., Bernsten, T. K., Bian, H., Bellouin, N.,
864 Chin, M., Diehl, T., Easter, R. C., Feichter, J., Ghan, S. J., Hauglustaine, D., Iversen, T., Kinne, S.,
865 Kirkevåg, A., Lamarque, J. F., Lin, G., Liu, X., Lund, M. T., Luo, G., Ma, X., van Noije, T., Penner, J.
866 E., Rasch, P. J., Ruiz, A., Seland, Ø., Skeie, R. B., Stier, P., Takemura, T., Tsigaridis, K., Wang, P.,
867 Wang, Z., Xu, L., Yu, H., Yu, F., Yoon, J. H., Zhang, K., Zhang, H., and Zhou, C.: Radiative forcing
868 of the direct aerosol effect from AeroCom Phase II simulations, *Atmos. Chem. Phys.*, 13, 1853-1877,
869 10.5194/acp-13-1853-2013, 2013b.

870 O'Connor, F. M., Johnson, C. E., Morgenstern, O., Abraham, N. L., Braesicke, P., Dalvi, M., Folberth,
871 G. A., Sanderson, M. G., Telford, P. J., Voulgarakis, A., Young, P. J., Zeng, G., Collins, W. J., and
872 Pyle, J. A.: Evaluation of the new UKCA climate-composition model – Part 2: The Troposphere,
873 *Geosci. Model Dev.*, 7, 41-91, 10.5194/gmd-7-41-2014, 2014.

874 O'Connor, F. M., Abraham, N. L., Dalvi, M., Folberth, G., Griffiths, P., Hardacre, C., Johnson, B. T.,
875 Kahana, R., Keeble, J., Kim, B., Morgenstern, O., Mulcahy, J. P., Richardson, M. G., Robertson, E.,
876 Seo, J., Shim, S., Teixeira, J. C., Turnock, S., Williams, J., Wiltshire, A., and Zeng, G.: Assessment of
877 pre-industrial to present-day anthropogenic climate forcing in UKESM1, *Atmos. Chem. Phys. Discuss.*,
878 2020, 1-49, 10.5194/acp-2019-1152, 2020.

879 O'Connor, F. M., Abraham, N. L., Dalvi, M., Folberth, G., Griffiths, P., Hardacre, C., Johnson, B. T.,
880 Kahana, R., Keeble, J., Kim, B., Morgenstern, O., Mulcahy, J. P., Richardson, M. G., Robertson, E.,
881 Seo, J., Shim, S., Teixeira, J. C., Turnock, S., Williams, J., Wiltshire, A., and Zeng, G.: Assessment of
882 pre-industrial to present-day anthropogenic climate forcing in UKESM1, *Atmospheric Chemistry and*
883 *Physics*, Submitted, 2020a.

884 O'Connor, F. M., Jamil, O., Andrews, T., Johnson, B. T., Mulcahy, J. P., and Manners, J.:
885 Apportionment of the Pre-Industrial to Present-Day Climate Forcing by Methane using UKESM1,
886 *JAMES*, submitted, 2020b.

887 Oshima, N., Yukimoto, S., Deushi, M., Koshiro, T., Kawai, H., Tanaka, T. Y., and Yoshida, K.: Global
888 and Arctic effective radiative forcing of anthropogenic gases and aerosols in MRI-ESM2.0, *Prog. Earth.*
889 *Planet. Sci.*, 7, <https://doi.org/10.1186/s40645-020-00348-w>, 2020.

890 Pendergrass, A. G., Conley, A., and Vitt, F. M.: Surface and top-of-atmosphere radiative feedback
891 kernels for CESM-CAM5, *Earth Syst. Sci. Data*, 10, 317-324, 10.5194/essd-10-317-2018, 2018.

892 Pincus, R., and Baker, M. B.: Effect of precipitation on the albedo susceptibility of clouds in the marine
893 boundary layer, *Nature*, 372, 250-252, 10.1038/372250a0, 1994.

- 894 Pincus, R., Forster, P. M., and Stevens, B.: The Radiative Forcing Model Intercomparison Project
895 (RFMIP): experimental protocol for CMIP6, *Geosci. Model Dev.*, 9, 3447-3460, 10.5194/gmd-9-3447-
896 2016, 2016.
- 897 Samset, B. H., and Myhre, G.: Climate response to externally mixed black carbon as a function of
898 altitude, *Journal of Geophysical Research: Atmospheres*, 120, 2913-2927, 10.1002/2014jd022849,
899 2015.
- 900 Samset, B. H., Myhre, G., Forster, P. M., Hodnebrog, Ø., Andrews, T., Faluvegi, G., Fläschner, D.,
901 Kasoar, M., Kharin, V., Kirkevåg, A., Lamarque, J.-F., Olivie, D., Richardson, T., Shindell, D., Shine,
902 K. P., Takemura, T., and Voulgarakis, A.: Fast and slow precipitation responses to individual climate
903 forcings: A PDRMIP multimodel study, *Geophysical Research Letters*, 43, 2782-2791,
904 10.1002/2016gl068064, 2016.
- 905 Saunio, M., Stavert, A. R., Poulter, B., Bousquet, P., Canadell, J. G., Jackson, R. B., Raymond, P. A.,
906 Dlugokencky, E. J., Houweling, S., Patra, P. K., Ciais, P., Arora, V. K., Bastviken, D., Bergamaschi,
907 P., Blake, D. R., Brailsford, G., Bruhwiler, L., Carlson, K. M., Carrol, M., Castaldi, S., Chandra, N.,
908 Crevoisier, C., Crill, P. M., Covey, K., Curry, C. L., Etiope, G., Frankenberg, C., Gedney, N., Hegglin,
909 M. I., Höglund-Isaksson, L., Hugelius, G., Ishizawa, M., Ito, A., Janssens-Maenhout, G., Jensen, K. M.,
910 Joos, F., Kleinen, T., Krummel, P. B., Langenfelds, R. L., Laruelle, G. G., Liu, L., Machida, T.,
911 Maksyutov, S., McDonald, K. C., McNorton, J., Miller, P. A., Melton, J. R., Morino, I., Müller, J.,
912 Murguía-Flores, F., Naik, V., Niwa, Y., Noce, S., O'Doherty, S., Parker, R. J., Peng, C., Peng, S., Peters,
913 G. P., Prigent, C., Prinn, R., Ramonet, M., Regnier, P., Riley, W. J., Rosentretter, J. A., Segers, A.,
914 Simpson, I. J., Shi, H., Smith, S. J., Steele, L. P., Thornton, B. F., Tian, H., Tohjima, Y., Tubiello, F.
915 N., Tsuruta, A., Viovy, N., Voulgarakis, A., Weber, T. S., van Weele, M., van der Werf, G. R., Weiss,
916 R. F., Worthy, D., Wunch, D., Yin, Y., Yoshida, Y., Zhang, W., Zhang, Z., Zhao, Y., Zheng, B., Zhu,
917 Q., Zhu, Q., and Zhuang, Q.: The Global Methane Budget 2000–2017, *Earth Syst. Sci. Data*, 12, 1561-
918 1623, 10.5194/essd-12-1561-2020, 2020.
- 919 Séférian, R., Nabat, P., Michou, M., Saint-Martin, D., Voltaire, A., Colin, J., Decharme, B., Delire, C.,
920 Berthet, S., Chevallier, M., Sénési, S., Franchisteguy, L., Vial, J., Mallet, M., Joetzjer, E., Geoffroy, O.,
921 Guérémy, J.-F., Moine, M.-P., Msadek, R., Ribes, A., Rocher, M., Roehrig, R., Salas-y-Méla, D.,
922 Sanchez, E., Terray, L., Valcke, S., Waldman, R., Aumont, O., Bopp, L., Deshayes, J., Éthé, C., and
923 Madec, G.: Evaluation of CNRM Earth-System model, CNRM-ESM 2-1: role of Earth system
924 processes in present-day and future climate, *Journal of Advances in Modeling Earth Systems*, n/a,
925 10.1029/2019ms001791, 2019.
- 926 Seland, Ø., Bentsen, M., Seland Graff, L., Olivie, D., Toniazzo, T., Gjermundsen, A., Debernard, J. B.,
927 Gupta, A. K., He, Y., Kirkevåg, A., Schwinger, J., Tjiputra, J., Schancke Aas, K., Bethke, I., Fan, Y.,
928 Griesfeller, J., Grini, A., Guo, C., Ilicak, M., Hafsahl Karset, I. H., Landgren, O., Liakka, J., Onsum
929 Moseid, K., Nummelin, A., Spensberger, C., Tang, H., Zhang, Z., Heinze, C., Iverson, T., and Schulz,
930 M.: The Norwegian Earth System Model, NorESM2 - Evaluation of theCMIP6 DECK and historical
931 simulations, *Geosci. Model Dev. Discuss.*, 2020, 1-68, 10.5194/gmd-2019-378, 2020.
- 932 Sellar, A. A., Jones, C. G., Mulcahy, J., Tang, Y., Yool, A., Wiltshire, A., O'Connor, F. M., Stringer,
933 M., Hill, R., Palmieri, J., Woodward, S., de Mora, L., Kuhlbrodt, T., Rumbold, S., Kelley, D. I., Ellis,
934 R., Johnson, C. E., Walton, J., Abraham, N. L., Andrews, M. B., Andrews, T., Archibald, A. T., Berthou,
935 S., Burke, E., Blockley, E., Carslaw, K., Dalvi, M., Edwards, J., Folberth, G. A., Gedney, N., Griffiths,
936 P. T., Harper, A. B., Hendry, M. A., Hewitt, A. J., Johnson, B., Jones, A., Jones, C. D., Keeble, J.,
937 Liddicoat, S., Morgenstern, O., Parker, R. J., Predoi, V., Robertson, E., Siahann, A., Smith, R. S.,
938 Swaminathan, R., Woodhouse, M. T., Zeng, G., and Zerroukat, M.: UKESM1: Description and
939 evaluation of the UK Earth System Model, *Journal of Advances in Modeling Earth Systems*, n/a,
940 10.1029/2019ms001739, 2020.

941 Sherwood, S. C., Bony, S., Boucher, O., Bretherton, C., Forster, P. M., Gregory, J. M., and Stevens, B.:
942 Adjustments in the Forcing-Feedback Framework for Understanding Climate Change, *Bulletin of the*
943 *American Meteorological Society*, 96, 217-228, 10.1175/bams-d-13-00167.1, 2015.

944 Shine, K. P., Cook, J., Highwood, E. J., and Joshi, M. M.: An alternative to radiative forcing for
945 estimating the relative importance of climate change mechanisms, *Geophysical Research Letters*, 30,
946 10.1029/2003gl018141, 2003.

947 Skeie, R. B., Myhre, G., Hodnebrog, Ø., Cameron-Smith, P. J., Deushi, M., Hegglin, M. I., Horowitz,
948 L. W., Kramer, R. J., Michou, M., Mills, M. J., Olivíe, D. J. L., O'Connor, F. M., Paynter, D., Samset,
949 B. H., Sellar, A., Shindell, D., Takemura, T., Tilmes, S., and Wu, T.: Historical total ozone radiative
950 forcing derived from CMIP6 simulations, *npj Climate and Atmospheric Science* 2020.

951 Smith, C. J., Kramer, R. J., Myhre, G., Forster, P. M., Soden, B. J., Andrews, T., Boucher, O., Faluvegi,
952 G., Fläschner, D., Hodnebrog, Ø., Kasoar, M., Kharin, V., Kirkevåg, A., Lamarque, J.-F., Mülmenstädt,
953 J., Olivíe, D., Richardson, T., Samset, B. H., Shindell, D., Stier, P., Takemura, T., Voulgarakis, A., and
954 Watson-Parris, D.: Understanding Rapid Adjustments to Diverse Forcing Agents, *Geophysical*
955 *Research Letters*, 45, 12,023-012,031, doi:10.1029/2018GL079826, 2018.

956 Smith, C. J., Kramer, R. J., Myhre, G., Alterskjær, K., Collins, W., Sima, A., Boucher, O., Dufresne, J.
957 L., Nabat, P., Michou, M., Yukimoto, S., Cole, J., Paynter, D., Shiogama, H., O'Connor, F. M.,
958 Robertson, E., Wiltshire, A., Andrews, T., Hannay, C., Miller, R., Nazarenko, L., Kirkevåg, A., Olivíe,
959 D., Fiedler, S., Pincus, R., and Forster, P. M.: Effective radiative forcing and adjustments in CMIP6
960 models, *Atmos. Chem. Phys.*, 20, 9591-9618, 10.5194/acp-20-9591-2020, 2020a.

961 Smith, C. J., Kramer, R. J., and Sima, A.: The HadGEM3-GA7.1 radiative kernel: the importance of a
962 well-resolved stratosphere, *Earth Syst. Sci. Data Discuss.*, 2020, 1-16, 10.5194/essd-2019-254, 2020b.

963 Soden, B. J., Held, I. M., Colman, R., Shell, K. M., Kiehl, J. T., and Shields, C. A.: Quantifying Climate
964 Feedbacks Using Radiative Kernels, *Journal of Climate*, 21, 3504-3520, 10.1175/2007jcli2110.1, 2008.

965 Stevenson, D. S., Young, P. J., Naik, V., Lamarque, J. F., Shindell, D. T., Voulgarakis, A., Skeie, R.
966 B., Dalsoren, S. B., Myhre, G., Berntsen, T. K., Folberth, G. A., Rumbold, S. T., Collins, W. J.,
967 MacKenzie, I. A., Doherty, R. M., Zeng, G., van Noije, T. P. C., Strunk, A., Bergmann, D., Cameron-
968 Smith, P., Plummer, D. A., Strode, S. A., Horowitz, L., Lee, Y. H., Szopa, S., Sudo, K., Nagashima, T.,
969 Josse, B., Cionni, I., Righi, M., Eyring, V., Conley, A., Bowman, K. W., Wild, O., and Archibald, A.:
970 Tropospheric ozone changes, radiative forcing and attribution to emissions in the Atmospheric
971 Chemistry and Climate Model Intercomparison Project (ACCMIP), *Atmos. Chem. Phys.*, 13, 3063-
972 3085, 10.5194/acp-13-3063-2013, 2013.

973 Stevenson, D. S., Zhao, A., Naik, V., O'Connor, F. M., Tilmes, S., Zeng, G., Murray, L. T., Collins, W.
974 J., Griffiths, P., Shim, S., Horowitz, L. W., Sentman, L., and Emmons, L.: Trends in global tropospheric
975 hydroxyl radical and methane lifetime since 1850 from AerChemMIP, *Atmos. Chem. Phys. Discuss.*,
976 2020, 1-25, 10.5194/acp-2019-1219, 2020.

977 Stjern, C. W., Samset, B. H., Myhre, G., Forster, P. M., Hodnebrog, Ø., Andrews, T., Boucher, O.,
978 Faluvegi, G., Iversen, T., Kasoar, M., Kharin, V., Kirkevåg, A., Lamarque, J.-F., Olivíe, D., Richardson,
979 T., Shawki, D., Shindell, D., Smith, C. J., Takemura, T., and Voulgarakis, A.: Rapid Adjustments Cause
980 Weak Surface Temperature Response to Increased Black Carbon Concentrations, *Journal of*
981 *Geophysical Research: Atmospheres*, 122, 11,462-411,481, 10.1002/2017jd027326, 2017.

982 Suzuki, K., and Takemura, T.: Perturbations to Global Energy Budget Due to Absorbing and Scattering
983 Aerosols, *Journal of Geophysical Research: Atmospheres*, 124, 2194-2209, 10.1029/2018jd029808,
984 2019.

- 985 Takemura, T., Nozawa, T., Emori, S., Nakajima, T. Y., and Nakajima, T.: Simulation of climate
986 response to aerosol direct and indirect effects with aerosol transport-radiation model, *Journal of*
987 *Geophysical Research: Atmospheres*, 110, 10.1029/2004jd005029, 2005.
- 988 Takemura, T., and Suzuki, K.: Weak global warming mitigation by reducing black carbon emissions,
989 *Scientific Reports*, 9, 4419, 10.1038/s41598-019-41181-6, 2019.
- 990 Takemura, T., et al: Development of a global aerosol climate model SPRINTARS, CGER's
991 Supercomputer Monograph Report, 24, 2018.
- 992 Tang, T., Shindell, D., Faluvegi, G., Myhre, G., Olivié, D., Voulgarakis, A., Kasoar, M., Andrews, T.,
993 Boucher, O., Forster, P. M., Hodnebrog, Ø., Iversen, T., Kirkevåg, A., Lamarque, J.-F., Richardson, T.,
994 Samset, B. H., Stjern, C. W., Takemura, T., and Smith, C.: Comparison of Effective Radiative Forcing
995 Calculations Using Multiple Methods, Drivers, and Models, *Journal of Geophysical Research:*
996 *Atmospheres*, 124, 4382-4394, 10.1029/2018jd030188, 2019.
- 997 Tatebe, H., Ogura, T., Nitta, T., Komuro, Y., Ogochi, K., Takemura, T., Sudo, K., Sekiguchi, M., Abe,
998 M., Saito, F., Chikira, M., Watanabe, S., Mori, M., Hirota, N., Kawatani, Y., Mochizuki, T., Yoshimura,
999 K., Takata, K., O'Ishi, R., Yamazaki, D., Suzuki, T., Kurogi, M., Kataoka, T., Watanabe, M., and
1000 Kimoto, M.: Description and basic evaluation of simulated mean state, internal variability, and climate
1001 sensitivity in MIROC6, *Geoscientific Model Development*, 12, 2727-2765,
1002 <http://dx.doi.org/10.5194/gmd-12-2727-2019>, 2019.
- 1003 Thornhill, G., Collins, W., Olivié, D., Archibald, A., Bauer, S., Checa-Garcia, R., Fiedler, S., Folberth,
1004 G., Gjermundsen, A., Horowitz, L., Lamarque, J. F., Michou, M., Mulcahy, J., Nabat, P., Naik, V.,
1005 O'Connor, F. M., Paulot, F., Schulz, M., Scott, C. E., Seferian, R., Smith, C., Takemura, T., Tilmes, S.,
1006 and Weber, J.: Climate-driven chemistry and aerosol feedbacks in CMIP6 Earth system models, *Atmos.*
1007 *Chem. Phys. Discuss.*, 2020, 1-36, 10.5194/acp-2019-1207, 2020.
- 1008 Tilmes, S., Hodzic, A., Emmons, L. K., Mills, M. J., Gettelman, A., Kinnison, D. E., Park, M.,
1009 Lamarque, J. F., Vitt, F., Shrivastava, M., Campuzano-Jost, P., Jimenez, J. L., and Liu, X.: Climate
1010 Forcing and Trends of Organic Aerosols in the Community Earth System Model (CESM2), *Journal of*
1011 *Advances in Modeling Earth Systems*, n/a, 10.1029/2019MS001827, 2019.
- 1012 Twomey, S.: Pollution and the planetary albedo, *Atmospheric Environment* (1967), 8, 1251-1256,
1013 [https://doi.org/10.1016/0004-6981\(74\)90004-3](https://doi.org/10.1016/0004-6981(74)90004-3), 1974.
- 1014 van Marle, M. J. E., Kloster, S., Magi, B. I., Marlon, J. R., Daniau, A. L., Field, R. D., Arneeth, A.,
1015 Forrest, M., Hantson, S., Kehrwald, N. M., Knorr, W., Lasslop, G., Li, F., Mangeon, S., Yue, C., Kaiser,
1016 J. W., and van der Werf, G. R.: Historic global biomass burning emissions for CMIP6 (BB4CMIP)
1017 based on merging satellite observations with proxies and fire models (1750–2015), *Geosci. Model Dev.*,
1018 10, 3329-3357, 10.5194/gmd-10-3329-2017, 2017.
- 1019 Vial, J., Dufresne, J.-I., and Bony, S.: On the interpretation of inter-model spread in CMIP5 climate
1020 sensitivity estimates, *Climate Dynamics*, 41, 3339-3362, [http://dx.doi.org/10.1007/s00382-013-1725-](http://dx.doi.org/10.1007/s00382-013-1725-9)
1021 [9](http://dx.doi.org/10.1007/s00382-013-1725-9), 2013.
- 1022 Watanabe, M., Suzuki, T., O'ishi, R., Komuro, Y., Watanabe, S., Emori, S., Takemura, T., Chikira, M.,
1023 Ogura, T., Sekiguchi, M., Takata, K., Yamazaki, D., Yokohata, T., Nozawa, T., Hasumi, H., Tatebe,
1024 H., and Kimoto, M.: Improved Climate Simulation by MIROC5: Mean States, Variability, and Climate
1025 Sensitivity, *Journal of Climate*, 23, 6312-6335, 10.1175/2010jcli3679.1, 2010.
- 1026 Woodward, S.: Modeling the atmospheric life cycle and radiative impact of mineral dust in the Hadley
1027 Centre climate model, *Journal of Geophysical Research: Atmospheres*, 106, 18155-18166,
1028 10.1029/2000jd900795, 2001.

- 1029 Wu, T., Lu, Y., Fang, Y., Xin, X., Li, L., Li, W., Jie, W., Zhang, J., Liu, Y., Zhang, L., Zhang, F.,
1030 Zhang, Y., Wu, F., Li, J., Chu, M., Wang, Z., Shi, X., Liu, X., Wei, M., Huang, A., Zhang, Y., and Liu,
1031 X.: The Beijing Climate Center Climate System Model (BCC-CSM): the main progress from CMIP5
1032 to CMIP6, *Geosci. Model Dev.*, 12, 1573-1600, 10.5194/gmd-12-1573-2019, 2019.
- 1033 Wu, T., Zhang, F., Zhang, J., Jie, W., Zhang, Y., Wu, F., Li, L., Liu, X., Lu, X., Zhang, L., Wang, J.,
1034 and Hu, A.: Beijing Climate Center Earth System Model version 1 (BCC-ESM1): Model Description
1035 and Evaluation, *Geosci. Model Dev.*, 13, 977-1005, 10.5194/gmd-2019-172, 2020.
- 1036 Yukimoto, S., Kawai, H., Koshiro, T., Oshima, N., Yoshida, K., Urakawa, S., Tsujino, H., Deushi, M.,
1037 Tanaka, T., Hosaka, M., Yabu, S., Yoshimura, H., Shindo, E., Mizuta, R., Obata, A., Adachi, Y., and
1038 Ishii, M.: The Meteorological Research Institute Earth System Model Version 2.0, MRI-ESM2.0:
1039 Description and Basic Evaluation of the Physical Component, *J. Meteor. Soc. Japan*, 97, 931-965,
1040 10.2151/jmsj.2019-051, 2019.
- 1041 Zelinka, M. D., Andrews, T., Forster, P. M., and Taylor, K. E.: Quantifying components of aerosol-
1042 cloud-radiation interactions in climate models, *Journal of Geophysical Research: Atmospheres*, 119,
1043 7599-7615, 10.1002/2014jd021710, 2014.
- 1044

1 **Supplementary Material for**
2 **Effective radiative forcing from emissions of reactive gases and**
3 **aerosols – a multi-model comparison**

4 Gillian D. Thornhill¹, William J. Collins¹, Ryan J. Kramer², Dirk Olivie³, Ragnhild B. Skeie⁴,
5 Fiona O'Connor⁵, Nathan L. Abraham⁶, Ramiro Checa Garcia⁷, Susanne E. Bauer⁸, Makoto
6 Deushi⁹, Louisa K. Emmons¹⁰, Piers M. Forster¹¹, Larry W. Horowitz¹², Ben Johnson⁵, James
7 Keeble⁶, Jean-Francois Lamarque¹⁰, Martine Michou¹³, Michael J. Mills¹⁰, Jane P. Mulcahy⁵,
8 Gunnar Myhre⁴, Pierre Nabat¹³, Vaishali Naik¹², Naga Oshima⁹, Michael Schulz³, Christopher
9 J. Smith¹¹, Toshihiko Takemura¹⁴, Simone Tilmes¹⁰, Tongwen Wu¹⁵, Guang Zeng¹⁶, Jie
10 Zhang¹⁵.

11 ¹Department of Meteorology, University of Reading, Reading, RG6 6BB, UK

12 ²Climate and Radiation Laboratory, NASA Goddard Space Flight Center, Greenbelt, MD 20771, USA, and
13 Universities Space Research Association, 7178 Columbia Gateway Drive, Columbia, MD 21046, USA

14 ³Norwegian Meteorological Institute, Oslo, Norway

15 ⁴CICERO – Centre for International Climate and Environmental Research Oslo, Oslo, Norway

16 ⁵Met Office, Exeter, UK

17 ⁶Department of Chemistry, University of Cambridge, Lensfield Road, Cambridge, CB2 1EW, U.K., National
18 Centre for Atmospheric Science, U.K.

19 ⁷IPSL/LSCE CEA-CNRS-UVSQ-UPSaclay UMR Gif sur Yvette, FRANCE

20 ⁸NASA Goddard Institute for Space Studies, USA

21 ⁹Meteorological Research Institute, Tsukuba, Japan

22 ¹⁰National Center for Atmospheric Research, Boulder, CO, USA

23 ¹¹University of Leeds, Leeds, UK and International Institute for Applied Systems Analysis (IIASA), Laxenburg,
24 Austria

25 ¹²NOAA, Geophysical Fluid Dynamics Laboratory (GFDL), Princeton, NJ 08540-6649

26 ¹³Centre National de Recherches Météorologiques, Meteo-France, Toulouse Cedex, France

27 ¹⁴Research Institute for Applied Mechanics, Kyushu University, Japan

28 ¹⁵Climate System Modeling Division, Beijing Climate Center, Beijing, China

29 ¹⁶NIWA, Wellington, New Zealand

30 *Correspondence to:* Gillian D. Thornhill (g.thornhill@reading.ac.uk)

31

32

33

34

35 **S1 Table of model characteristics**

36 **The table of models used in the paper with information on resolution and aerosol and chemistry modules.**

37 **Table S 1 Table of model properties, aerosol schemes, and chemistry (SU = sulphate; OA = organic aerosol; BC = black**
 38 **carbon; DU = dust; SS = sea salt; NO3 =nitrate)**

Earth System Model (component models)	Resolution	Description of aerosol module	References
IPSL-CM6A-LR (LMDz, INCA)	1.25°(lat) x 2.5°(lon) 79 vertical levels LMDzORIN CA Two	LMDzORINCA Two-moment (mass and number) aerosol scheme with 5 lognormal modes. The IPSLCM6A-LR-INCA model used for this analysis has interactive aerosols but a limited gas-phase model. Aerosol scheme is based a sectional approach with to represent the size distribution of dust, Sea- salt (which has an additional super-coarse mode to model largest emission of spray-salt aerosols), BC, NH4, NO3, SO4, SO2 and OA with a combination of accumulation and coarse log-normal modes with both, soluble and insoluble, treated as independent modes. DMS emissions are prescribed and not interactively calculated. BC is modelled as internally mixed with sulphate (Wang et al., 2016), where the refractive index is relies on Garnet-Maxwell method. Its emissions are derived from inventories. A new dust refractive index is implemented (Di Biagio et al., 2019). Well mixed trace gases concentrations/emissions are forced with AMIP/CMIP6 datasets (Lurton et al., 2020) ozone by (Checa-Garcia et al., 2018) and solar forcing by (Matthes et al., 2017) Components included: SU, BC, OA, SS, DU, NO3	(Balkanski et al., 2010) (Hauglustaine et al., 2014)

<p>UKESM11 (HadGEM3, UKCA, JULES)</p>	<p>1.25°(lat) x 1.88°(lon) 85 vertical levels</p>	<p>UKCA contains the GLOMAP-mode aerosol microphysics scheme</p> <p>Two-moment (mass and number) aerosol scheme with 5 lognormal modes (nucleation soluble, Aitken soluble, Aitken insoluble, accumulation soluble, coarse soluble)</p> <p>Components included: SU, BC, OA, SS, DU*</p> <p>*Dust component tracked independently in six size bins</p> <p>UKCA contains a stratosphere-troposphere chemistry scheme, consisting of 84 tracers, 81 species, 199 bimolecular reactions, 25 uni- or termolecular reactions, 5 heterogeneous, 3 aqueous phase reactions, and 59 photolytic reactions. Secondary aerosol formation of sulphate and secondary organic aerosol is determined by the interactive oxidants.</p> <p>The UKCA aerosol scheme, called GLOMAP-mode, is a two-moment scheme for the simulation of tropospheric black carbon (BC), organic carbon (OC), SO₄, and sea salt. Dust is modelled independently using the bin scheme of Woodward (2001). The UKCA chemistry and aerosol schemes are coupled such that the secondary aerosol (SO₄, OA) formation rates depend on oxidants from the stratosphere-troposphere chemistry scheme. Aerosol particles are activated into cloud droplets using the activation scheme of Abdul-Razzak and Ghan (2000) which is dependent on aerosol size distribution, aerosol composition, and meteorological conditions. Changes in CDNC affect cloud droplet effective radius ((Jones et al., 2001) and the auto conversion of cloud liquid water in to rain water (Khairoutdinov and Kogan, 2000), which both influence cloud albedo. Stratospheric aerosols (aerosol optical depth and surface area density) are prescribed in the model (Sellar et al., 2019b).</p>	<p>(Sellar et al.) (Williams et al., 2018) (Walters et al., 2019) (Kuhlbrodt et al., 2018) GLOMAP-mode by (Mann et al., 2010) (Mulcahy et al., 2018) (Morgenstern et al., 2009) (O'Connor et al., 2014) (Archibald et al., 2020;Sellar et al., 2020;Mulcahy et al., 2020)</p>
---	---	--	---

<p>CNRM-ESM2-1 (ARPEGEclimatv6.3, ISBA-CTRIP, TACTIC, REPROBUS, PISCES)</p>	<p>1.4°(lat) x 1.4°(lon) 91 vertical levels</p>	<p>Aerosols: TACTIC_v2 tropospheric aerosol bin scheme. 12 bins in total for SU, BC, OA, SS, DU, with 3 bins for SS, and 3 bins for DD.</p> <p>REPROBUS_v2 stratospheric chemistry scheme with 63 variables, 44 transported by the model large-scale transport scheme, and 168 chemical reactions, among which 39 photolysis and 9 heterogeneous reactions</p>	<p>(Séférian et al., 2016; Michou et al., 2015)</p> <p>(Séférian et al.) 2019</p> <p>Michou et al 2019</p> <p>Model description website: http://www.umrcnrm.fr/cmip6/spip.php?article10</p>
<p>NorESM2 CAM6-Nor, CLM5)</p>	<p>1.9°(lat) x 2.5°(lon) 32 vertical levels</p>	<p>OsloAero6</p> <p>Production-tagged aerosol module with background lognormal modes (Aitken, accumulation, coarse). Process tracers can alter the shape and composition of the initially lognormal background modes to generate mixtures.</p> <p>OsloAero6 aerosol module which contains some slight updates since (Kirkevåg et al., 2018) describes the formation and evolution of BC, OC, SO₄, dust, sea-salt and SOA. There is a limited gas-phase chemistry describing the oxidation of the aerosol precursors DMS, SO₂, isoprene, and monoterpenes. Oxidant fields of OH, HO₂, NO₃ and O₃ are prescribed climatological fields. As there is no ozone chemistry in the model, prescribed monthly-varying ozone fields are used for the radiation.</p> <p>Components included: SU, BC, OA, SS, DU</p>	<p>(Kirkevåg et al., 2018)</p>

MRI-ESM2	<p>MRI-AGCM3.5: TL159; 320 x 160 lon/lat,</p> <p>MASINGAR mk-2r4c: TL95; 192 x 96 lon/lat,</p> <p>MRI-CCM2.1: T42; 128 x 64 lon/lat, with 80 vertical levels</p>	<p>MASINGAR mk-2r4c is an aerosol model that is a component of MRI-ESM2.0. MASINGAR mk-2r4c treats atmospheric aerosol physical and chemical processes (e.g., emission, transport, diffusion, chemical reactions, and dry and wet depositions). The size distributions of sea salt and mineral dust are divided into 10 discrete bins and those of other aerosols are represented by lognormal size distributions.</p> <p>Components included: SU, BC, OA, SS, DU</p>	<p>(Yukimoto et al., 2019)</p> <p>(Oshima et al., 2020)</p>
MIROC6	1.4° (lat) x 1.4° (lon)	<p>Spectral Radiation-Transport Model for Aerosol Species (SPRINTARS) predicts mass mixing ratios of the main tropospheric aerosols, and models aerosol-cloud interactions in which aerosols alter cloud microphysical properties and affect the radiation budget by acting as cloud condensation and ice nuclei. The SO₄, BC and OC aerosols are treated as externally mixed in this model. The CDNC and ice crystal number are used to calculate the aerosol indirect effect and cloud nucleation process</p> <p>Components included: SU, BC, OA, SS, DU</p>	<p>(Takemura et al., 2005; Watanabe et al., 2010; Takemura and Suzuki, 2019; Takemura, 2018; Tatebe et al., 2019)</p>

<p>BCC-ESM1 (BCC-AGCM3-Chem, BCC-AVIM2, MOM4-L40, SIS)</p>	<p>2.8125° (lat) x 2.8125° (lon) 26 vertical levels with top level at 2.914 hPa</p>	<p>The model prognoses mass distribution of five aerosol types including sulfate, dust, black carbon, organic carbon, and sea salt based on their emissions (and precursor emissions), chemical production for sulfate and secondary organics, dry and wet (rainout and washout) deposition, transport by advection, and dry and wet convection.</p> <p>It uses the BCC-AGCM3-Chem atmospheric chemistry model based on MOZART2 (Horowitz et al., 2003) It uses the BCC-AGCM3-Chem atmospheric chemistry model based on MOZART2 (Horowitz et al., 2003) which does not include stratospheric chemistry, so concentrations of O₃, CH₄, and N₂O at the top two model levels are the zonally and monthly values derived from the CMIP6 data package.</p> <p>Components included: SU, BC, OA, SS, DU</p> <p>Effects of aerosols on radiation, cloud, and precipitation are treated.</p>	<p>(Wu et al., 2020)</p>
--	---	--	--------------------------

GFDL-ESM4	(C96 96x96 cells) 49 vertical levels	The model includes 56 prognostic (transported) tracers and 36 diagnostic (non-transported) chemical tracers, with 43 photolysis reactions, 190 gas-phase kinetic reactions, and 15 heterogeneous reactions. The tropospheric chemistry includes reactions for the NO _x -HO _x -O _x -CO-CH ₄ system and oxidation schemes for other non-methane volatile organic compounds. The stratospheric chemistry accounts for the major ozone loss cycles (O _x , HO _x , NO _x , ClO _x , and BrO _x) and heterogeneous reactions on liquid and solid stratospheric aerosols as in Austin et al. (2013). The bulk aerosol scheme, including 18 transported aerosol tracers, is similar to that in AM4.0 (Zhao et al., 2018), with the following updates: (1) ammonium and nitrate aerosols are treated explicitly, with ISORROPIA (Fountoukis and Nenes, 2007) used to simulate the sulfate–nitrate–ammonia thermodynamic equilibrium; (2) oxidation of sulfur dioxide and dimethyl sulfide to produce sulfate aerosol is driven by the gas-phase oxidant concentrations (OH, H ₂ O ₂ , and O ₃) and cloud pH simulated by the online chemistry scheme, and (3) the rate of aging of black and organic carbon aerosols from hydrophobic to hydrophilic forms varies with calculated concentrations of hydroxyl radical (OH). Aerosol species, including sulfate, BC, organic aerosols, sea-salt, dust and nitrate are treated explicitly.	(Horowitz et al., 2020)(Dunne et al., 2020)
GISS-E2-1 (p3 variant)	2° latitude by 2.5° in longitude 40 vertical layers surface to 0.1 hPa in	Aerosols and ozone are calculated prognostically using the One-Moment Aerosol (OMA). Aerosol scheme is coupled to the tropospheric chemistry scheme which includes inorganic chemistry of O _x , NO _x , HO _x , CO, and organic chemistry of CH ₄ and higher hydrocarbons using the CBM4 scheme and the stratospheric chemistry scheme which includes chlorine and bromine chemistry together with polar stratospheric clouds.	(Bauer et al., 2020;Shindell et al., 2001;Shindell et al., 2003;Gery et al., 1989;Shindell et al., 2006)

CESM2-WACCM	0.9 (lat) x 1.25 (lon), 70 levels	Chemistry and aerosols for the troposphere, stratosphere, mesosphere and lower thermosphere are calculated interactively. It simulates 228 compounds, including the 4-mode Modal Aerosol Model (MAM4). This version of MAM4 is modified to allow for the simulation of stratospheric aerosols from volcanic eruptions (from their SO ₂ emissions) and oxidation of OCS. The representation of secondary organic aerosols follows the Volatility Basis Set approach.	(Emmons et al., 2020; Danabasoglu, 2019; Danabasoglu, 2019; Gettelman et al., 2019; Tilmes et al., 2019) Mills et al., 2016)
-------------	---	--	--

39

40 (Table for European models updated from:

41 Crescendo Report Horizon 2020

42 H2020-SC5-2014 Advanced Earth-system models

43 (Grant Agreement 641816)

44 Coordinated Research in Earth Systems and Climate: Experiments, kNowledge, Dissemination and
45 Outreach Deliverable D_6.2

46

47 **S2 Tables of ERF and ERF_ts for all models analysed**

48 By removing the adjustment due to the changes in the land surface temperature (as calculated from radiative
49 kernels) we show the ERF_ts for those models where the adjustment was available in the following table.

50 The tables below give the 1850-2014 ERF and the ERF_ts calculated from the TOA flux differences for each
51 model for each experiment.

52

53 **Table S 2 ERFs and ERF_ts for the aerosols, including multi-model means with standard errors.**

ERF	aer		BC		OC		SO2		NH3	
	ERF	ERF_ts	ERF	ERF_ts	ERF	ERF_ts	ERF	ERF_ts	ERF	ERF_ts
CNRM-ESM2	-0.74	-0.79	0.11	0.11	-0.17	-0.18	-0.75	-0.78		
UKESM1	-1.10	-1.15	0.37	0.36	-0.21	-0.23	-1.36	-1.41		
MRI-ESM2	-1.21	-1.24	0.25	0.27	-0.32	-0.32	-1.37	-1.42		
BCC-ESM1	-1.47	-1.54	0.21	0.21			-1.54	-1.62		

	0.0212	-0.0094	-0.0147	-0.0013	0.0010	0.0007	0.1200	0.0048
--	--------	---------	---------	---------	--------	--------	--------	--------

61

62

63 S3 Kernel Breakdown of atmospheric adjustments for each experiment

64 The full breakdowns of the rapid adjustments as calculated from the kernels is shown for each of the models and
 65 experiments where the relevant data was available and shows the differences in models for how the rapid
 66 adjustments from different processes contributed to the overall rapid adjustment.

67 Table S5a Adjustments for piClim-aer experiment

piClim-aer	CNRM-ESM2	UKESM1	MRI-ESM2	BCC-ESM1	MIROC6	NorESM2	GFDL-ESM4	GISS-E2-1
albedo	-0.017	-0.049	-0.009	-0.095	-0.026	-0.015	-0.044	0.003
cloud	-0.661	-0.915	-0.842	-0.900	-0.945	-1.093	-0.452	-0.581
W.V.	-0.055	0.017	0.169	-0.008	-0.085	0.029	0.094	-0.046
T_trop	0.107	0.023	-0.243	0.092	0.183	0.038	-0.138	0.137
T_strat	-0.015	-0.006	-0.014	-0.038	0.010	-0.054	-0.027	-0.038
T_surface	0.054	0.049	0.032	0.075	0.059	0.001	0.035	0.052

68

69 Table S5b Adjustments for piClim-BC experiment

piClim-BC	CNRM-ESM2	UKESM1	MRI-ESM2	BCC-ESM1	MIROC6	NorESM2	GISS-E2-1
albedo	0.003	-0.013	0.067	0.015	-0.002	0.076	0.046
cloud	-0.010	-0.013	0.163	0.053	-0.282	-0.067	-0.184
W.V.	0.060	0.057	0.329	0.076	-0.042	0.097	0.038
T_trop	-0.088	-0.137	-0.509	-0.131	0.033	-0.137	-0.051
T_strat	-0.003	0.043	0.021	-0.004	-0.008	-0.025	-0.003
T_surface	0.001	0.005	-0.022	-0.002	0.021	-0.003	0.003

70

71 Table S5c Adjustments for piClim-OC experiment

piClim-OC	CNRM-ESM2	UKESM	MRI	MIROC6	NorESM2	GISS-E2-1
albedo	0.008	-0.015	-0.006	-0.017	0.002	0.001
cloud	-0.083	0.052	-0.129	-0.087	-0.100	-0.290
W.V.	0.000	-0.018	-0.009	-0.004	-0.008	-0.054
T_trop	0.025	0.023	-0.016	0.029	0.066	0.057
T_strat	-0.019	-0.003	-0.010	-0.008	-0.016	-0.015
T_surface	0.011	0.015	0.009	0.035	0.010	0.012

72

73

74

75

76 **Table S5d Adjustments for piClim-SO2 experiment**

piClim-SO2	CNRM-ESM2	UKESM1	MRI-ESM2	BCC-ESM1	MIROC6	NorESM2	GISS-E2-1
albedo	0.01	-0.03	-0.04	-0.10	-0.02	-0.09	-0.04
cloud	-0.49	-0.79	-0.73	-0.43	-0.40	-0.96	-0.02
W.V.	-0.04	-0.10	-0.05	-0.07	-0.06	-0.05	-0.06
T_trop	0.10	0.20	0.08	0.22	0.11	0.16	0.14
T_strat	-0.01	-0.02	-0.02	-0.03	0.00	-0.03	-0.01
T_surface	0.03	0.04	0.06	0.07	0.04	0.01	0.03

77

78 **Table S5e Adjustments for piClim-CH4 experiment**

piClim-CH4	CNRM-ESM2	UKESM1	MRI-ESM2	BCC-ESM1	NorESM2	GFDL-ESM4	GISS-E2-1	CESM2-WACCM
albedo	0.019	0.019	0.013	0.031	0.010	0.014	0.007	0.023
cloud	-0.038	0.242	-0.056	0.008	-0.041	-0.054	0.035	0.045
W.V.	0.071	0.109	0.070	0.055	0.018	0.117	0.021	0.068
T_trop	-0.084	-0.162	-0.138	-0.127	-0.080	-0.147	-0.056	-0.082
T_strat	0.114	0.115	0.124	0.039	0.057	0.109	0.053	0.103
T_surface	-0.017	-0.031	-0.028	-0.046	-0.018	-0.023	-0.019	-0.031

79

80 **Table S5f Adjustments for piClim-HC experiment**

piClim-HC	CNRM-ESM2	UKESM1	MRI-ESM2	GFDL-ESM4	GISS-E2-1	CESM2-WACCM
albedo	0.01	-0.02	0.00	0.00	-0.01	0.01
cloud	-0.05	-0.09	-0.02	-0.03	0.03	0.06
W.V.	-0.02	-0.09	0.02	-0.01	-0.01	0.01
T_trop	0.03	0.10	-0.03	-0.03	-0.01	0.00
T_strat	0.21	0.47	0.16	0.26	0.30	0.16
T_surface	0.00	0.01	0.00	-0.02	-0.01	-0.03

81

82 **Table S5g Adjustments for piClim-N2O experiment**

piClim-NO2	CNRM-ESM2	UKESM1	MRI-ESM2	NorESM2	GISS-E2-1	CESM2-WACCM
albedo	0.021	0.001	0.005	0.003	0.000	0.008
cloud	-0.010	0.047	0.004	0.059	0.026	0.119

W.V.	0.038	-0.002	-0.015	-0.012	-0.006	0.016
T_trop	-0.035	-0.006	-0.022	-0.037	-0.002	-0.014
T_strat	0.094	0.074	0.108	0.003	0.130	0.089
T_surface	-0.016	-0.011	-0.005	-0.014	0.005	-0.016

83

84 **Table S5h Adjustments for piClim-NOx experiment**

piClim-NOx	UKESM1	MRI-ESM2	BCC-ESM1	GFDL-ESM4	GISS-E2-1	CESM2-WACCM
albedo	-0.005	0.018	0.023	0.010	0.003	0.041
cloud	-0.036	-0.041	0.007	-0.065	-0.052	0.104
Spec. Hum.	-0.003	-0.040	0.031	0.029	0.005	0.062
T_trop	0.002	-0.014	-0.063	-0.057	-0.001	-0.056
T_strat	-0.024	-0.161	0.029	0.038	0.056	0.095
T_surface	-0.012	-0.012	-0.026	-0.025	-0.001	-0.030

85

86 **Table S5i Adjustments for piClim-O3 experiment**

piClim-O3	UKESM1	MRI-ESM2	BCC-ESM1	GFDL-ESM4	GISS-E2-1
albedo	0.001	0.002	0.026	0.009	-0.003
cloud	0.091	-0.126	0.096	-0.079	-0.021
W.V.	0.006	0.010	0.054	0.082	-0.004
T_trop	-0.034	-0.062	-0.115	-0.083	-0.021
T_strat	0.009	-0.036	0.047	0.094	0.113
T_surface	-0.016	-0.010	-0.037	-0.015	0.002

87

88 **Table S5j Adjustments for piClim-VOC experiment**

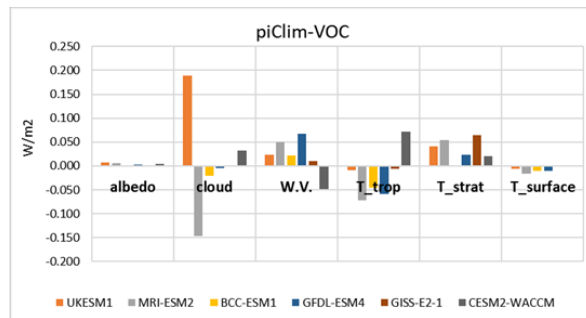
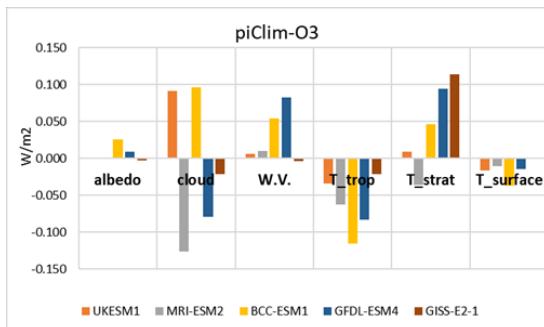
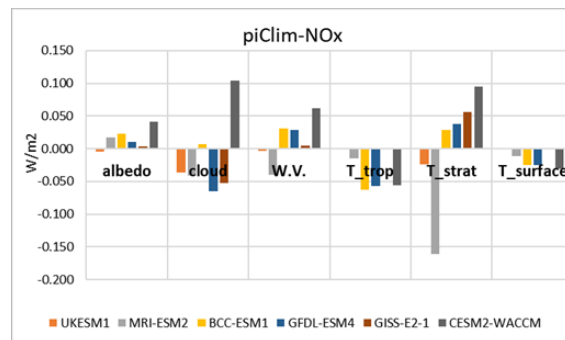
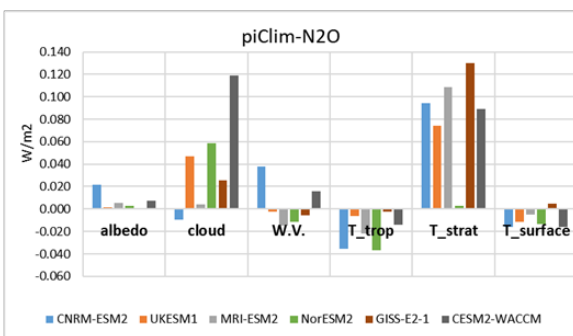
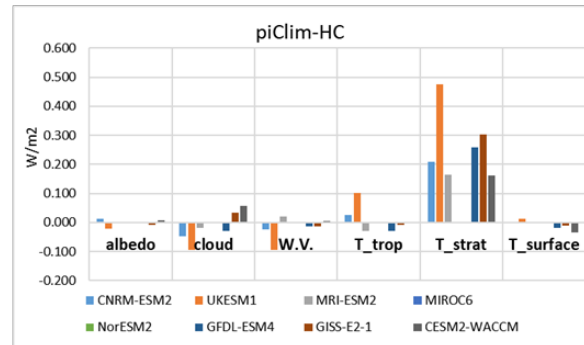
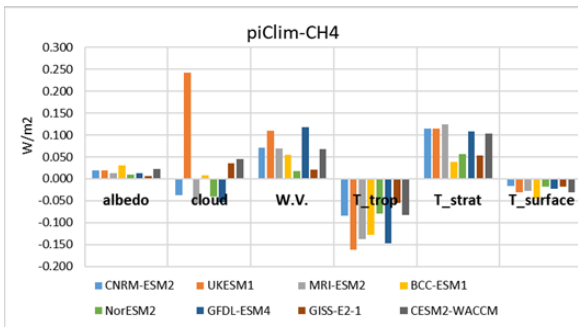
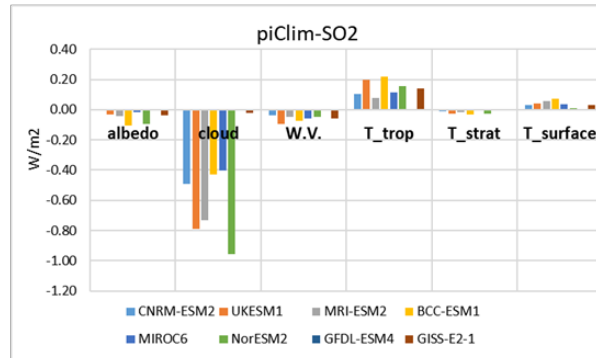
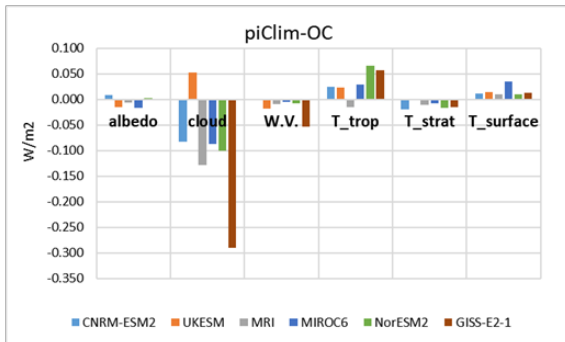
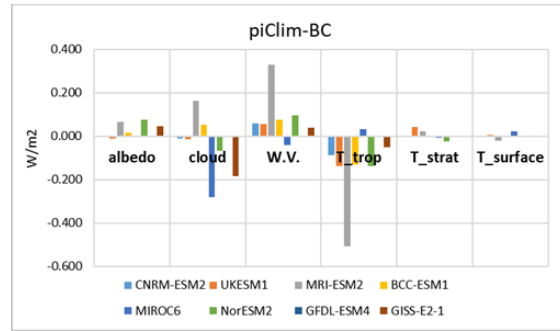
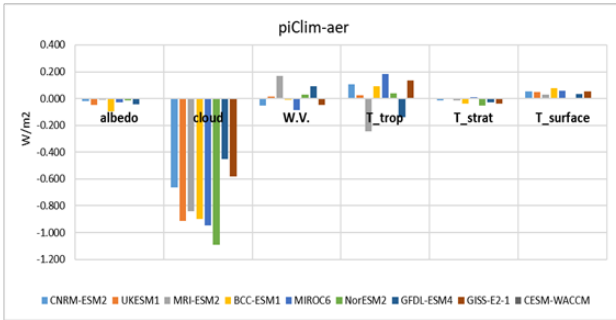
piClim-VOC	UKESM1	MRI-ESM2	BCC-ESM1	GFDL-ESM4	GISS-E2-1	CESM2-WACCM
albedo	0.008	0.006	0.000	0.002	-0.001	0.004
cloud	0.190	-0.147	-0.020	-0.004	-0.001	0.033
W.V.	0.023	0.050	0.022	0.067	0.010	-0.049
T_trop	-0.009	-0.072	-0.046	-0.059	-0.006	0.072
T_strat	0.042	0.054	-0.001	0.024	0.064	0.021
T_surface	-0.006	-0.016	-0.011	-0.011	0.002	0.000

89

90

91

92 Bar charts showing the atmospheric adjustments calculated from the kernel analysis are included below,
93 showing adjustments for surface albedo, cloud, water vapour, tropospheric temperature, stratospheric
94 temperature, and surface temperature.



96

97 **Figure S 1** Plots showing the breakdown of rapid adjustments for all experiments and models with the appropriate
 98 **diagnostics**

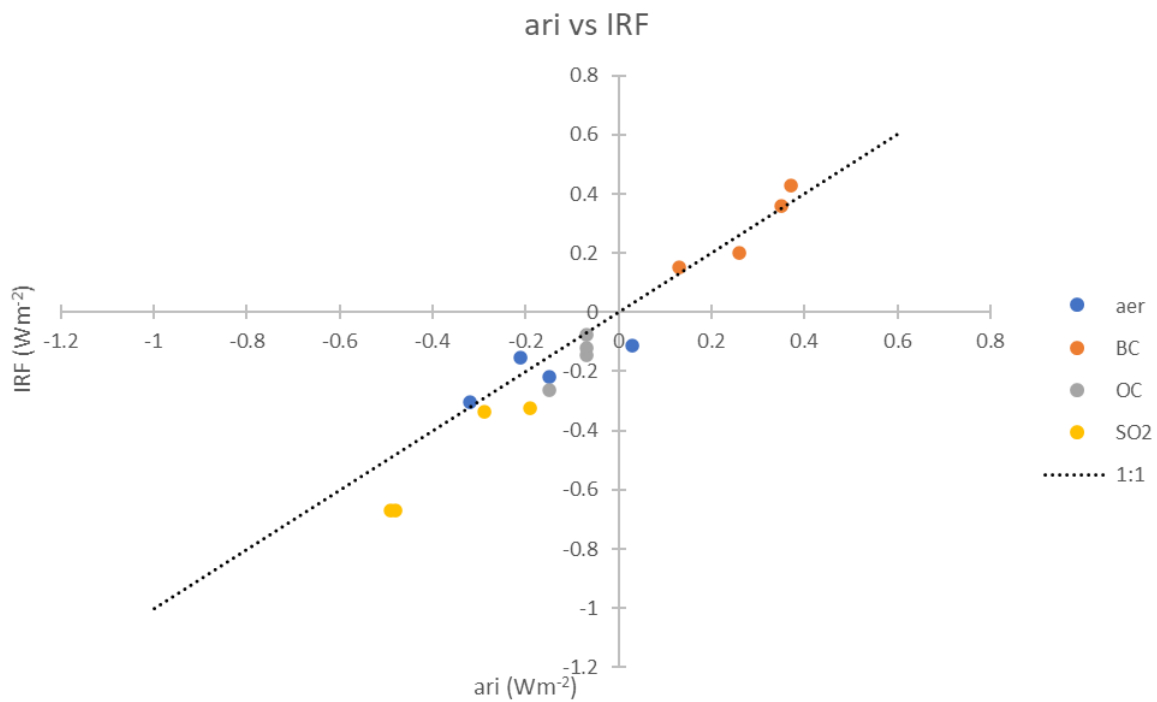
99

100 **Table S 5** Comparison of IRF and cloud adjustment with Smith et al. (2020) for piClim-aer experiment.

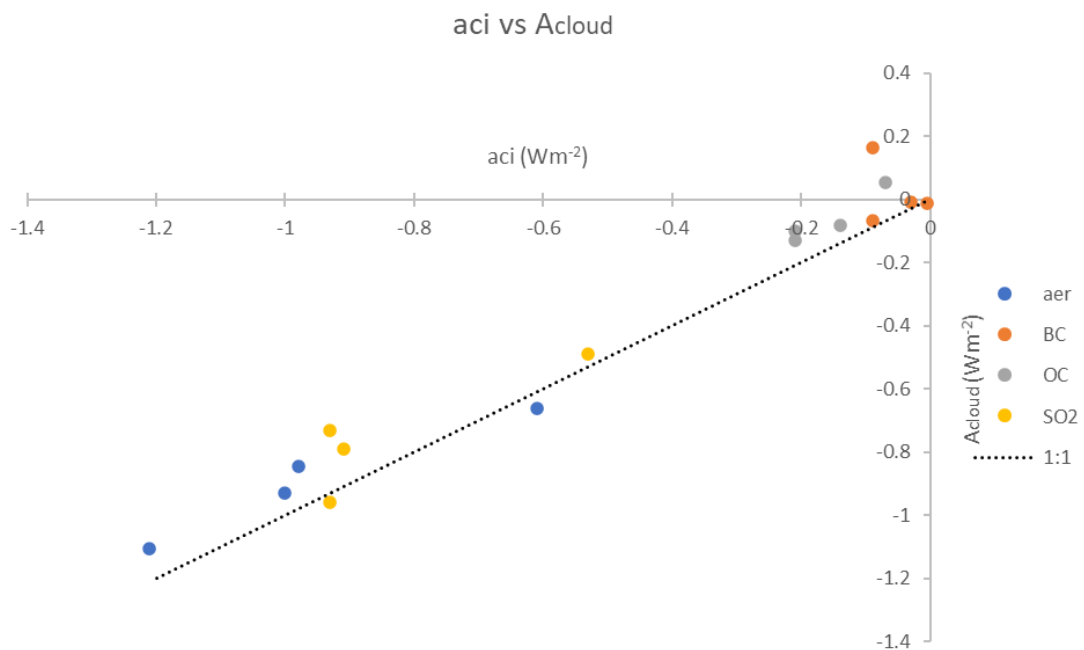
piClim-aer (Wm⁻²)	IRF (This work)	IRF (Smith et al., 2020))	IRF Diff	Cloud adj. (This work)	Cloud adj. (Smith et al., 2020)	Cloud adj. Diff	IRF+Cld Adj (this work)	IRF+Cloud Adj. (Smith et al., 2020)	Total Diff	% Diff
CNRM- ESM2-1	-0.15	-0.75	0.60	-0.66	-0.06	-0.60	-0.82	-0.81	-0.01	0.63
GFDL- ESM4	-0.16	-0.37	0.21	-0.45	-0.26	-0.19	-0.61	-0.63	0.02	-2.77
GISS-E2- 1-G (p3)	-0.42	-1.00	0.58	-0.60	-0.01	-0.59	-1.02	-1.01	-0.01	1.33
MIROC6	-0.21	-1.13	0.92	-0.95	-0.02	-0.93	-1.16	-1.15	-0.01	0.80
MRI- ESM2-0	-0.30	-0.46	0.16	-0.85	-0.68	-0.17	-1.15	-1.14	-0.01	0.79
NorESM2- LM	-0.11	-1.09	0.98	-1.11	-0.08	-1.03	-1.22	-1.17	-0.05	4.28
UKESM1- 0-LL	-0.22	-0.97	0.75	-0.93	-0.18	-0.75	-1.15	-1.15	0.00	0.17
Mean	-0.23	-0.82	0.60	-0.79	-0.18	-0.61	-1.02	-1.01	-0.01	1.01

101

102 (a)



103



104 (b)

105

106 **Figure S 2** Scatter plots comparing direct and indirect aerosol effects from Ghan diagnostics (x-axes) with
107 kernel-derived breakdown (y-axes). Points are from 4 models that included Ghan diagnostics (CNRM-
108 ESM1, UKESM1, MRI-ESM2, NorESM2) (a) Comparison of IRFari with kernel IRF. (b) Comparison of
109 ERFaci with kernel cloud adjustment (Acloud).

110

111 **S4 AOD scaling**

112 In Fig (S2) we compare the ERF originally calculated from the radiative fluxes for the (piClim-xx –piClim-
 113 control) experiments – referred to as Calc ERF to the ERF contributions obtained from using the AOD scaling,



Figure S 3 Comparison of the ERF calculated from radiative fluxes with that from the ERF from AOD-scaled values.

114 e.g. the BC AOD in the piClim-BC experiment. In general, the change in the single species is responsible for
 115 most of the change in the ERF in these experiments, however in the MIROC6 piClim-OC experiment there is a
 116 significant contribution from the organic carbon, indicating this is not as clean a method for obtaining the
 117 scaling in this case as for the other models and experiments. In the case of NorESM2 for the SO₂ experiment we
 118 also have some contribution from the OA, which may be attributable to the way the nucleation scheme works in
 119 NorESM2. Their nucleation scheme looks at the combination of H₂SO₄ and low-volatile organic vapours
 120 (precursors of SOA), so changing the SO₂ emissions might therefore indirectly change the pathway for the SOA
 121 precursors, leading to a shift in how much nucleates and how much condensates. This might lead to a difference
 122 in lifetime of SOA (which is part of OM), leading to differences in the OM burden or AOD. (Dirk Olive, pers.
 123 Communication).

124

125 In Table S6 the ERF per Tg burden is shown for the piClim-BC, piClim-SO₂ and piClim-OC experiments.

126 Table S 6 Table of ERF/burden for individual aerosol experiments

ERF/burden (Wm ⁻² Tg ⁻¹)	CNRM-ESM2	MIROC6	NorESM2	UKESM1	GISS-E2-1	MRI-ESM2	BCC-ESM1	IPSL-INCA
piClim-BC	1.43	-2.49	2.38	4.07	0.92	1.74	1.63	0.90
piClim-OC	-0.68	-0.67	-0.55	-0.45	-1.42	-1.02		-0.35
piClim-SO2	-1.12	-0.93	-1.17	-1.34	-1.01	-1.47	-1.33	-0.64

127

128

129 **S5 Detailed plot of the atmospheric adjustments for the piClim-CH4 model results**

130 The rapid adjustments for the CH4 experiment are broken down to show the model differences and the
 131 contributions of the individual rapid adjustments to the overall rapid adjustment contribution to the ERF.

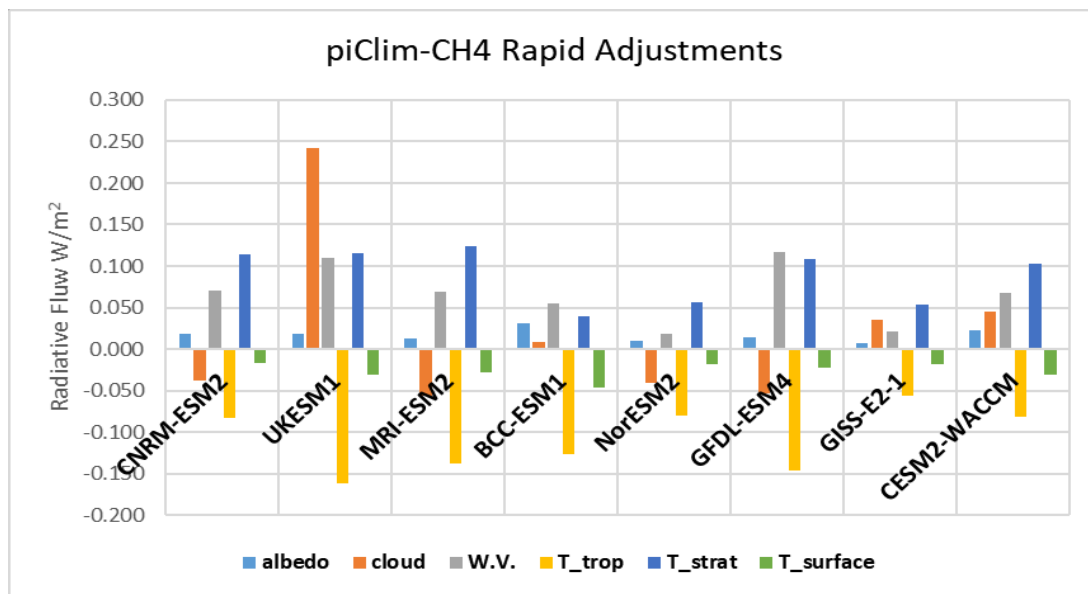


Figure S 4 Plots showing the rapid adjustments for the piClim-CH4 experiments

132

133 **S5 Plots of the Ghan Calculations**

134 We also plotted the breakdown of the ERF into the ERFari, ERFcloud and the ERFcs,af (clear sky, no aerosol)
 135 for models with the appropriate diagnostics, shown in Fig. S4 below.

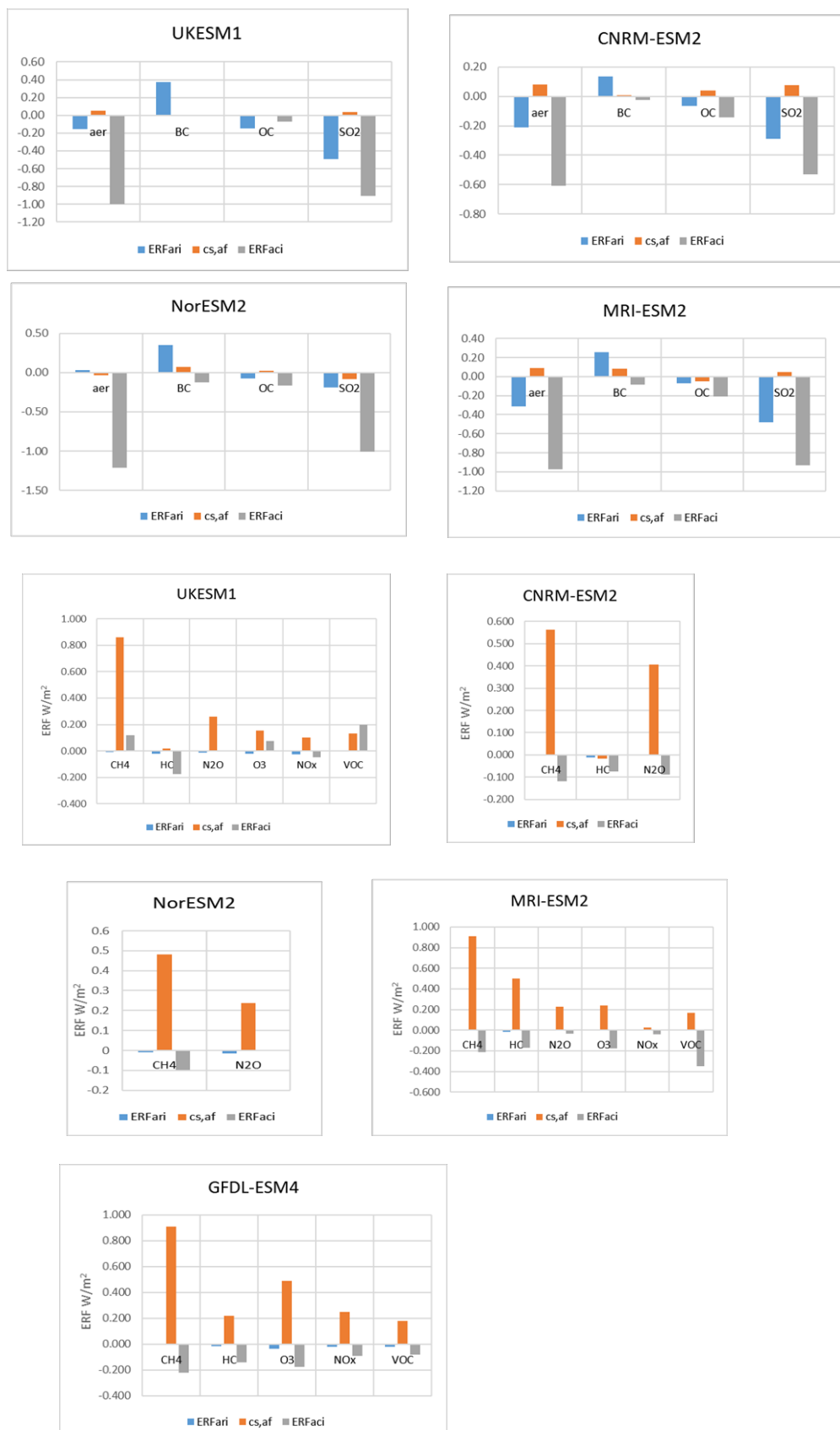


Figure S 5 Breakdown of the ERFs using the double-call method, showing IRFari, ERFcs,af and ERFaci

136

137 **S6 Experiments using NorESM2 to examine adding 2014 aerosols to an atmosphere with 2014**
138 **oxidants.**

139 The following sensitivity experiments were done with the NorESM2 aerosol scheme. To study the
140 effect of SO₂ emissions, we have done a few extra simulations in addition to piClim-control and
141 piClim-SO₂ : two additional experiments which we called piClim-oxid and piClim-oxidSO₂.

142

143 These experiments are :

144 (1) piClim-control : SO₂ emissions are 1850, oxidants are 1850

145 (2) piClim-SO₂ : SO₂ emissions are 2014, oxidants are 1850

146 (3) piClim-oxid : SO₂ emissions are 1850, oxidants are 2014

147 (4) piClim-oxid+SO₂ : SO₂ emissions are 2014, oxidants are 2014

148

149 The standard results in this paper compare (2) with (1) : this gives ERF = -1.303 W/m² (N.B the
150 calculations here were done over 25 years, not 30 years as in the rest of the paper). It reflects the
151 impact of adding SO₂ emissions in a clean pre-industrial atmosphere (both (1) and (2) have the
152 oxidants on 1850 levels, as if NO_x, CO, VOC, ... emissions are all 1850).

153 However, if we compare (4) with (3) : this gives -1.479 W/m². It is the impact of adding SO₂
154 emissions, already in a polluted atmosphere where NO_x, CO, VOC, ... emissions are at 2014 levels,
155 and therefore high oxidant values.

156 It shows that we have differences of the order of 13% : ERF = -1.303 W/m² compared to -1.479
157 W/m².

158 Similar experiments for all aerosols together result in the following :

159 (1) piClim-control : aerosol emissions are 1850, oxidants are 1850

160 (2) piClim-aer : aerosol emissions are 2014, oxidants are 1850

161 (3) piClim-oxid : aerosol emissions are 1850, oxidants are 2014

162 (4) piClim-oxid+aer : aerosol emissions are 2014, oxidants are 2014

163

164 Comparing here (2) with (1) gives ERF = -1.214 W/m² and comparing (4) with (3) gives ERF = -
165 1.458 W/m². This gives a difference of around 20%.

166 This result is only obtained in a simplified setup (prescribed oxidants), but it might give an indication
167 of how the "chemical climate" affects the result.

168 The climate conditions (different temperature and deposition rates in 1850 and 2014) are of course not
169 covered by the above experiment. It remains in an 1850 climate.

170 Finally, the impact of large emission reductions (like 100% for SO₂) can show a different sensitivity
171 than smaller mitigation-type reduction sizes due to non-linearity.

172 (D. Olivie, pers. Comm).

173

174

175 **S7 Breakdown of Ozone changes**

176 Table S 7 Column ozone, and ozone changes resulting from changes concentrations (CH₄, N₂O, HC) or emissions (NO_x, VOC, O₃, NTCF) of reactive gases. The multi
 177 model mean does not include the results for CNRM-ESM2 for tropospheric ozone.

Experiment	CNRM-ESM2		UKSM1		MRI-ESM2		BCC-ESM1		GFDL-ESM4		GISS-E2		CESM2-WACCM		Multi-model	
	trop	strat	trop	strat	trop	Strat	trop	strat	trop	strat	trop	strat	trop	strat	trop	strat
Control DU		303.0 ±0.2	25.71 ±0.06	313.2 ±0.6	19.88 ±0.04	294.8 ±0.4	23.20 ±0.03		20.15 ±0.02	267.0 ±0.2	20.45 ±0.04	258.5 ±0.1	20.33 ±0.04	260.3 ±0.2	22.3 ±2.60	283 ±20
CH ₄ DU		+6.1±0.3	3.02 ±0.08	+2.0 ±0.6	+2.48 ±0.04	+2.9 ±0.5	+2.42 ±0.03		2.50 ±0.04	+2.1 ±0.2	2.17 ±0.05	+5.3 ±0.2	+3.15 ±0.04	+2.9±0.2	+2.6 ±0.3	+4 ±2
NO _x DU			5.20 ±0.08	+4.6 ±0.6	+4.09 ±0.05	+10.5 ±0.5	7.23 ±0.03		6.61 ±0.03	+1.1 ±0.2	9.19 ±0.05	+1.0 ±0.2	+6.97 ±0.04	+0.1 ±0.2	+6.5 ±1.6	+3 ±3
VOC DU			1.47 ±0.08	+1.6 ±0.6	+1.99 ±0.05	+2.0 ±0.5	0.79 ±0.03		1.94 ±0.03	+2.5 ±0.2	1.90 ±0.05	-1.9 ±0.3	+1.57 ±0.05	+2.0 ±0.2	+1.6 ±0.4	+1 ±1
O ₃ DU			6.86 ±0.08	+5.1 ±0.6	+7.51 ±0.04	7.2 ±0.5	8.52 ±0.03		9.46 ±0.03	+2.8 ±0.2	11.38 ±0.06	-0.6 ±0.3			+8.7 ±1.6	+4 ±3
N ₂ O DU		-6.7 ±0.3	0.16 ± 0.08	-3.1 ±0.6	--0.05 ±0.04	-4.7 ±0.5					0.23 ±0.05	-7.6 ±0.2	+0.41 ±0.04	-4.5 ±0.2	+0.2 ±0.2	-5 ±1
HC DU		-23.4 ±0.8	-2.12± 0.08	-38.2 ±0.6	-0.41 ±0.05	-13.4 ±0.5			-1.51 ±0.0	-23.3 ±0.2	-2.54 ±0.05	-24.2 ±0.2	-0.61 ±0.06	-22.7 ±0.4	-1.4 ±0.8	-23 ±8

178

179

180 Table S 8 Percentage change in total aerosol mass (sulphate, nitrate and secondary organic) from the reactive gas experiments.

Experiment	UKESM	MRI-ESM2	BCC-ESM2	GFDL-ESM4			GISS-E2			CESM2-WACCM	
				SO4	NO3	SOA	SO4	NO3	SOA	SO4	SOA
CH4	-2	+2	+1	+6	0	0	-1	-11	+1	-1	-1
NOx	-2	0	+9	-8	+200	+1	-19	+120	+19	+2	-10
VOC	-3	+1	0	+4	-5	+8	-2	0	+1	-2	+34
O3	-4	+1	+10	-3	+190	+7	-21	+130	+21		
N2O	+1	+1					+1	+7	+1	+1	+1
HC	+2	+1		+1	0	+1	+1	-11	+1	-1	+1

193

194

195

196 **S8 Methane Lifetime**

197

198 **Table S 9 Methane lifetime (years), and change due to each experiment (%). Multi-model mean and**
199 **standard deviation. Lifetimes assume a soil loss of 120 years. Stratospheric loss is included in the model**
200 **calculations.**

Experiment	UKESM1	CESM2-WACCM	GFDL-ESM4	BCC	GISS-E2	MRI-ESM2	Multi-model
Control years	8.0	8.7	9.6	6.3	13.4	10.1	10.0 ±1.9
CH4 %	+22	+22	+21	+26	+18	+22	22±3
NOx %	-25	-35	-33		-46	-26	-33±8
VOC %	+11		+15		+27	+21	+19±6
O3 %	-19		-24		-40	-20	-16±9
HC %	-4.9		-7.5		-0.6	-2.4	-3.7 ±2.4
N2O	-1.2	-2.8			-3.9	-1.3	-2.0 ±1.1

201

202

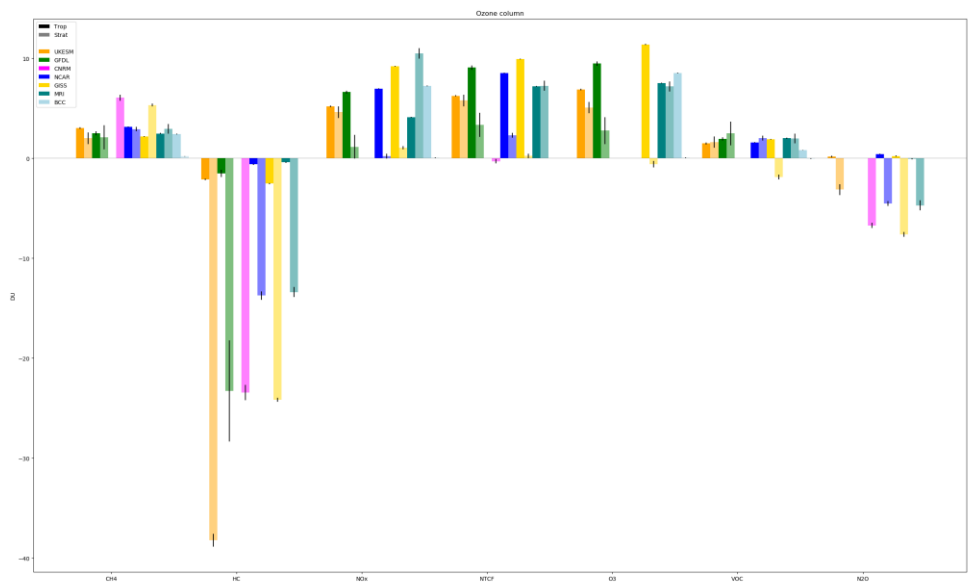
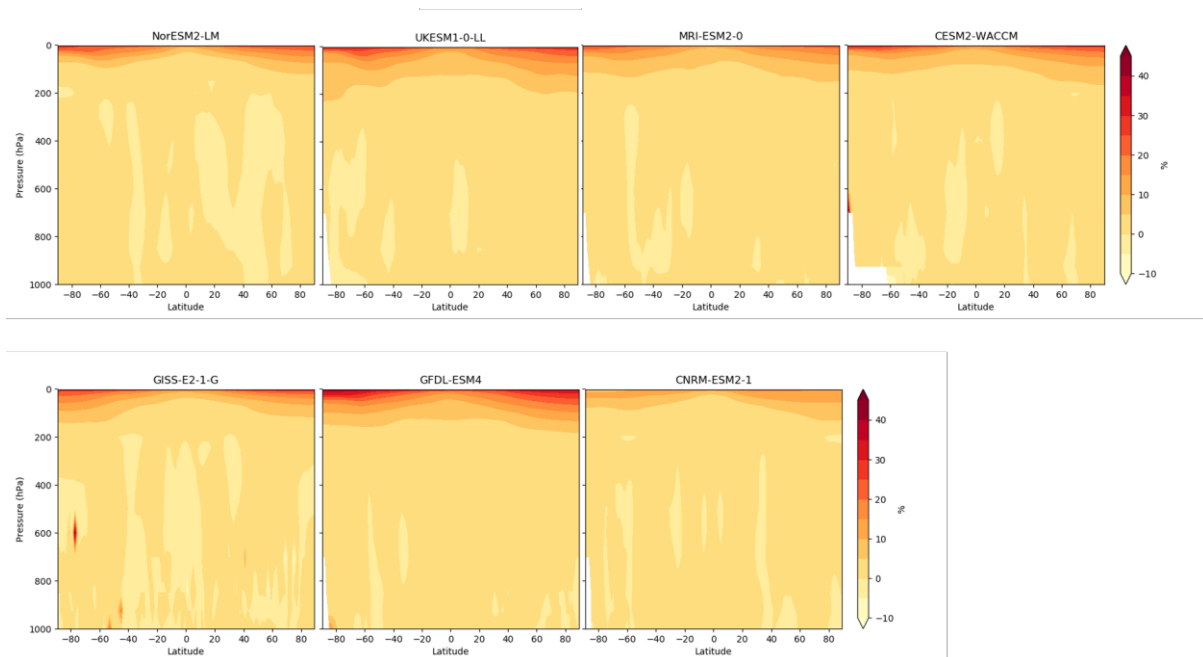


Figure S 6 Ozone column values for the troposphere and stratosphere for the reactive greenhouse gas experiments

203



204
205

Figure S 7 Percentage changes in water vapour from the piClim-CH4 experiments.

206

207 Abdul-Razzak, H., and Ghan, S. J.: A parameterization of aerosol activation: 2. Multiple aerosol
208 types, *Journal of Geophysical Research: Atmospheres*, 105, 6837-6844, 10.1029/1999jd901161, 2000.

209 Archibald, A. T., O'Connor, F. M., Abraham, N. L., Archer-Nicholls, S., Chipperfield, M. P., Dalvi,
210 M., Folberth, G. A., Dennison, F., Dhomse, S. S., Griffiths, P. T., Hardacre, C., Hewitt, A. J., Hill, R.,
211 Johnson, C. E., Keeble, J., Köhler, M. O., Morgenstern, O., Mulchay, J. P., Ordóñez, C., Pope, R. J.,

- 212 Rumbold, S., Russo, M. R., Savage, N., Sellar, A., Stringer, M., Turnock, S., Wild, O., and Zeng, G.:
213 Description and evaluation of the UKCA stratosphere-troposphere chemistry scheme (StratTrop v1.0)
214 implemented in UKESM1, *Geosci. Model Dev. Discuss.*, 2019, 1-82, 10.5194/gmd-2019-246,
215 2020.
- 216 Balkanski, Y., Myhre, G., Gauss, M., Rädcl, G., Highwood, E. J., and Shine, K. P.: Direct radiative
217 effect of aerosols emitted by transport: from road, shipping and aviation, *Atmos. Chem. Phys.*, 10,
218 4477-4489, 10.5194/acp-10-4477-2010, 2010.
- 219 Bauer, S. E., Tsigaridis, K., Faluvegi, G., Kelley, M., Lo, K. K., Miller, R. L., Nazarenko, L.,
220 Schmidt, G. A., and Wu, J.: Historical (1850–2014) Aerosol Evolution and Role on Climate Forcing
221 Using the GISS ModelE2.1 Contribution to CMIP6, *Journal of Advances in Modeling Earth Systems*,
222 12, e2019MS001978, 10.1029/2019ms001978, 2020.
- 223 Checa-Garcia, R., Hegglin, M. I., Kinnison, D., Plummer, D. A., and Shine, K. P.: Historical
224 Tropospheric and Stratospheric Ozone Radiative Forcing Using the CMIP6 Database, *Geophysical
225 Research Letters*, 45, 3264-3273, 10.1002/2017gl076770, 2018.
- 226 Danabasoglu, G.: NCAR CESM2-WACCM model output prepared for CMIP6 CMIP historical,
227 <https://doi.org/10.22033/ESGF/CMIP6.10071>, <https://doi.org/10.22033/ESGF/CMIP6.10071>, 2019.
- 228 Danabasoglu, G.: NCAR CESM2-WACCM model output prepared for CMIP6 ScenarioMIP,
229 <https://doi.org/10.22033/ESGF/CMIP6.10026>, [http://cera-
www.dkrz.de/WDCC/meta/CMIP6/CMIP6.ScenarioMIP.NCAR.CESM2-WACCM](http://cera-
230 www.dkrz.de/WDCC/meta/CMIP6/CMIP6.ScenarioMIP.NCAR.CESM2-WACCM), 2019.
- 231 Di Biagio, C., Formenti, P., Balkanski, Y., Caponi, L., Cazaunau, M., Pangui, E., Journet, E., Nowak,
232 S., Andreae, M., Kandler, K., Saeed, T., Piketh, S., Seibert, D., Williams, E., and Doussin, J.-F.:
233 Complex refractive indices and single scattering albedo of global dust aerosols in the shortwave
234 spectrum and relationship to iron content and size, *Atmospheric Chemistry and Physics Discussions*,
235 1-42, 10.5194/acp-2019-145, 2019.
- 236 Dunne, J. P., Horowitz, L. W., Adcroft, A. J., Ginoux, P., Held, I. M., John, J. G., Krasting, J. P.,
237 Malyshev, S., Naik, V., Paulot, F., Shevliakova, E., Stock, C. A., Zadeh, N., Balaji, V., Blanton, C.,
238 Dunne, K. A., Dupuis, C., Durachta, J., Dussin, R., Gauthier, P. P. G., Griffies, S. M., Guo, H.,
239 Hallberg, R. W., Harrison, M., He, J., Hurlin, W., McHugh, C., Menzel, R., Milly, P. C. D., Nikonov,
240 S., Paynter, D. J., Ploshay, J., Radhakrishnan, A., Rand, K., Reichl, B. G., Robinson, T.,
241 Schwarzkopf, D. M., Sentman, L. T., Underwood, S., Vahlenkamp, H., Winton, M., Wittenberg, A.
242 T., Wyman, B., Zeng, Y., and Zhao, M.: The GFDL Earth System Model version 4.1 (GFDL-ESM
243 4.1): Overall coupled model description and simulation characteristics, *Journal of Advances in
244 Modeling Earth Systems*, n/a, e2019MS002015, 10.1029/2019ms002015, 2020.
- 245 Emmons, L. K., Schwantes, R. H., Orlando, J. J., Tyndall, G., Kinnison, D., -F., L. J., Marsh, D.,
246 Mills, M., Tilmes, S., Bardeen, C., Buchholz, R. R., Conley, A., Gettelman, A., Garcia, R., Simpson,
247 I., Blake, D. R., Meinardi, S., and Pétron, G.: The Chemistry Mechanism in the Community Earth
248 System Model version 2 (CESM2), *J. Advances in Modeling Earth Systems*, 12,
249 <https://doi.org/10.1029/2019MS001882>, 2020.
- 250 Gery, M. W., Whitten, G. Z., Killus, J. P., and Dodge, M. C.: A photochemical kinetics mechanism
251 for urban and regional scale computer modeling., *Journal of Geophysical Research*, 94, 925-956,
252 1989.
- 253 Gettelman, A., Mills, M. J., Kinnison, D. E., Garcia, R. R., Smith, A. K., Marsh, D. R., Tilmes, S.,
254 Vitt, F., Bardeen, C. G., McInerny, J., Liu, H. L., Solomon, S. C., Polvani, L. M., Emmons, L. K.,
255 Lamarque, J. F., Richter, J. H., Glanville, A. S., Bacmeister, J. T., Phillips, A. S., Neale, R. B.,
256 Simpson, I. R., DuVivier, A. K., Hodzic, A., and Randel, W. J.: The Whole Atmosphere Community

257 Climate Model Version 6 (WACCM6), *Journal of Geophysical Research: Atmospheres*, n/a,
258 10.1029/2019JD030943, 2019.

259 Hauglustaine, D. A., Balkanski, Y., and Schulz, M.: A global model simulation of present and future
260 nitrate aerosols and their direct radiative forcing of climate, *Atmos. Chem. Phys.*, 14, 11031-11063,
261 10.5194/acp-14-11031-2014, 2014.

262 Horowitz, L. W., Walters, S., Mauzerall, D. L., Emmons, L. K., Rasch, P. J., Granier, C., Tie, X.,
263 Lamarque, J.-F., Schultz, M. G., Tyndall, G. S., Orlando, J. J., and Brasseur, G. P.: A global
264 simulation of tropospheric ozone and related tracers: Description and evaluation of MOZART,
265 version 2, *Journal of Geophysical Research: Atmospheres*, 108, 10.1029/2002jd002853, 2003.

266 Horowitz, L. W., Naik, V., Paulot, F., Ginoux, P. A., Dunne, J. P., Mao, J., Schnell, J., Chen, X., He,
267 J., John, J. G., Lin, M., Lin, P., Malyshev, S., Paynter, D., Shevliakova, E., and Zhao, M.: The GFDL
268 Global Atmospheric Chemistry-Climate Model AM4.1: Model Description and Simulation
269 Characteristics, *Journal of Advances in Modeling Earth Systems*, n/a, e2019MS002032,
270 10.1029/2019ms002032, 2020.

271 Jones, A., Roberts, D. L., Woodage, M. J., and Johnson, C. E.: Indirect sulphate aerosol forcing in a
272 climate model with an interactive sulphur cycle, *Journal of Geophysical Research: Atmospheres*, 106,
273 20293-20310, 10.1029/2000jd000089, 2001.

274 Khairoutdinov, M., and Kogan, Y.: A New Cloud Physics Parameterization in a Large-Eddy
275 Simulation Model of Marine Stratocumulus, *Monthly Weather Review*, 128, 229-243, 10.1175/1520-
276 0493(2000)128<0229:ancppi>2.0.co;2, 2000.

277 Kirkevåg, A., Grini, A., Olivie, D., Seland, Ø., Alterskjær, K., Hummel, M., Karset, I. H. H.,
278 Lewinschal, A., Liu, X., Makkonen, R., Bethke, I., Griesfeller, J., Schulz, M., and Iversen, T.: A
279 production-tagged aerosol module for Earth system models, OsloAero5.3 – extensions and updates for
280 CAM5.3-Oslo, *Geosci. Model Dev.*, 11, 3945-3982, 10.5194/gmd-11-3945-2018, 2018.

281 Kuhlbrodt, T., Jones, C. G., Sellar, A., Storkey, D., Blockley, E., Stringer, M., Hill, R., Graham, T.,
282 Ridley, J., Blaker, A., Calvert, D., Copsey, D., Ellis, R., Hewitt, H., Hyder, P., Ineson, S., Mulcahy, J.,
283 Siahann, A., and Walton, J.: The Low-Resolution Version of HadGEM3 GC3.1: Development and
284 Evaluation for Global Climate, *Journal of Advances in Modeling Earth Systems*, 10, 2865-2888,
285 10.1029/2018ms001370, 2018.

286 Lurton, T., Balkanski, Y., Bastrikov, V., Bekki, S., Bopp, L., Braconnot, P., Brockmann, P., Cadule,
287 P., Contoux, C., Cozic, A., Cugnet, D., Dufresne, J.-L., Éthé, C., Foujols, M.-A., Ghattas, J.,
288 Hauglustaine, D., Hu, R.-M., Kageyama, M., Khodri, M., Lebas, N., Levvasseur, G., Marchand, M.,
289 Ottlé, C., Peylin, P., Sima, A., Szopa, S., Thiéblemont, R., Vuichard, N., and Boucher, O.:
290 Implementation of the CMIP6 Forcing Data in the IPSL-CM6A-LR Model, *Journal of Advances in
291 Modeling Earth Systems*, 12, e2019MS001940, 10.1029/2019ms001940, 2020.

292 Mann, G. W., Carslaw, K. S., Spracklen, D. V., Ridley, D. A., Manktelow, P. T., Chipperfield, M. P.,
293 Pickering, S. J., and Johnson, C. E.: Description and evaluation of GLOMAP-mode: a modal global
294 aerosol microphysics model for the UKCA composition-climate model, *Geosci. Model Dev.*, 3, 519-
295 551, 10.5194/gmd-3-519-2010, 2010.

296 Matthes, K., Funke, B., Andersson, M. E., Barnard, L., Beer, J., Charbonneau, P., Clilverd, M. A.,
297 Dudok de Wit, T., Haberreiter, M., Hendry, A., Jackman, C. H., Kretzschmar, M., Kruschke, T.,
298 Kunze, M., Langematz, U., Marsh, D. R., Maycock, A. C., Misios, S., Rodger, C. J., Scaife, A. A.,
299 Seppälä, A., Shangguan, M., Sinnhuber, M., Tourpali, K., Usoskin, I., van de Kamp, M., Verronen, P.,
300 T., and Versick, S.: Solar forcing for CMIP6 (v3.2), *Geosci. Model Dev.*, 10, 2247-2302,
301 10.5194/gmd-10-2247-2017, 2017.

302 Michou, M., Nabat, P., and Saint-Martin, D.: Development and basic evaluation of a prognostic
303 aerosol scheme (v1) in the CNRM Climate Model CNRM-CM6, *Geosci. Model Dev.*, 8, 501-531,
304 10.5194/gmd-8-501-2015, 2015.

305 Morgenstern, O., Braesicke, P., O'Connor, F. M., Bushell, A. C., Johnson, C. E., Osprey, S. M., and
306 Pyle, J. A.: Evaluation of the new UKCA climate-composition model – Part 1: The stratosphere,
307 *Geosci. Model Dev.*, 2, 43-57, 10.5194/gmd-2-43-2009, 2009.

308 Mulcahy, J. P., Jones, C., Sellar, A., Johnson, B., Boutle, I. A., Jones, A., Andrews, T., Rumbold, S.
309 T., Mollard, J., Bellouin, N., Johnson, C. E., Williams, K. D., Grosvenor, D. P., and McCoy, D. T.:
310 Improved Aerosol Processes and Effective Radiative Forcing in HadGEM3 and UKESM1, *Journal of*
311 *Advances in Modeling Earth Systems*, 10, 2786-2805, 10.1029/2018ms001464, 2018.

312 Mulcahy, J. P., Johnson, C., Jones, C. G., Povey, A. C., Scott, C. E., Sellar, A., Turnock, S. T.,
313 Woodhouse, M. T., Abraham, N. L., Andrews, M. B., Bellouin, N., Browse, J., Carslaw, K. S., Dalvi,
314 M., Folberth, G. A., Glover, M., Grosvenor, D., Hardacre, C., Hill, R., Johnson, B., Jones, A.,
315 Kipling, Z., Mann, G., Mollard, J., O'Connor, F. M., Palmieri, J., Reddington, C., Rumbold, S. T.,
316 Richardson, M., Schutgens, N. A. J., Stier, P., Stringer, M., Tang, Y., Walton, J., Woodward, S., and
317 Yool, A.: Description and evaluation of aerosol in UKESM1 and HadGEM3-GC3.1 CMIP6 historical
318 simulations, *Geosci. Model Dev. Discuss.*, 2020, 1-59, 10.5194/gmd-2019-357, 2020.

319 O'Connor, F. M., Johnson, C. E., Morgenstern, O., Abraham, N. L., Braesicke, P., Dalvi, M.,
320 Folberth, G. A., Sanderson, M. G., Telford, P. J., Voulgarakis, A., Young, P. J., Zeng, G., Collins, W.
321 J., and Pyle, J. A.: Evaluation of the new UKCA climate-composition model – Part 2: The
322 Troposphere, *Geosci. Model Dev.*, 7, 41-91, 10.5194/gmd-7-41-2014, 2014.

323 Oshima, N., Yukimoto, S., Deushi, M., Koshiro, T., Kawai, H., Tanaka, T. Y., and Yoshida, K.:
324 Global and Arctic effective radiative forcing of anthropogenic gases and aerosols in MRI-ESM2.0,
325 *Prog. Earth. Planet. Sci.*, 2020.

326 Séférian, R., Nabat, P., Michou, M., Saint-Martin, D., Voldoire, A., Colin, J., Decharme, B., Delire,
327 C., Berthet, S., Chevallier, M., Sénési, S., Franchisteguy, L., Vial, J., Mallet, M., Joetzjer, E.,
328 Geoffroy, O., Guérémy, J.-F., Moine, M.-P., Msadek, R., Ribes, A., Rocher, M., Roehrig, R., Salas-y-
329 Mélia, D., Sanchez, E., Terray, L., Valcke, S., Waldman, R., Aumont, O., Bopp, L., Deshayes, J.,
330 Éthé, C., and Madec, G.: Evaluation of CNRM Earth-System model, CNRM-ESM 2-1: role of Earth
331 system processes in present-day and future climate, *Journal of Advances in Modeling Earth Systems*,
332 n/a, 10.1029/2019ms001791.

333 Séférian, R., Delire, C., Decharme, B., Voldoire, A., Salas Y Melia, D., Chevallier, M., Saint-Martin,
334 D., Aumont, O., Calvet, J.-C., Carrer, D., Douville, H., Franchistéguy, L., Joetzjer, E., and Sénési, S.:
335 Development and evaluation of CNRM Earth system model – CNRM-ESM1, *Geoscientific Model*
336 *Development*, 9, 1423-1453, 10.5194/gmd-9-1423-2016, 2016.

337 Sellar, A. A., Jones, C. G., Mulcahy, J., Tang, Y., Yool, A., Wiltshire, A., O'Connor, F. M., Stringer,
338 M., Hill, R., Palmieri, J., Woodward, S., de Mora, L., Kuhlbrodt, T., Rumbold, S., Kelley, D. I., Ellis,
339 R., Johnson, C. E., Walton, J., Abraham, N. L., Andrews, M. B., Andrews, T., Archibald, A. T.,
340 Berthou, S., Burke, E., Blockley, E., Carslaw, K., Dalvi, M., Edwards, J., Folberth, G. A., Gedney, N.,
341 Griffiths, P. T., Harper, A. B., Hendry, M. A., Hewitt, A. J., Johnson, B., Jones, A., Jones, C. D.,
342 Keeble, J., Liddicoat, S., Morgenstern, O., Parker, R. J., Predoi, V., Robertson, E., Siahann, A., Smith,
343 R. S., Swaminathan, R., Woodhouse, M. T., Zeng, G., and Zerroukat, M.: UKESM1: Description and
344 evaluation of the UK Earth System Model, *Journal of Advances in Modeling Earth Systems*, n/a,
345 10.1029/2019ms001739.

346 Sellar, A. A., Jones, C. G., Mulcahy, J., Tang, Y., Yool, A., Wiltshire, A., O'Connor, F. M., Stringer,
347 M., Hill, R., Palmieri, J., Woodward, S., de Mora, L., Kuhlbrodt, T., Rumbold, S., Kelley, D. I., Ellis,

348 R., Johnson, C. E., Walton, J., Abraham, N. L., Andrews, M. B., Andrews, T., Archibald, A. T.,
349 Berthou, S., Burke, E., Blockley, E., Carslaw, K., Dalvi, M., Edwards, J., Folberth, G. A., Gedney, N.,
350 Griffiths, P. T., Harper, A. B., Hendry, M. A., Hewitt, A. J., Johnson, B., Jones, A., Jones, C. D.,
351 Keeble, J., Liddicoat, S., Morgenstern, O., Parker, R. J., Predoi, V., Robertson, E., Siahann, A., Smith,
352 R. S., Swaminathan, R., Woodhouse, M. T., Zeng, G., and Zerroukat, M.: UKESM1: Description and
353 evaluation of the UK Earth System Model, *Journal of Advances in Modeling Earth Systems*, n/a,
354 10.1029/2019ms001739, 2020.

355 Shindell, D. T., Grenfell, J. L., Rind, D., Grewe, V., and Price, C.: Chemistry-climate interactions in
356 the Goddard Institute for Space Studies general circulation model: 1. Tropospheric chemistry model
357 description and evaluation, *Journal of Geophysical Research: Atmospheres*, 106, 8047-8075,
358 10.1029/2000jd900704, 2001.

359 Shindell, D. T., Faluvegi, G., and Bell, N.: Preindustrial-to-present-day radiative forcing by
360 tropospheric ozone from improved simulations with the GISS chemistry-climate GCM, *Atmos. Chem.*
361 *Phys.*, 3, 1675-1702, 10.5194/acp-3-1675-2003, 2003.

362 Shindell, D. T., Faluvegi, G., Unger, N., Aguilar, E., Schmidt, G. A., Koch, D. M., Bauer, S. E., and
363 Miller, R. L.: Simulations of preindustrial, present-day, and 2100 conditions in the NASA GISS
364 composition and climate model G-PUCCINI, *Atmos. Chem. Phys.*, 6, 4427-4459, 10.5194/acp-6-
365 4427-2006, 2006.

366 Smith, C. J., Kramer, R. J., Myhre, G., Alterskjær, K., Collins, W., Sima, A., Boucher, O., Dufresne,
367 J. L., Nabat, P., Michou, M., Yukimoto, S., Cole, J., Paynter, D., Shiogama, H., O'Connor, F. M.,
368 Robertson, E., Wiltshire, A., Andrews, T., Hannay, C., Miller, R., Nazarenko, L., Kirkevåg, A.,
369 Olivié, D., Fiedler, S., Pincus, R., and Forster, P. M.: Effective radiative forcing and adjustments in
370 CMIP6 models, *Atmos. Chem. Phys.*, 20, 9591-9618, 10.5194/acp-20-9591-2020, 2020.

371 Takemura, T., Nozawa, T., Emori, S., Nakajima, T. Y., and Nakajima, T.: Simulation of climate
372 response to aerosol direct and indirect effects with aerosol transport-radiation model, *Journal of*
373 *Geophysical Research: Atmospheres*, 110, 10.1029/2004jd005029, 2005.

374 Takemura, T., and Suzuki, K.: Weak global warming mitigation by reducing black carbon emissions,
375 *Scientific Reports*, 9, 4419, 10.1038/s41598-019-41181-6, 2019.

376 Takemura, T., et al: Development of a global aerosol climate model SPRINTARS, CGER's
377 Supercomputer Monograph Report, 24, 2018.

378 Tatebe, H., Ogura, T., Nitta, T., Komuro, Y., Ogochi, K., Takemura, T., Sudo, K., Sekiguchi, M.,
379 Abe, M., Saito, F., Chikira, M., Watanabe, S., Mori, M., Hirota, N., Kawatani, Y., Mochizuki, T.,
380 Yoshimura, K., Takata, K., O'Ishi, R., Yamazaki, D., Suzuki, T., Kurogi, M., Kataoka, T., Watanabe,
381 M., and Kimoto, M.: Description and basic evaluation of simulated mean state, internal variability,
382 and climate sensitivity in MIROC6, *Geoscientific Model Development*, 12, 2727-2765,
383 <http://dx.doi.org/10.5194/gmd-12-2727-2019>, 2019.

384 Tilmes, S., Hodzic, A., Emmons, L. K., Mills, M. J., Gettelman, A., Kinnison, D. E., Park, M.,
385 Lamarque, J. F., Vitt, F., Shrivastava, M., Campuzano-Jost, P., Jimenez, J. L., and Liu, X.: Climate
386 Forcing and Trends of Organic Aerosols in the Community Earth System Model (CESM2), *Journal of*
387 *Advances in Modeling Earth Systems*, n/a, 10.1029/2019MS001827, 2019.

388 Walters, D., Baran, A. J., Boutle, I., Brooks, M., Earnshaw, P., Edwards, J., Furtado, K., Hill, P.,
389 Lock, A., Manners, J., Morcrette, C., Mulcahy, J., Sanchez, C., Smith, C., Stratton, R., Tennant, W.,
390 Tomassini, L., Van Weverberg, K., Vosper, S., Willett, M., Browse, J., Bushell, A., Carslaw, K.,
391 Dalvi, M., Essery, R., Gedney, N., Hardiman, S., Johnson, B., Johnson, C., Jones, A., Jones, C.,
392 Mann, G., Milton, S., Rumbold, H., Sellar, A., Ujiie, M., Whitall, M., Williams, K., and Zerroukat,

393 M.: The Met Office Unified Model Global Atmosphere 7.0/7.1 and JULES Global Land 7.0
394 configurations, *Geosci. Model Dev.*, 12, 1909-1963, 10.5194/gmd-12-1909-2019, 2019.

395 Wang, R., Balkanski, Y., Boucher, O., Ciais, P., Schuster, G. L., Chevallier, F., Samset, B. H., Liu, J.,
396 Piao, S., Valari, M., and Tao, S.: Estimation of global black carbon direct radiative forcing and its
397 uncertainty constrained by observations, *Journal of Geophysical Research: Atmospheres*, 121, 5948-
398 5971, 10.1002/2015jd024326, 2016.

399 Watanabe, M., Suzuki, T., O'ishi, R., Komuro, Y., Watanabe, S., Emori, S., Takemura, T., Chikira,
400 M., Ogura, T., Sekiguchi, M., Takata, K., Yamazaki, D., Yokohata, T., Nozawa, T., Hasumi, H.,
401 Tatebe, H., and Kimoto, M.: Improved Climate Simulation by MIROC5: Mean States, Variability,
402 and Climate Sensitivity, *Journal of Climate*, 23, 6312-6335, 10.1175/2010jcli3679.1, 2010.

403 Williams, K. D., Copsey, D., Blockley, E. W., Bodas-Salcedo, A., Calvert, D., Comer, R., Davis, P.,
404 Graham, T., Hewitt, H. T., Hill, R., Hyder, P., Ineson, S., Johns, T. C., Keen, A. B., Lee, R. W.,
405 Megann, A., Milton, S. F., Rae, J. G. L., Roberts, M. J., Scaife, A. A., Schiemann, R., Storkey, D.,
406 Thorpe, L., Watterson, I. G., Walters, D. N., West, A., Wood, R. A., Woollings, T., and Xavier, P. K.:
407 The Met Office Global Coupled Model 3.0 and 3.1 (GC3.0 and GC3.1) Configurations, *Journal of*
408 *Advances in Modeling Earth Systems*, 10, 357-380, 10.1002/2017ms001115, 2018.

409 Woodward, S.: Modeling the atmospheric life cycle and radiative impact of mineral dust in the
410 Hadley Centre climate model, *Journal of Geophysical Research: Atmospheres*, 106, 18155-18166,
411 10.1029/2000jd900795, 2001.

412 Wu, T., Zhang, F., Zhang, J., Jie, W., Zhang, Y., Wu, F., Li, L., Liu, X., Lu, X., Zhang, L., Wang, J.,
413 and Hu, A.: Beijing Climate Center Earth System Model version 1 (BCC-ESM1): Model Description
414 and Evaluation, *Geosci. Model Dev.*, 13, 977-1005, 10.5194/gmd-2019-172, 2020.

415 Yukimoto, S., Kawai, H., Koshiro, T., Oshima, N., Yoshida, K., Urakawa, S., Tsujino, H., Deushi,
416 M., Tanaka, T., Hosaka, M., Yabu, S., Yoshimura, H., Shindo, E., Mizuta, R., Obata, A., Adachi, Y.,
417 and Ishii, M.: The Meteorological Research Institute Earth System Model Version 2.0, MRI-ESM2.0:
418 Description and Basic Evaluation of the Physical Component, *J. Meteor. Soc. Japan*, 97, 931-965,
419 10.2151/jmsj.2019-051, 2019.

420